2010

Wnt5b signaling in zebrafish development and disease

Shengda Lin
University of Iowa

WNT5B SIGNALING IN ZEBRAFISH DEVELOPMENT AND DISEASE

by

Shengda Lin

An Abstract

Of a thesis submitted in partial fulfillment
of the requirements for the Doctor of
Philosophy degree in Biology
in the Graduate College of
The University of Iowa

December 2010

Thesis Supervisor: Professor Diane C. Slusarski

ABSTRACT

Wnts are secreted glycoproteins that activate signaling pathways important in development and disease. The canonical Wnt pathway activates nuclear localization of ß-catenin, a multi-functional protein involved in cell adhesion and transcription. Other Wnt pathways, which appear to be independent of nuclear ß-catenin, are collectively categorized as non-canonical pathways. Non-canonical Wnt pathways are involved in a variety of biological processes such as establishing planar cell polarity (PCP), stimulating intra-cellular calcium release and antagonizing canonical Wnt signaling.

Wnt proteins share remarkable structural similarity, yet can trigger diverse pathways that lead to distinct or even opposing signaling outputs. To address this central question in biology, we focused on two fundamental aspects of Wnt signaling: the differential expression of Wnt ligands and the action of Wnt receptors. We specifically studied how zebrafish embryos regulate the expression of Wnt5, a particular Wnt protein capable of inducing all known Wnt pathways, and whether/how alternative Wnt receptors Frizzled (Fz) and Related to Tyrosine Kinase (Ryk) convey Wnt5 signals to distinguishable cellular molecular responses.

Non-canonical Wnts are largely believed to act as permissive cues for embryonic development via Fz receptors in vertebrate cell movement. In this thesis, I provide evidence that Wnt5b acts as an instructive cue during gastrulation, and spatial-temporal control of Wnt5b expression is essential for its function in embryogenesis. I integrated *in silico* and *in vivo* methods to identify *cis*-regulatory elements that modulate embryonic expression pattern of zebrafish *wnt5b*. I further showed that epigenetic changes of these elements may be contributing to increased tumor incidence in adult zebrafish.

In addition to Fz, Wnt ligands can signal through an alternative receptor Ryk. However, Wnt-Ryk signaling during embryogenesis is less well characterized. We found that Ryk deficiency impairs Wnt5b-induced calcium activity and directional cell

movement. Upon Wnt5b stimulation, Fz2, but not Ryk, recruits Disheveled to the cell membrane, suggesting that Fz2 and Ryk mediate separate pathways. We further demonstrated that Ryk-expressing cells migrate away from the Wnt5b source by promoting polarized protrusive activity and conclude that full-length Ryk transduces directional Wnt5b signals in development.

Abstract Approved: _____
Thesis Supervisor

_____
Title and Department

_____
Date

WNT5B SIGNALING IN ZEBRAFISH DEVELOPMENT AND DISEASE

by

Shengda Lin

A thesis submitted in partial fulfillment
of the requirements for the Doctor of
Philosophy degree in Biology
in the Graduate College of
The University of Iowa

December 2010

Thesis Supervisor: Professor Diane C. Slusarski

Graduate College
The University of Iowa
Iowa City, Iowa

CERTIFICATE OF APPROVAL

_____

PH.D. THESIS

_____

This is to certify that the Ph.D. thesis of

Shengda Lin

has been approved by the Examining Committee
for the thesis requirement for the Doctor of Philosophy
degree in Biology at the December 2010 graduation.

Thesis Committee: _____
Diane C. Slusarski, Thesis Supervisor

_____
Robert A. Cornell

_____
Douglas W. Houston

_____
Jim J.-C. Lin

_____
Christopher S. Stipp

ABSTRACT

Wnts are secreted glycoproteins that activate signaling pathways important in development and disease. The canonical Wnt pathway activates nuclear localization of ß-catenin, a multi-functional protein involved in cell adhesion and transcription. Other Wnt pathways, which appear to be independent of nuclear ß-catenin, are collectively categorized as non-canonical pathways. Non-canonical Wnt pathways are involved in a variety of biological processes such as establishing planar cell polarity (PCP), stimulating intra-cellular calcium release and antagonizing canonical Wnt signaling.

Wnt proteins share remarkable structural similarity, yet can trigger diverse pathways that lead to distinct or even opposing signaling outputs. To address this central question in biology, we focused on two fundamental aspects of Wnt signaling: the differential expression of Wnt ligands and the action of Wnt receptors. We specifically studied how zebrafish embryos regulate the expression of Wnt5, a particular Wnt protein capable of inducing all known Wnt pathways, and whether/how alternative Wnt receptors Frizzled (Fz) and Related to Tyrosine Kinase (Ryk) convey Wnt5 signals to distinguishable cellular molecular responses.

Non-canonical Wnts are largely believed to act as permissive cues for embryonic development via Fz receptors in vertebrate cell movement. In this thesis, I provide evidence that Wnt5b acts as an instructive cue during gastrulation, and spatial-temporal control of Wnt5b expression is essential for its function in embryogenesis. I integrated *in silico* and *in vivo* methods to identify *cis*-regulatory elements that modulate embryonic expression pattern of zebrafish *wnt5b*. I further showed that epigenetic changes of these elements may be contributing to increased tumor incidence in adult zebrafish.

In addition to Fz, Wnt ligands can signal through an alternative receptor Ryk. However, Wnt-Ryk signaling during embryogenesis is less well characterized. We found that Ryk deficiency impairs Wnt5b-induced calcium activity and directional cell

movement. Upon Wnt5b stimulation, Fz2, but not Ryk, recruits Disheveled to the cell membrane, suggesting that Fz2 and Ryk mediate separate pathways. We further demonstrated that Ryk-expressing cells migrate away from the Wnt5b source by promoting polarized protrusive activity and conclude that full-length Ryk transduces directional Wnt5b signals in development.

TABLE OF CONTENTS

LIST OF TABLES

Table

LIST OF FIGURES

Figure

LIST OF ABBREVIATIONS

AO	Acridine Orange
AP	Anterior-Posterior
bp	base-pairs
Ca^{2+}	Calcium
CaMKII	Calcium/calmodulin-dependent protein kinase II
CDS	Coding sequence
CE	Convergent extension
CRD	Cystine-riched domain
DFC	Dorsal forerunner cell
DA	Dorsal aorta
DAG	Diacylglycerol
DMSO	Dimethyl sulfoxide
dpf	Day post-fertilization
DAAM	Dishevelled-associated activator of morphogenesis
DV	Dorsal-Ventral
Dvl	Dishevelled
ECD	Extracellular domain
ER	Endoplasmic reticulum
EVL	Enveloping layer
FRET	Fluorescence resonance energy transfer
Fz	Frizzled
GPCR	G-protein coupled receptors
GSK3	Glycogen synthase kinase3
hpf	Hour post-fertilization
ICD	Intracellular domain

Ig	Immunoglobulin
IPL	Inner plexiform layer
IRES	Internal ribosome entry site
IS	Intersegmental vessel
JNK	JUN N-terminal kinase
Kny	Knypek
KV	Kupffer’s vesicle
LEF/TCF	Lymphoid Enhancer Factor/T-Cell Factor
LPM	Lateral plate mesoderm
LR	Left-Right
MBT	Mid-blastrula transition
MO	Morpholino
Nkd	Naked cuticle
PCP	Planar cell polarity
PCV	Posterior cardinal vein
PLC	Phospholipase C
ROCK	regulation of Rho-associated protein kinase
RTK	Receptor tyrosine kinase
Ryk	Related to tyrosine kinase
TM	Transmembrane
TGF	Transforming growth factor
wg	*wingless*
WMISH	Whole-mount in situ hybridization
UTR	Untranslated region
YSL	Yolk syncytial layer

CHAPTER I
INTRODUCTION

The Wnt signaling network

Wnts are a large family of secreted cystine-rich glycoproteins that activate receptor-mediated signaling pathways. Wnt signaling regulates a wide range of biological processes including embryonic patterning, cell proliferation, and stem cell maintenance (Alonso and Fuchs, 2003; van Es et al., 2003; Veeman et al., 2003a). Based on genetic and biochemical studies, Wnt proteins are classified into two groups: the canonical Wnts, which activate nuclear localization of ß-catenin, and the non-canonical Wnts, whose function is independent of nuclear ß-catenin (Moon et al., 2004; Veeman et al., 2003a). Canonical and non-canonical Wnt pathways share a set of signaling components (Simons and Mlodzik, 2008) and non-canonical Wnts are often antagonistic to canonical Wnt signaling (Buratovich et al., 2000; Gieseler et al., 1999; Slusarski et al., 1997b; Westfall et al., 2003a), suggesting that different Wnt pathways crosstalk and collectively make a signaling network.

Canonical and non-canonical Wnt pathways

The canonical Wnt pathway, also known as the Wnt/ß-catenin pathway, is triggered by a subset of Wnt ligands including *Drosophila* Wingless (Wg) and the vertebrate Wnt1, Wnt3a and Wnt8 (Dale, 1998). In the absence of Wnt ligands, cytosolic β-catenin is rapidly turned over by a degradation complex containing Axin, the tumor suppressor protein APC and the serine threonine kinase [Glycogen synthase kinase 3β (GSK3β)] (Nelson and Nusse, 2004). GSK3 phosphorylation of β-catenin targets the latter for proteasomal degradation. The interaction of Wnt with the serpentine receptor Frizzled (Fz) and its co-receptors (low-density lipoprotein receptor-related protein) LRP5/6 activates the phosphoprotein Dishevelled (Dvl). The activation of Dvl inhibits the degradation complex by two mechanisms: 1) recruiting the degradation complex to

the membrane, where Axin binds to LRP5/6 and is degraded and 2) inhibiting GSK3, which alleviates the phosphorylation and degradation of β-catenin (Nelson and Nusse, 2004). Stabilized β-catenin protein is accumulated in the nuclei and interacts with the LEF/TCF transcription factors to promote the transcription of downstream genes (Moon et al., 2004) (Figure 1 A). Multiple lines of evidence support the notion that canonical Wnt signaling is the determining factor in dorsal-ventral patterning of early embryos: nuclear β-catenin is found in the future dorsal side of blastula, overexpression of canonical Wnt ligands leads to dorsalization of the embryos with ectopic axes, and negative regulation of canonical Wnt signaling, such as overexpressing the Wnt inhibitor Dkk, often results in ventralization of the embryos (Schier and Talbot, 2005).

In addition to β-catenin-dependent function, Fz homologs also mediate β-catenin-independent activities, such as the establishment of cell polarity, axon guidance and cell movements. It appears that all these activities require a similar set of factors with the Dvl protein as an essential component (Gao and Chen, 2010). Depending on the most prominent cellular/molecular response in a given context, different terms have been applied to Fz-mediated non-canonical Wnt signaling, among which are the Wnt/planar cell polarity (PCP), the Wnt/Calcium (Ca^{2+}), and the Wnt/JNK pathways (Kohn and Moon, 2005). Nevertheless, these pathways exhibit substantial overlap and likely comprise a complicated yet unified signaling network (Figure 1 A).

The Wnt/PCP pathway was first described in *Drosophila* and the term PCP refers to the epithelial cell polarity on the plane perpendicular to apical-basal axis. Such planar polarity is characterized by the asymmetric distribution of the “core PCP components”, which include Fz, Dvl, Strabismus, Prickle and Diego. Briefly, Fz/Dvl proteins and Strabismus/Prickle proteins are located to the opposite side of individual epithelial planes (Zallen, 2007). It is noteworthy that, 1) Wnt ligands do not present directional information to Fz for cell polarity, as *Drosophila* PCP appears to be independent of Wnt (Lawrence et al., 2002) and ubiquitous/non-directional expression of exogenous *wnt11*

rescues *wnt11* mutant in zebrafish (Ulrich et al., 2003), and 2) the Fz/PCP system is not the only mechanism underlying planar cell polarity, as genetics studies showed that an independent Fat/Dachsous system act in parallel with the Fz/PCP systems in *Drosophila* (Lawrence et al., 2007). Indeed, a recent report demonstrated that the final orientation of planar cell polarity in *Drosophila* wing cells is largely driven by anisotropic mechanical stress and Dachsous-mediated tissue re-modeling (Aigouy et al., 2010).

Fz receptors are structurally similar to members of the G-protein coupled receptors (GPCR) superfamily. Studies have shown that non-canonical Wnts (Wnt5, Wnt4 and Wnt11), components of the Wnt/PCP including Fz, Prickle and Dvl, and Regulator of G protein signaling 3 (RGS3) modulate Ca^{2+} dynamics in zebrafish (Freisinger et al., 2010; Sheldahl et al., 2003; Slusarski et al., 1997a; Veeman et al., 2003b). Zebrafish *wnt5b/pipetail* (*ppt*) genetic mutants display reduced Ca^{2+} release (Westfall et al., 2003a) as well as cell movement defects (Hammerschmidt et al., 1996; Rauch et al., 1997a).

Another function of non-canonical Wnt signaling involves the regulation of actin cytoskeleton by small GTPases Rho and Rac. An actin re-modeling complex consisting of Dishevelled-associated activator of morphogenesis 1 (DAAM1), Dvl and Rho, activates the regulation of Rho-associated protein kinase 1 (ROCK1) to modify cytoskeleton. Alternatively, the Dvl-DAAM1-Rho complex leads to JUN N-terminal kinase (JNK)-mediated actin remodeling, which is also regulated by a Dvl–Rac complex (Angers and Moon, 2009). Wnt11, Fz7, Dvl and RhoA are colocalized in cell-cell interface during contact inhibition of locomotion (Carmona-Fontaine et al., 2008).

In vertebrate embryonic development, gastrulation is characterized by directional cell migration toward the midline, resulting in the narrowing/lengthening of tissues known as convergent extension (CE) (Solnica-Krezel, 2005). β-catenin independent, or non-canonical, Wnt signaling is pivotal in vertebrate CE, as loss-of-function of components in non-canonical Wnt often results in CE defects (Rohde and Heisenberg,

2007).

Diversity of Wnt receptors

Although whether a particular Wnt protein belongs to the canonical type or β-catenin independent/non-canonical type can be tested by functional assays, this usual classification is not determined by distinctive sequence or structural motifs shared by individual members of the Wnt protein family. The discrepancy between seemingly similar signaling initiators (namely, the Wnt ligands) and diverse functional outputs has spurred thoughts on how a particular Wnt signaling output is determined and why canonical and non-canonical Wnt signaling pathways are antagonistic.

A logical proposition is that the presence of particular receptors, as opposed to the type of Wnt ligands, dictates the signaling output. Supporting this hypothesis, purified Wnt5a inhibits Wnt3a–induced canonical Wnt signaling through Ror2 receptor, but also activates β-catenin signaling when Frizzled4 is present (Mikels and Nusse, 2006). However, earlier experiments demonstrated that overexpressing different classes of Wnt ligands in the same receptor context led to distinct or even opposite signaling outputs in multiple systems (Kohn and Moon, 2005). For example, while canonical Wnts induce dorsalization of early *Xenopus* embryos and transformation of C57MG mammary epithelial cells, Wnt4, Wnt5A, and Wnt11 do not exhibit the same effect (Du et al., 1995; Wong et al., 1994), but antagonize canonical Wnts in ectopic axis formation (Gieseler et al., 1999; Torres et al., 1996). Therefore, the identity of Wnt ligands plays a role in signaling decision, and the specificity of ligand-receptor interaction cannot be neglected.

Another possibility is that canonical and non-canonical Wnts compete for the same receptors. It has been demonstrated that Fz2 mediates both Wnt5a-induced non-canonical signaling and Wnt3a-induced canonical signaling; Wnt5a seems to compete with Wnt3a for Fz2 and inhibit Wnt3a-dependent β-catenin accumulation in cultured cells (Sato et al., 2010). However, ligand competition alone does not explain why the

same receptor, Fz2, mediates both canonical and non-canonical pathways. In fact, Wnt5a-specific receptors Ror1 or Ror2 are required for inhibition of Wnt3a-induced canonical signaling in these experiments (Mikels and Nusse, 2006; Sato et al., 2010). It is also noteworthy that the Wnt co-receptors LRP5/6 are specific to canonical Wnts (He et al., 2004) and a possible co-receptor specific to non-canonical Wnt signaling, Knypek (Kny), has also been identified (Topczewski et al., 2001). Therefore, the diversity of different Wnt receptors and co-receptors as well as their interaction can potentially generate significant complexity which may underlie distinct Wnt signaling outputs.

In addition to Frizzled, membrane receptors ROR homologs and Ryk homologs have been shown to transduce Wnt signaling (Angers and Moon, 2009; Zhang et al., 2004) (Figure 1B). Both Ror-type and Ryk-type receptors are evolutionarily conserved, perhaps as conserved as the Frizzled receptors. The extracellular portion of most Ror homologs possesses repetitive extracellular immunoglobulin-like (Ig) domains, a Frizzled-like cystine-rich domain (CRD), and a Kringle domain, which is missing in human Musk homolog (Angers and Moon, 2009; Zhang et al., 2004). The extracellular portion of Ryk homologs possessed a Wnt-inhibitory factor (WIF) domain, which is also present in the secreted Wnt antagonist WIF (Kroiher et al., 2001). Although Ror-type and Ryk-type receptors vary in their extracellular domains, they share several interesting features: both are structurally similar to receptor tyrosine kinase (RTK) in the intracellular domain, function in a tyrosine kinase activity independent manner, and, homologs of both types of receptors are found to regulate neuronal migration and vulval patterning in worms (Angers and Moon, 2009; Green et al., 2008; Inoue et al., 2004; Zhang et al., 2004).

Discovered in a screen for genes upregulated by LIM1 in *Xenopus* animal caps (Hikasa et al., 2002), Ror2 was identified as a Wnt receptor. Overexpression of Ror2 inhibits CE movements in *Xenopus*, reminiscent of gene knockdown of non-canonical Wnt using antisense morpholino oligonucleotides. Misexpression of two different Ror2

mutants, a kinase domain point mutant or kinase domain deletion, are equally potent in inducing the CE defects, implying that the kinase activity of *Xenopus* Ror2 may not be essential (Hikasa et al., 2002). Wnt5A is likely to be the primary ligand for Ror2. First, Ror2 knock-out mice showed similar phenotype to *Wnt5a* mutant (Oishi et al., 1999). Second, Wnt5A binds to Ror2 *in vitro* (Mikels and Nusse, 2006; Oishi et al., 2003). Third, Wnt5A and Ror2 activate JUN N-terminal kinase (JNK) to regulate PAPC in *Xenopus* CE (Schambony et al., 2003). It has been proposed that Ror2 mediates antagonism of canonical Wnt signaling by Wnt5A (Mikels and Nusse, 2006). This was demonstrated by experiments showing that Wnt5A negatively regulates Wnt3A-stimulated β-catenin signaling in human HEK293 cells expressing Ror2, but lacks similar activity in mouse L cell line, which expresses significantly lower level of Ror2 (Mikels and Nusse, 2006).

Many properties of Ror2 in *Xenopus* and cultured cells are recapitulated by its homologs in other systems. In *C. elegans*, interaction between a Ror2 homolog CAM-1 and a Wnt ligand EGL-20 orients the polarity of the P7.p cell, in the direction opposite to that predisposed by Wnt/Fz signaling (Green et al., 2008). Interestingly, a truncated CAM-1 lacking the intracellular domain fully rescues HSN cell migration defects in cam-1 mutants, suggesting that the kinase activity of CAM-1 is not essential for this particular process (Forrester et al., 2004). Zebrafish *unplugged* gene encodes a muscle-specific Ror2 homolog that functions in axonal pathway choice (Zhang et al., 2004). It was revealed that Wnt11r signals the unplugged/MuSK Receptor to determine the organization of the central muscle zone where acetylcholine receptors are clustered (Jing et al., 2009). Expressing a dominant negative form of Dvl (XDsh–DEP+), which specifically blocks non-canonical Wnt signaling, disrupts such patterning, indicating that the Wnt/MuSK pathway is non-canonical in nature (Jing et al., 2009).

Ryk homologs represent another type of Wnt receptors. The *Drosophila* Ryk homolog, *derailed,* is known to regulate mid-line crossing of the axons in commissural

neurons (Callahan et al., 1996). Another *Drosophila* Ryk homolog, *doughnut*, is expressed and functions in invaginating cells during embryogenesis (Savant-Bhonsale et al., 1999). The interaction between Wnt5a and Derailed was first identified in a genetic screen for genes suppressing Derailed misexpression phenotypes (Yoshikawa et al., 2001). Later experiments in other systems confirmed that Wnt ligands bind Ryk *in vivo* and *in vitro* (Keeble et al., 2006; Kim et al., 2008; Lin et al., 2010; Liu et al., 2005). Ryk protein consists of an extracellular domain similar to Wif and an intracellular domain highly similar to that of RTKs. Interestingly, the kinase domain in Ryk is predicted to be kinase inactive (Hovens et al., 1992), indicating that Ryk may not function as a typical RTK. However, overexpression of a truncated Ryk lacking the C-terminal domain does not lead to ectopic routing of commissural axons (Wouda et al., 2008).

The exact mechanism by which Ryk transduces Wnt signals is not clear. Diverse molecular events downstream of Ryk have been reported, including heterodimerization with other RTKs (Halford et al., 2000), Src kinase activation (Wouda et al., 2008), Fz binding (Kim et al., 2008; Lu et al., 2004) and additionally, Wnt induces the nuclear translocation of the Ryk intracellular domain (ICD) to promote neuronal differentiation (Lyu et al., 2008). It is also unknown whether the Ryk-mediated pathway is related to the Fz-mediated pathway or not. In *Drosophila*, the Wnt5A-Derailed pathway seems to be independent of Fz-mediated pathways; instead, Derailed undergoes phosphorylation, recruits and activates Src kinase (Wouda et al., 2008). During vulval cell patterning in *C. elegans*, a Wnt ligand MOM-2 activates the Ryk homolog LIN-18 to signal a pathway separate from Fz homolog LIN-17 mediated pathways (Inoue et al., 2004). In contrast, experiments using HEK293T cells showed that Wnt1, Ryk and Frizzled form a ternary complex (Lu et al., 2004). Overexpressed DVL and RYK interact with each other using the PDZ domain of Dvl and the C-terminal tail of RYK; RYK is required for Wnt3a-mediated canonical Wnt signaling (Lu et al., 2004). Vertebrate Ryk proteins are constitutively cleaved by γ-secretase at a position close to the transmembrane domain

(Lin et al., 2010; Lyu et al., 2008). A recent study reported that Wnt3a simulates the cleaved Ryk product to enter the nucleus and function as a transcriptional factor during neuronal differentiation; importantly, this function of Ryk is independent of Fz (Lyu et al., 2008). Studies conducted in different systems suggest that the exact pathway that Ryk participates in may depend upon a given context.

Calcium (Ca^{2+}) dynamics and the crosstalk of Wnt pathways

Competition between canonical and non-canonical Wnts for the same receptors has been proposed as a mechanism for the antagonism of β-catenin signaling by non-canonical pathways (Sato et al., 2010). However, strong genetic and biochemical experiments have shown that intracellular calcium signaling as a result of non-canonical Wnt signaling antagonizes nuclear localization of β-catenin and expression of β-catenin target genes (Schneider et al., 2008; Westfall et al., 2003a; Westfall et al., 2003b). Mounting evidence suggests calcium dynamics as an important mechanism regulating crosstalk of Wnt pathways.

In zebrafish, overexpression of Wnt5 leads to increases in the frequency, as well as the amplitude, of intracellular Ca^{2+} release events in a pertussis toxin sensitive manner, indicating that G-protein signaling is involved (Slusarski et al., 1997a; Slusarski et al., 1997b). Moreover, use of inhibitors identified a requirement for the phosphatidylinositol cycle in calcium release (Schneider et al., 2008; Westfall et al., 2003b). Activation of calcium release and inhibition of PI cycle have opposing impact on nuclear localization of β-catenin and downstream canonical Wnt signaling (Westfall et al., 2003b). Thus, both canonical Wnt signaling, mediated by nuclear β-catenin, and non-canonical Wnt signaling, mediated by intracellular Ca^{2+} release, are subjected to regulation by inositol 1,4,5-trisphosphate (IP3)-dependent Ca^{2+} release and a hypothesis that Wnt/Ca^{2+} signaling mediates the crosstalk of canonical and non-canonical Wnt pathways, resulting in a complex yet unified Wnt signaling network, has been proposed (Freisinger et al.,

2008a).

In *Xenopus* and zebrafish embryos, overexpression of non-canonical Wnts antagonizes β-catenin signaling, as ectopic axis formation induced by canonical Wnt ligands, e.g. Wnt8, can be suppressed when Wnt5 is co-expressed (Moon et al., 1993; Slusarski et al., 1997b). Stimulating Ca^{2+} release, via G-protein signaling through exogenous serotonin receptor and its agonist 5HT, also antagonizes Wnt8-induced expansion of dorsal domains (Slusarski et al., 1997b), indicating that the Wnt5 mediates antagonism of β-catenin signaling by modulating intracellular Ca^{2+} release. Consistently, attenuation of the Wnt/Ca^{2+} signaling by pharmacological or genetic approaches in zebrafish embryos and mouse limb buds results in ectopic accumulation of nuclear β-catenin and its transcriptional targets (Topol et al., 2003b; Westfall et al., 2003a; Westfall et al., 2003b). It was also reported that inhibition of G-protein function dorsalizes *Xenopus* embryos (Kume et al., 2000).

In non-excitable cells, IP3-sensitive Ca^{2+} channels mediate a majority of intracellular Ca^{2+} release from the endoplasmic reticulum (ER) membrane (Berridge et al., 2003). Two predominant receptor classes, the G-protein coupled receptor (GPCR) and the receptor tyrosine kinase (RTK) have been shown to activate the PI cycle in response to a variety of secreted proteins. GPCR-activated signaling pathways are mediated by four sub-classes of G-proteins: Gαs, Gαi, Gαo, Gαq/11, and Gα12/13. The Gαq/11 pathway activates phospholipase C-β (PLCβ), which catalyzes proteolytic cleavage of the membrane bound phosphatidylinositol (4,5)-biphosphate (PIP2) into inositol (1,4,5) triphosphate (IP3) and diacylglycerol (DAG). IP3 receptors located on the ER trigger the release of Ca^{2+}, and DAG stimulates protein kinase C (PKC) on the plasma membrane. PKC can also be activated by intracellular Ca^{2+} (Wettschureck and Offermanns, 2005). Activation of RTKs by ligands leads to dimerization of the receptors on the membrane and subsequent autophosphorylation of tyrosine residues in the intracellular domain. Once phosphorylated, the receptors can activate Src homology 2

(SH2) and phosphotyrosine binding (PTB) domain containing proteins, including phospholipase Cγ (PLCγ) (Pawson, 1995). PLCγ, like PLCβ, mediates cleavage of PIP2 and the release of IP3 to stimulate intracellular Ca^{2+} release events (Berridge, 1993).

Model system and tools

Zebrafish (*Danio rerio*)

We used the zebrafish, *Danio rerio*, as primary model for this study. Zebrafish is a tropical freshwater fish originating from the Ganges River in the Indian subcontinent. It commonly inhabits streams, canals, ditches, ponds, and slow-flowing water bodies (Spence et al., 2008). Fecundity, small size (4-6 cm), external fertilization, transparency and quick development make zebrafish an ideal model system to study vertebrate development. Zebrafish reach breeding age within 3-4 months and individual mature females produce hundreds of eggs in a single cross. Fertilized zebrafish eggs develop rapidly and remain transparent for 24 hours post fertilization, making easy optical observation of internal organs possible (Kimmel et al., 1995). Additionally, genetic, embryonic, and physiological research tools have been advanced in past years. Furthermore, the zebrafish research community enjoys a high-level of resource sharing in recent years.

Forward and reverse genetics

Zebrafish belongs to the minnow family (*Cyprinidae*) of order *Cypriniformes*. The zebrafish genome contains 25 chromosomes of ~1.7 billion base-pairs (bp) and mitochondrial DNA of 16,596 bp (Broughton et al., 2001). The ninth assembly of the zebrafish genome (Zv9) by Sanger Institute comprises a total sequence length of 1.4 Gb in 4,560 scaffolds. The zebrafish genome underwent whole-genome-duplication events after the divergence of ray-finned fishes and lobe-finned fishes (Hoegg et al., 2004). Despite complications of the zebrafish genome, a number of commercial microarrays and

ChIP-on-chip are available for gene expression and promoter regulation studies, respectively.

Forward genetic and pharmacological screening for disease and development related traits in zebrafish have yielded valuable genetic knowledge for many years. Early chemical mutagenesis screens of different scales have identified mutations affecting many aspects of embryonic development (Baier et al., 1996; Malicki et al., 1996; Mullins et al., 1996; Solnica-Krezel et al., 1996; Whitfield et al., 1996). Notably, two large-scale screens revealed nearly ~2000 mutations affecting zebrafish development in 1996 (Driever et al., 1996; Haffter et al., 1996). In addition, transgenesis and retroviral-based mutagenesis are also available to generate zebrafish mutants (Amsterdam et al., 1999; Long et al., 1997). The zebrafish genetic mutants used in this thesis study are *wnt5b/pipetail* and *wnt11/silberblick.*

A common reverse genetic technique in zebrafish research is Morpholino antisense technology (Heasman, 2002). Morpholino oligonucleotides (MO) are stable, synthetic oligos that contain the same bases as DNA. MO reduces gene expression by binding to complementary RNA sequences to either block ribosomal entry or alter splicing, a process known as “knock-down”. MO diffuses between blastomeres when injected in embryos younger than 32-cells, as large molecules can shuffle between cells (Kimmel and Law, 1985a, b). When injected into individual cell of an embryo after the 32-cell stage, MO only affects the injected cells and their descendants. *In vitro* transcribed RNAs and circular DNAs are commonly used in rescue assays to verify the specificity of MO. RNAs and DNAs are generally less diffusible than MOs. Injecting RNAs at one-cell stage results in uniform expression at later stages. RNA expression from pCS2+ vector normally peaks at ~12hpf (measured by fluorescent intensity from injecting EGFP-coding RNA). Exogenous gene expression from DNA injections often shows a high degree of mosaic expression.

Transgenesis has become a popular approach since the introduction of the Tol2

transposon system in zebrafish (Kawakami et al., 2004). Isolated as an autonomous transposon from the medaka fish, Tol2 element encodes a transposase that catalyzes transposition of transposons, which contain DNA inserts as large as 11 kilobases and flanking sequences composed of terminal inverted repeats and subterminal sequences (Kawakami et al., 2004). A tool kit utilizing multi-site gateway cloning and common fluorescent tags has been developed to facilitate the generation of transgenic zebrafish (Kwan et al., 2007). High transgenesis efficiency in somatic cells allows for transient transgenic studies in injected embryos (Kwan et al., 2007).

In addition, the amenable traits of the zebrafish allow the integration of genetic, pharmaceutical tools and *in vivo* physiological analysis by Fura-2 calcium imaging. Biochemical assays have also been gradually optimized for zebrafish embryos.

Mosaic analysis and cultures

Mosaic analysis in zebrafish is particularly useful in studying cell-cell interaction, distinguishing cell autonomous and non-autonomous effects and parsing tissue-specific properties. The most commonly used technique in generating mosaic zebrafish is cell-transplantation. Typically, donor cells are grafted from 1000-cell to sphere-stage embryos when the differentiation of the donor cells are generally considered marginal, and transplanted into a host embryo at the same stage. The fate of the donor cells is usually determined by the transplant location in host embryos. Xenografting, heterografting, homografting, and allografting are all possible using zebrafish embryos.

Another method takes advantage of mosaic injection. Antisense oligos and/or *in vitro* transcribed RNAs can be injected into individual blastomeres to generate mosaic embryos. MOs are generally more diffusible than protein-coding RNAs and should be injected in embryos older than 32-cells to prevent its diffusion into other cells (Kimmel and Law, 1985a, b). Injecting MOs and/or RNAs into the yolk at late-blastrula stage targets the yolk syncytial layer (YSL) and dorsal forerunner cells (DFC) (Amack and

Yost, 2004). DNA injection which results in random mosaic expression even when performed at one-cell stage, although less commonly used, can also generate mosaic embryos. Other methods to create mosaic embryos including using RNAs containing both protein-coding sequences and 3'UTRs with strong RNA-localization signals, and introducing transgenes driven by tissue-specific promoter and/or enhancers.

Zebrafish tissues and cells can be cultured *in vitro*. Cells from adult fish can be isolated to make primary culture under generic procedure for other model systems. Due to the heterogeneity and tendency to undergo rapid differentiation in embryonic cells, it is less common to culture embryonic cells. An exception is the application of temporary culture of induced mesodermal cells. Primary zebrafish mesodermal cell cultures were obtained by injecting 1-cell stage embryos with *cyclops* mRNA to force mesendodermal differentiation and enzymatically disassociated at dome stage (Montero et al., 2003).

We and other groups have utilized zebrafish explant cultures to study cell-cell interaction. In the original design, two pieces of "animal-caps" were dissected from 1000-cell stage embryos, and juxtaposed in culture medium; after a period of time, interactions between cells from each animal-cap led to changes in cell distribution and the extent of intermingling of cells (Mellitzer et al., 1999). In this study, we experimented with explant cultures using normal and prolonged culture conditions to investigate repulsive cell migration (Lin et al., 2010) and vessel routing.

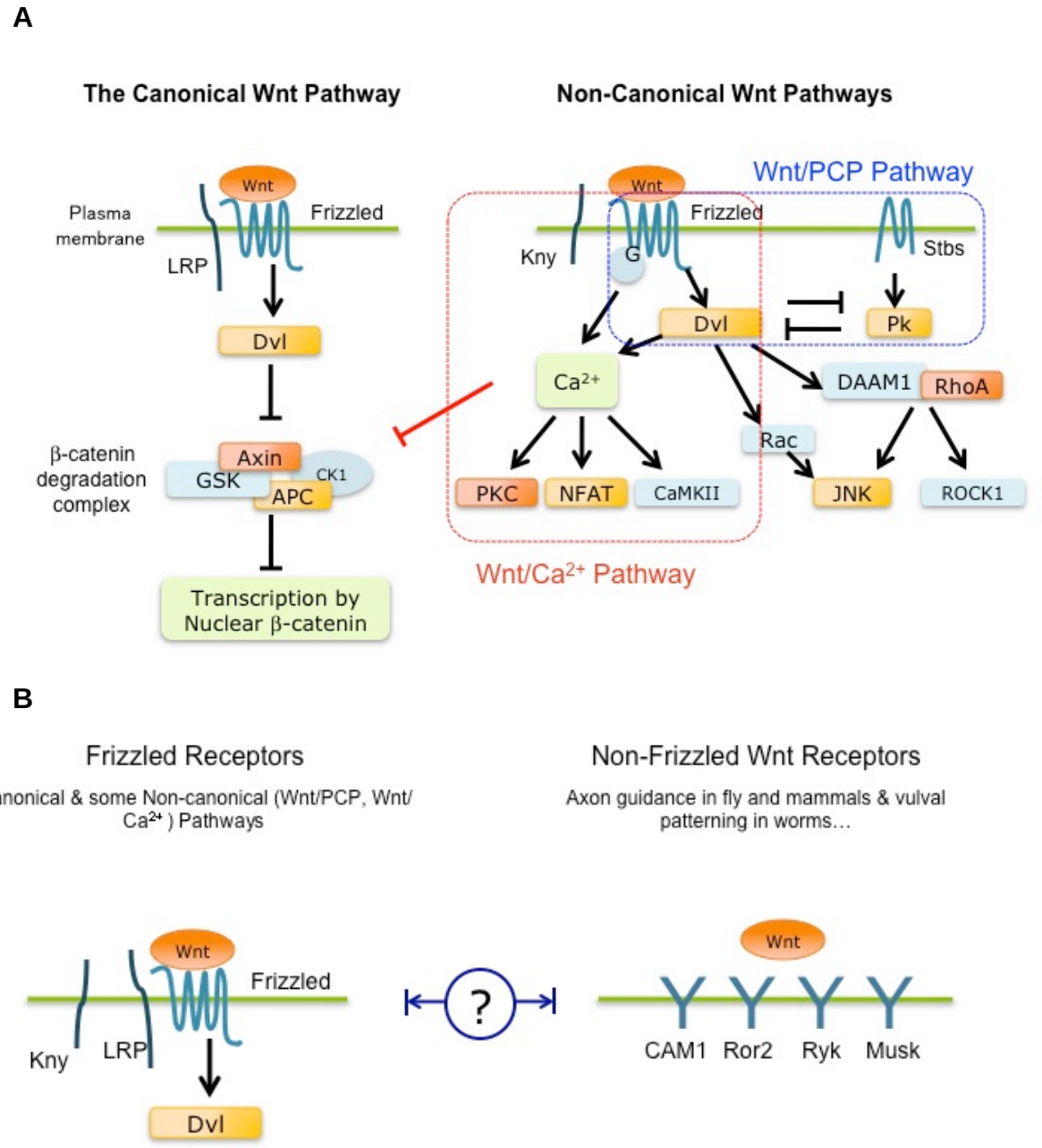

Figure 1: A schematic of the Wnt signaling network. (A) Frizzled-mediated Wnt pathways with β-catenin-dependent components to the left side and β-catenin-independent pathways to the right side. (B) Comparison of Fz and non-Fz Wnt receptors.

CHAPTER II
TRANSCRIPTIONAL REGULATION OF WNT5 HOMOLOGS IN ZEBRAFISH

Introduction

Wnt5 homologs have been implicated in fundamental developmental processes as well as various diseases, notably cancers (Chien et al., 2009; Lai et al., 2009; Moon et al., 2004). In contrast to most other Wnt ligands, whose functions are in conformity to the usual classification of canonical and non-canonical Wnt signaling, Wnt5 homologs are involved in all known Wnt-induced pathways (Angers and Moon, 2009). The diversity of Wnt5 stimulated signaling processes are partially due to the variety of Wnt5-interacting membrane receptors. Conversely, Wnt5-interacting receptors are potentially responsive to other Wnt homologs. A particular signaling direction is determined by the presence of specific receptors, as well as the presence of the Wnt5 ligands. We reason that the spatial, temporal and quantitative expression of Wnt5 homologs is under strict regulation, as ectopic signaling pathways can be triggered due to Wnt5's diverse signaling potential. Supporting this hypothesis, we and other groups found that zygotic loss of *wnt5b/pipetail* couldn't be rescued by exogenous *wnt5b* RNA injection at one-cell stage, which is in contrast to the *wnt11/silberblick* mutants that are rescued by *wnt11* RNA injection (Kilian et al., 2003; Westfall et al., 2003a). To elucidate the intricacy of Wnt5 expression during development, we cloned and analyzed zebrafish *wnt5* homologs in embryonic development, and studied subfunctionalization of vertebrate *wnt5* homologs from an evolutionary and comparative development perspective. We further integrated *in silico* and *in vivo* methods to identify *cis*-regulatory elements that modulate embryonic expression pattern of zebrafish and mammalian *wnt5* homologs.

Embryonic expression profiles of zebrafish *wnt5a* and *wnt5b* genes

Identification of alternative promoters of *wnt5b*

There are two *wnt5* homologs, *wnt5a* (chromosome 8) and *wnt5b* (chromosome 4) genes, in the zebrafish genome (Ensembl, Zv9). By 5'RACE, we also identified two transcripts from the *wnt5b* locus (Figure 2 A). We termed the transcript that is previously known and whose transcription start site is further away from coding sequence (CDS) *wnt5b.1*, and the transcript whose transcription start site is closer to the CDS *wnt5b.2*. The *wnt5b.1* transcript encodes a protein of 363 amino acids, and *wnt5b.2* encodes a protein with additional 17 amino acids at the N-terminal signaling peptide, assuming that the first AUG codon in the longest open-reading frame encodes for the initiation methionine for both transcripts (Figure 2 B). Zebrafish Wnt5b.1, Wnt5b.2 and Wnt5a share a high-degree of sequence similarity (Figure 2 B).

To validate the *wnt5b.2* promoter, we introduced Tol2-flanking transgenes into zebrafish embryos to access the capacity of putative *wnt5b.2* promoter to drive EGFP expression. We cloned a ~1.2 kb sequence upstream to *wnt5b.2* transcription start site, and then ligated the forward and reverse strand to the N-terminus of EGFP in the transgene vector, respectively. We found that the transient transgene with forward strand, but not the reverse strand, of *wnt5b.2* promoter drives the EGFP expression (Figure 2 C). Therefore *wnt5b.2* promoter region demonstrates orientation-specific ability in driving gene expression.

Spatial and temporal expression of *wnt5* transcripts

By semi-quantitative RT-PCR, we found that *wnt5a* is maternally expressed. Zygotic *wnt5a* is not expressed immediately after mid-blastrula transition (MBT) at 4phf; low expression levels of *wnt5a* can be detected at 6hpf; and the expression level gradually increases from 6hpf to 26hpf. *wnt5b.2* is not maternally expressed (at 1hpf), its zygotic expression is initiated immediately after MBT at 4hpf, the expression level

increases at gastrulation stages with the peak expression detected at 12hpf. *wnt5b.1* is both maternally and zygotically expressed. However, the onset of its zygotic expression trails that of *wnt5b.2* (Figure 3 A).

By whole-mount *in situ* hybridization, we found that *wnt5a* expression is not prominent during gastrulation stage. However, high level of *wnt5a* is found in the brain at 48hpf. The similarity between *wnt5b.1*, and *wnt5b.2* implies lack of specificity of riboprobes targeting individual transcripts. We therefore used a generic *wnt5b* riboprobe that corresponds to shared sequence of *wnt5b.1*, and *wnt5b.2* and detects both transcripts. Similar to previously reported *wnt5b* expression (Hammerschmidt et al., 1996; Rauch et al., 1997a), we found that *wnt5b* shows characteristic expression at the tail-bud and fin-bud regions (Figure 3 B), as is expected for vertebrate genomic regulatory blocks that encompass neighboring genes (Kikuta et al., 2007).

Phylogenetic and syntenic analysis of vertebrate *wnt5* homologs

The zebrafish *pipetail* gene has long been misannotated as a *wnt5a* homolog. Others and we showed that the *pipetail* gene encodes a protein that clusters with Wnt5b proteins from other species and a second Wnt5 homolog in zebrafish clusters with Wnt5a proteins (Stoick-Cooper et al., 2007) (Figure 4 A). Moreover, syntenic analysis on *wnt5* gene clusters reveals that the *pipetail* gene is a bona-fide *wnt5b* homolog (Figure 4 B and C). *wnt5a* homologs belong to a syntenic group composed of *erc2*, *wnt5a*, *lrtm1* and *cacna2d3* (Figure 4 B). This syntenic group is also accompanied by a proximal syntenic group marked by *selk* and *actr8*, and a distal syntenic group marked by *creld1* and *brpf1*, in the same chromosome (Figure 4 B). The syntenic group to which *wnt5b/pipetail* belongs is highly conserved in all the species we analyzed including zebrafish (Figure 4 C). This syntenic group contains *ERC1*, *WNT5B*, *FBXL14*, and *ADIPOR2*. Interestingly, *FBXL14* gene, which is transcribed in the opposite direction to that of *WNT5B*, is often

located between alternative transcription start sites of *WNT5B* gene (data not shown). Zebrafish *fbxl14* does not show an expression pattern similar to *wnt5b/pipetail* (data not shown), raising the possibility that the *fbxl14* locus may function as an insulator, separating alternative *wnt5b/pipetail* promoters.

Identification of *cis*-regulatory sequences regulating *wnt5a* and *wnt5b* expression

In silico screening of putative *wnt5* enhancers

Sequence conservation among *cis*-regulatory sequences has been shown to be an efficient and reliable method to predict enhancers (Pennacchio et al., 2006). However, functionally conserved enhancers often show poor sequence conservation in distantly-related species (Fisher et al., 2006). A previous study demonstrated that enhancers driving similar expression pattern of the *RET* gene show sequence similarity between closely-related species, such as human vs. mouse and zebrafish vs. fugu, but not between human and zebrafish (Fisher et al., 2006).

To facilitate the process of enhancer prediction, we separately aligned sequences from *tetrapoda* species and *teleostei* species, and then determined the conservation of enhancers identified in these two lineages by syntenic information (Figure 5 A). Dog, horse, mouse, rat and chicken sequences were aligned to human sequence to identify putative enhancers in the *tetrapoda* lineage. Fugu, medaka, and stickleback sequences were aligned to zebrafish sequence to identify putative enhancers in the *teleostei* lineage. We also found that syntenic enhancers often drive similar expression pattern (Figure 5 B and C).

Validation of *wnt5* enhancers by transgenic assays

We utilized a transgenesis-based enhancer reporting system to validate predicted enhancers in zebrafish (Fisher et al., 2006). Briefly, Tol2-flanking transgenes containing

the putative enhancer, c-fos minimal promoter and EGFP were introduced into zebrafish embryos at one-cell stage to generate transient-transgenic zebrafish. The expression pattern of EGFP was evaluated in embryos at 24hpf. Subsets of injected embryos were raised and crossed to wild-type zebrafish to identify germ-line transmission and establish permanent transgenic lines.

We identified multiple conserved *cis*-regulatory elements from human, mouse and zebrafish *wnt5* loci that drive tissue-specific expression similar to that of endogenous *wnt5* homologs (Figure 6 and Table 1). Various conserved *cis*-regulatory elements are shown to drive EGFP expression in tail, forebrain, and heart ventricle in an orientation-independent manner (Table 1). Notably, an enhancer sequence (hwnt5A-1 / h5A) derived from human genome that drives tail expression is a subset of a previously identified enhancer (WNT5A-ERC2) that drives a similar expression pattern in both transgenic mouse (Pennacchio et al., 2006) and zebrafish (Figure 6).

Subfunctionalization of *wnt5a* and *wnt5b* in zebrafish

Different roles of zygotic *wnt5a* and *wnt5b* in tail patterning

Mammalian *Wnt5A* and *Wnt5B* are expressed in similar domains (Summerhurst et al., 2008), and *Wnt5A* and *Wnt5B* individual knockouts created similar embryonic lethal defects in mice, notably reduced tail and limb extension (Agalliu et al., 2009; Yamaguchi et al., 1999). Zebrafish *wnt5b/pipetail* plays important roles in ventral–posterior patterning (Rauch et al., 1997b). Zygotic loss of *wnt5b* causes severe defects in tail extension, which earned the *wnt5b* mutant name *pipetail*. Expression pattern and function of *wnt5b* is conserved in vertebrates, as the *pipetail* phenotype is consistent with that of *Wnt5B* knock-out mice (Agalliu et al., 2009). In contrast, zebrafish *wnt5a* is not strongly expressed in tailbud region where *wnt5b/pipetail* is highly enriched (Figure 3 B). We characterized the expression profile of zebrafish *wnt5a* by semi-quantitative RT-PCR

and whole-mount *in situ* hybridization, and found that although zebrafish *wnt5a* is both maternally and zygotically expressed. In contrast to *wnt5b*, *wnt5a* expression levels are relatively low and not strongly associated with gastrulation (Figure 3).

We further explored the function of zebrafish *wnt5a* in ventral-posterior patterning. We used a combination of high-dose translational-blocking and splicing-blocking *wnt5a* MOs (10 pmol each) to knock down *wnt5a* function (Figure 7). At moderate dose (5 pmol each), *wnt5a* translational-blocker MO is sufficient to eliminate the expression of an EGFP construct with the MO-targeting sequence conjugated to the N-terminus of EGFP (Figure 7 B); *wnt5a* splicing-blocker MO is sufficient to eliminate the normal-size *wnt5a* mRNA and results in an RNA product with targeted intron included (Figure 7 B), which leads to frame-shifting and emergence of premature STOP codon in the aberrant RNA product (data not shown). Although *wnt5b* knock-down embryos display severe defects in ventral-posterior patterning, *wnt5a* knock-down embryos show normal tail extension resembling uninjected control embryos (Figure 7 A). These observations indicate that *wnt5b* encodes the predominant Wnt5 protein during ventral-posterior patterning, while *wnt5a*'s function is dispensable in this process during the gastrulation stage.

A hypothesis of species-specific evolution of *wnt5* homologs

Although zebrafish-specific loss of tail expression of *wnt5a* is not a result of gene order changes in the *wnt5a* syntenic cluster (Figure 8 A), loss of *cis*-regulatory elements such as promoters and enhancers may impact the expression of *wnt5a* gene. We hypothesize that loss of enhancer elements in zebrafish *wnt5a* locus, rather than changes of transcription factors, eliminates its expression in the developing tail.

A human *WNT5A* enhancer that drives tail expression in transgenic zebrafish (Figure 6, hwnt5A-1) is conserved in tetrapods. Its syntenic *cis*-regulatory element sequence is conserved among stickleback, fugu, and puffer fish, but not zebrafish (Figure

8 B). It is noticeable that this *cis*-regulatory sequence in zebrafish-excluded teleost species is similarly or even more conserved than the downstream *wnt5a* coding exons. In contrast, zebrafish *wnt5a* coding exons shows significant sequence conservation with stickleback *wnt5a*; but the upstream non-coding sequence shows poor conservation with corresponding region in stickleback, suggesting that the lack of conservation is unlikely due to further evolution distance between zebrafish and other teleosts (Figure 8 B). Therefore we speculated that the upstream *cis*-regulatory element responsible for *wnt5a* tail expression is not present in zebrafish genome.

Preliminary results and future directions

Although zebrafish *wnt5a* is not expressed in developing tail like other vertebrate *wnt5a* homologs, *WNT5A* enhancer from human genome still drives gene expression in the tail region. This phenomenon suggests that the transcriptional machinery driving the tail expression of vertebrate *wnt5a* is still present in zebrafish. And the fact that tail expression of zebrafish *wnt5b* compensates the loss of *wnt5a* in this area indicates that the same transcriptional machinery might drive tail expression of both *wnt5a* and *wnt5b* in vertebrates. Based on this assumption, we reasoned that the same type of transcription factor binding sites is present in both *wnt5a* and *wnt5b* enhancers originated from different species.

To identify transcription factors activating tissue-specific expression of *wnt5*, we analyzed functionally tested enhancer sequences in our transgenics studies. We utilized the rVISTA tools, as well as TRANSFAC public database of transcription factor binding matrices, to deduce candidate transcription factors responsible for activating *wnt5* expression in specific tissues. We scored the frequency of individual transcription factor binding sites in multiple enhancers driving the same expression pattern, and generated a list of possible transcription factors and the tissue where they drive gene expression. Our preliminary results suggest that *cdx1a* might be responsible for the tail expression of

Wnt5 homologs. Injecting *cdx1a* RNA into the hwnt5A-1 transient transgenic line increased EGFP expression at epiboly stages compared to control injection (Figure 8 C). We are currently in the process of verifying these results by quantitative RT-PCR and chromatin-IP.

Materials and methods

Zebrafish Husbandry

Zebrafish were maintained in a 14-hour light /10-hour dark cycle at 28°C. Embryos were collected from natural pairwise matings and staged by both hours post fertilization (hpf) at 28.5ºC and by using morphological criteria described in Kimmel et al. (Kimmel, Ballard et al. 1995). Collection of embryos was carried out as described by Westerfield (Westerfield 1995). Animal welfare assurance number: A3021-01.

Whole-mout *in situ* hybridization

Embryos were dechorionated and fixed overnight in 4% paraformaldehyde. Whole-mount *in situ* hybridization (WMISH) was performed as previously described (Thisse et al., 1993; Westfall et al., 2003a), using both digoxigenen-labeled antisense RNA probes and digoxigenen-labeled sense RNA probes (controls). Detection was carried out using BM purple (Roche Applied Science) and the reaction was stopped in phosphate-buffered saline (PBS). Embryos were mounted and photographed using a Zeiss Stemi M13 Stereoscope using Axiocam digital camera.

Sequence analysis

Genomic and protein sequences were retrieved from Ensembl (http://www.ensembl.org), NCBI Gene (http://www.ncbi.nlm.nih.gov/gene) and UCSC genome browser (http://genome.ucsc.edu/). Gene annotations were according to the Ensembl known transcripts database and compiled in the VISTA format. Comparative

genomics studies were performed using both UCSC genome browser's features and mVISTA (http://genome.lbl.gov/vista/) with LAGAN alignment algorithm (RankVISTA probability threshold set at 0.5). ClustalW alignment was performed to derive an unrooted phylogenetic tree for protein sequences and Primer3 program was used to design primers.

5' rapid amplification of cDNA ends (RACE)

Total RNAs from zebrafish embryos were isolated using TRIzol (Invitrogen, Carlsbad, Calif.). Single-strand cDNAs was synthesized with reverse-transcriptase. cDNA was processed by incorporating a SMART oligo (BD SMART RACE cDNA amplification Kit) at the 5' end and using CDS III–modified oligo-dT, according to the instructions of the manufacturer. PCRs were performed with a forward primer 5' RACE, 5'-CTAATACGACTCACTATAGGGCAAGCAGTGGTATCAACGCAGAGT-3' and corresponding 3' primers. Gel-purified PCR bands were subjected to automated DNA sequencing.

Microinjections

Zebrafish embryos were microinjected with a pressure injector (Harvard apparatus) with approximately 3 nanoliter volumes at the 1-cell stage. Embryos were placed into an injection dish coated with 1.5% agarose layers. Small depressions were formed by 1 mm capillaries and covered with egg water. The needle was positioned to penetrate the chorion, then gently inserted through the yolk into the blastodisc. Injection cartridge was injected with air pressure. The needle was then slowly withdrawn using forceps to support the embryo.

Transgenesis

Transgenic lines were generated by injecting a mixture of transposase RNA at 25ng/μL and plasmid DNA at 25ng/μL in a volume of ~5nL. Injection cartridge was

delivered to the cell body of one-cell stage embryos. Putative enhancer sequences were amplified from zebrafish genomic DNA by PCR and flanked by attL1 and attL2 sites by TA-cloning with pCR8/GW/TOPO vector (Invitrogen). The resulting entry clone was combined with the pT2cfosGW destination clone (Fisher et al., 2006) by LR-recombination reaction. Plasmid DNAs were purified by the "DNA clean and concentrator" kit (Zymo Research). We generally did not observe orientation-specific effects of enhancer elements (sense and anti-sense strand of the enhancer elements drive the same expression pattern).

Discussion

Spatial and temporal control of ligand expression is important for the regulation of signaling events. Here, we integrated *in silico* and *in vivo* methods to identify *cis*-regulatory elements that modulate embryonic expression pattern of zebrafish *wnt5b*. We characterized *cis*-elements that drive tissue-specific expression of Wnt5 homologs. The identification of multiple *cis*-elements revealed an unexpected level of intricacy of temporal and spatial control of *wnt5* expression.

We provided detailed analysis of the syntenic relationship between the coding sequence of zebrafish *wnt5a* and *wnt5b*, as well as *cis*-elements encompassing the coding area. We further characterized the expression profiles of zebrafish *wnt5a* and *wnt5b*. Together, these data suggest the *cis*-elements regulating *wnt5* loci undergo rapid evolution, which results in species-specific changes of the expression profiles.

In addition, we demonstrated an example in which syntenic information can be integrated into conserved transcription factor binding sites search. The method we developed, which utilized functionally verified sequences from multiple species, showed potential to extend to broader application that might greatly reduces false-positive hits in searching for conserved transcription factor binding sites.

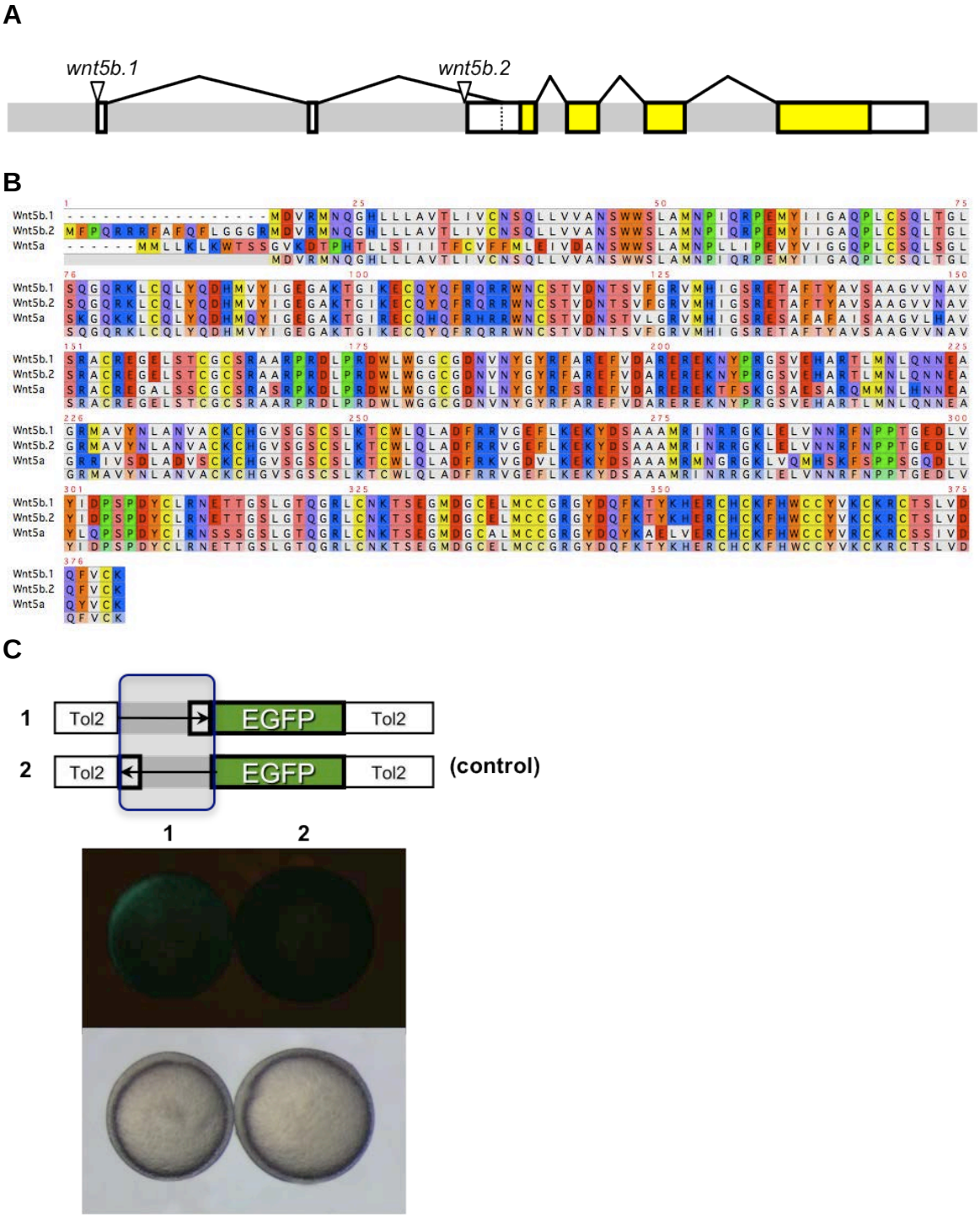

Figure 2: Zebrafish *wnt5a*, *wnt5b.1*, and *wnt5b.2*. (A) Transcripts of *wnt5b.1*, and *wnt5b.2* in the *wnt5b* locus. Transcription start sites noted by triangles; Coding sequence for mature Wnt5b protein in yellow. (B) Alignment of zebrafish Wnt5b.1, Wnt5b.2, and Wnt5a protein sequences. (C) *wnt5b.2* promoter region demonstrates orientation-specific ability in driving downstream EGFP expression.

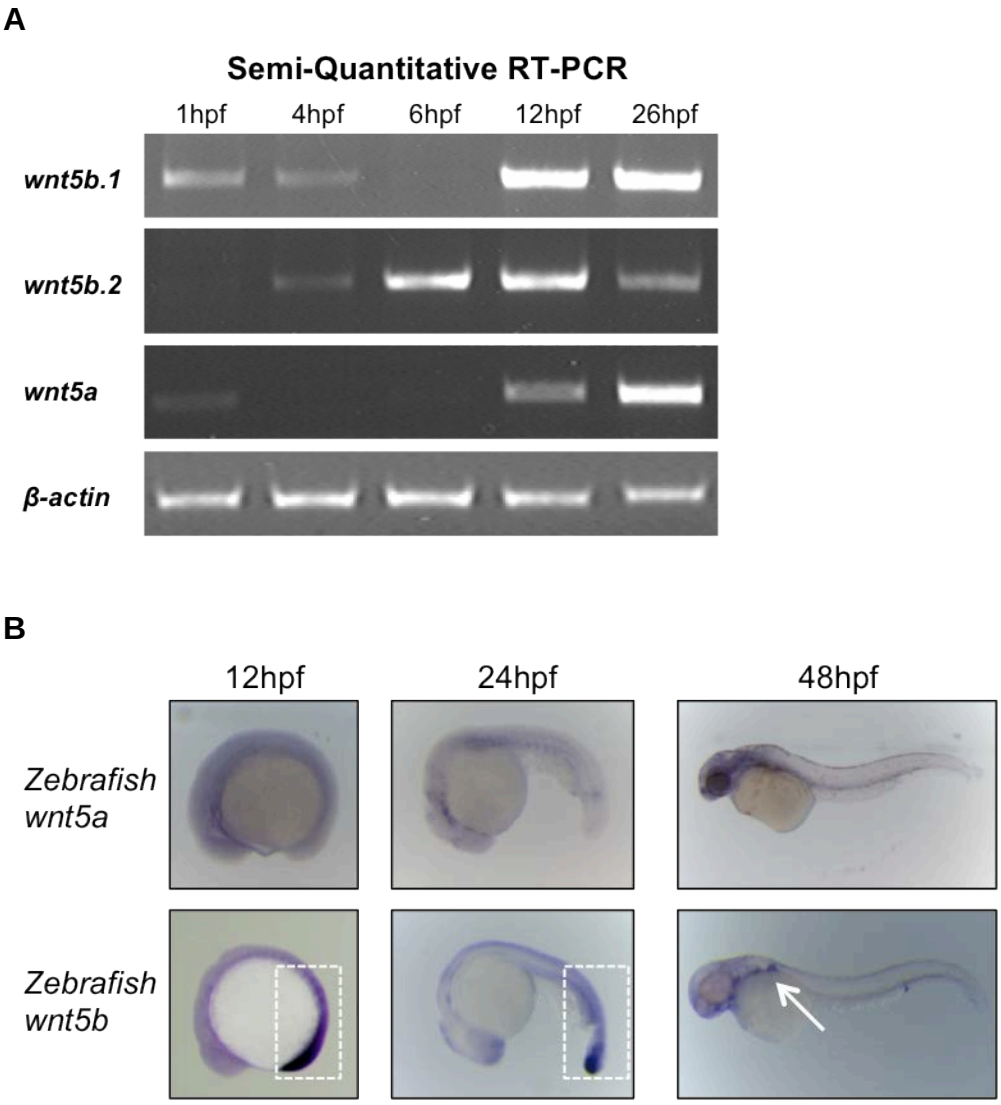

Figure 3: Expression profiles of zebrafish *wnt5a*, *wnt5b.1*, and *wnt5b.2*. (A) Semi-quantitative RT-PCR showing expression of *wnt5a*, *wnt5b.1*, and *wnt5b.2* with β-actin as loading control. (B) Whole-mount *in situ* hybridization reveals low expression level of *wnt5a* prior to 24hpf and enrichment in brain at 48hpf; in contrast, *wnt5b* shows characteristic expression at the tail-bud (box) and fin-buds (arrow). Stages and orientation: dorsal to the up and anterior to the left.

A

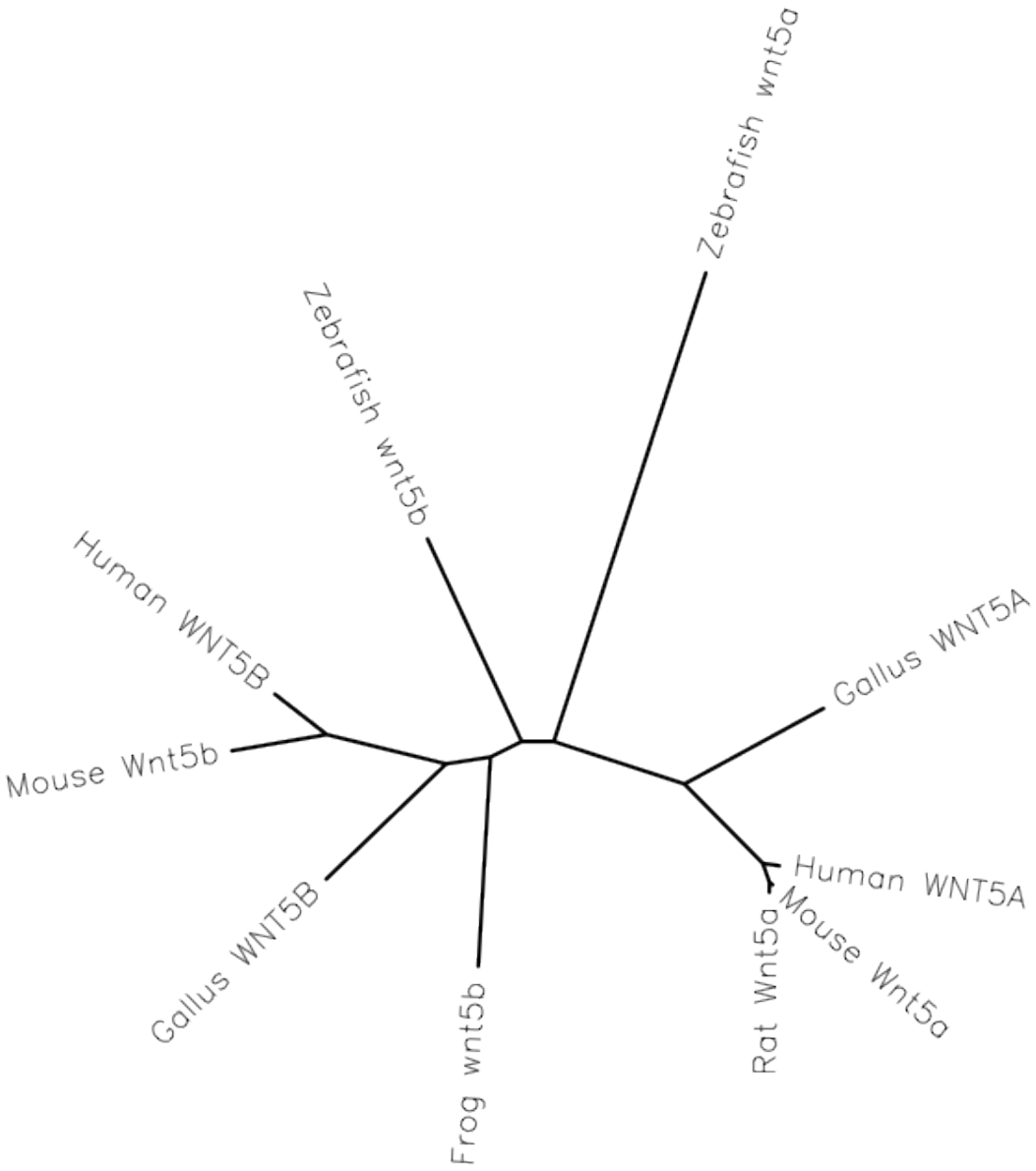

Figure 4: Phylogenetic and syntenic analysis of *wnt5* homologs. (A) Unrooted phylogenetic tree for Wnt5 proteins generated by ClustalW shows that zebrafish Wnt5a and Wnt5b cluster with respective homologs in vertebrate. (B) The *wnt5a* syntenic group (Zv8). A distal syntenic group composed of *selk* and *actr8*, and a proximal syntenic group composed of *creld1* and *brpf1* on the same chromosome, are also shown. (C) The *wnt5b* syntenic group (Zv8).

Figure 4 continued

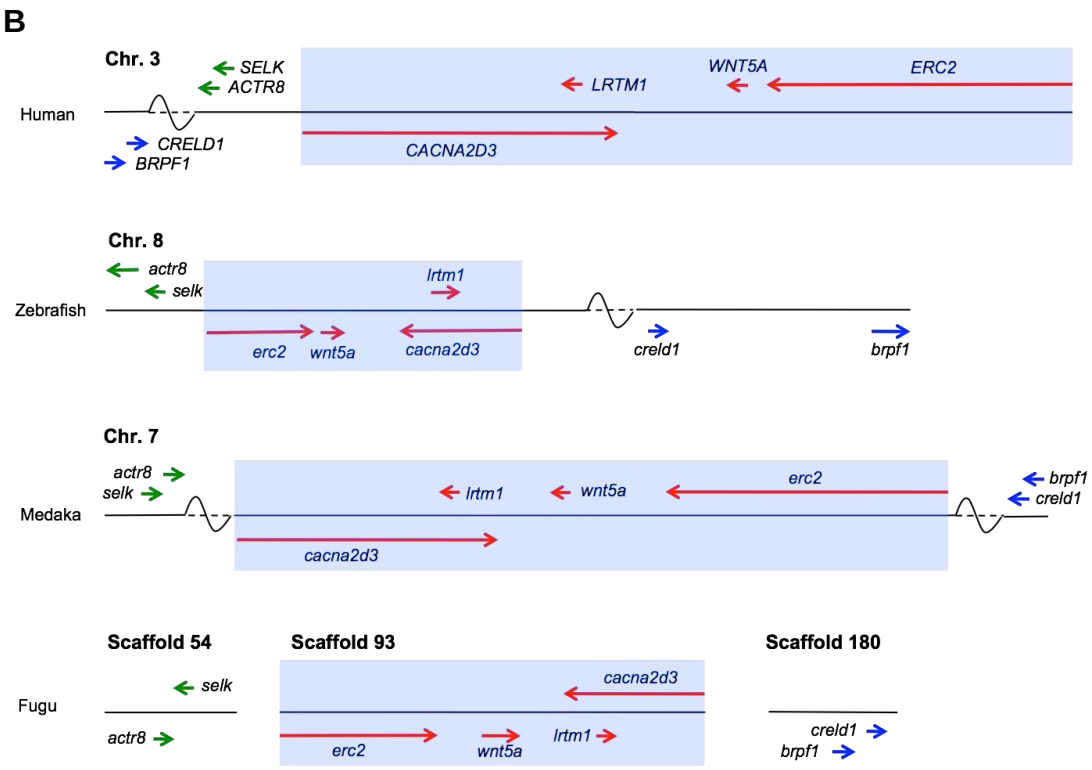

Figure 4 continued

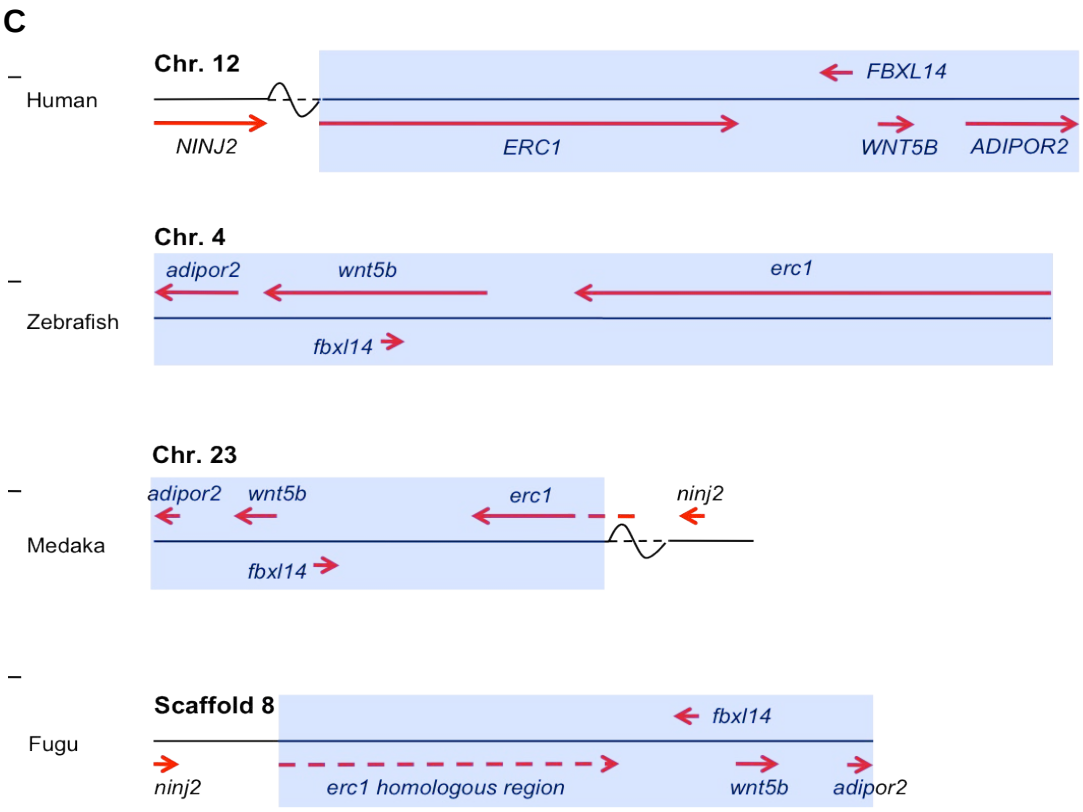

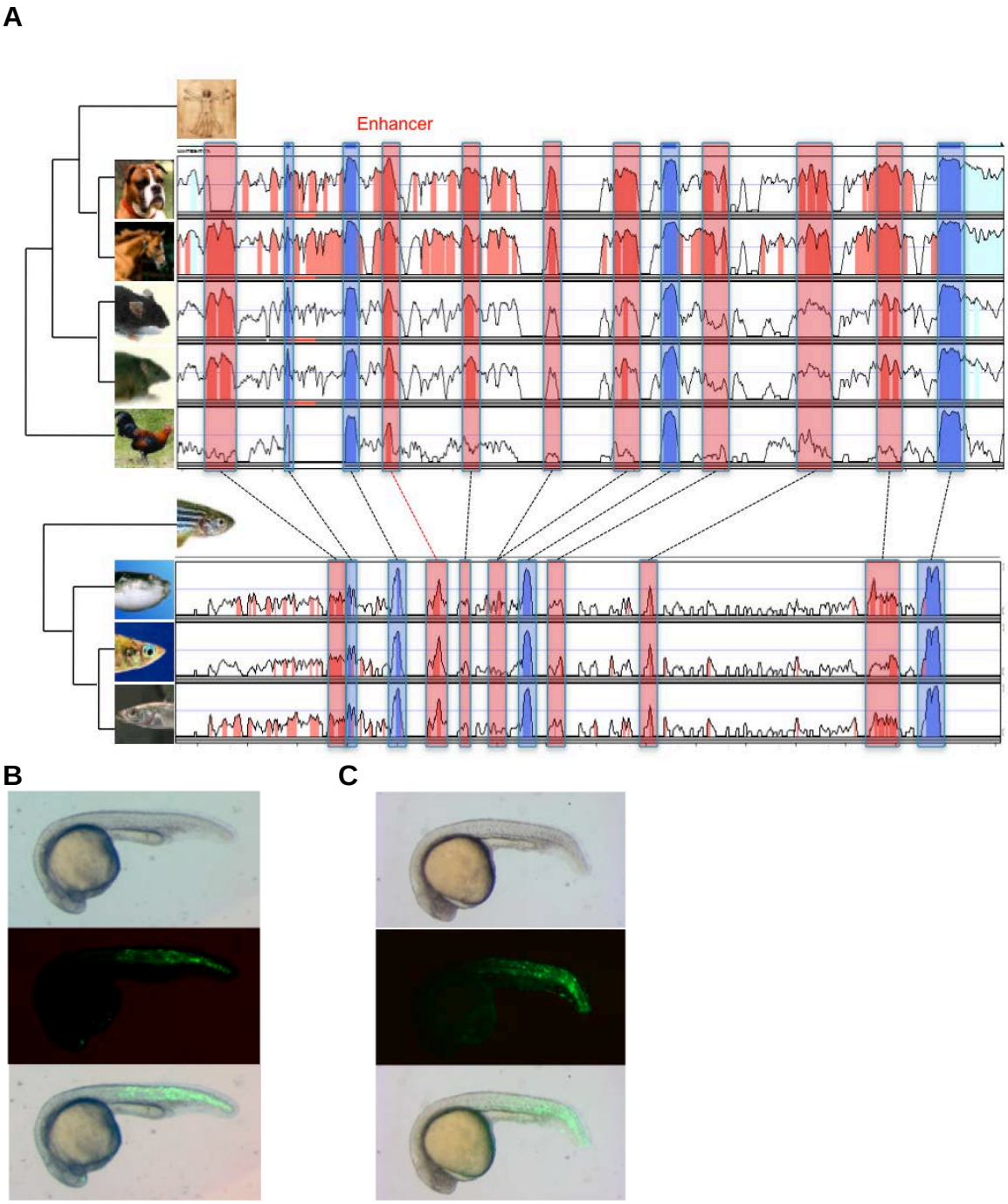

Figure 5: Synteny of conserved *cis*-regulatory elements in the *wnt5b* locus. (A) Multi-alignment of *wnt5b* genomic DNA in *tetrapoda* and *teleostei* lineages. Protein-coding exons are in blue and non-coding conserved regions are in red. Syntenic regions between *tetrapoda* (Top to down: dog, horse, mouse, rat, and chick aligned to human) and *teleostei* (Top to down: Fugu, Medaka, and stickback aligned to zebrafish) are connected by dashed lines. (B-C) Syntenic *cis*-regulatory elements in *tetrapoda* (B) and *teleostei* (C) drive similar expression pattern. 24hpf embryos shown with dorsal to the up and anterior to the left.

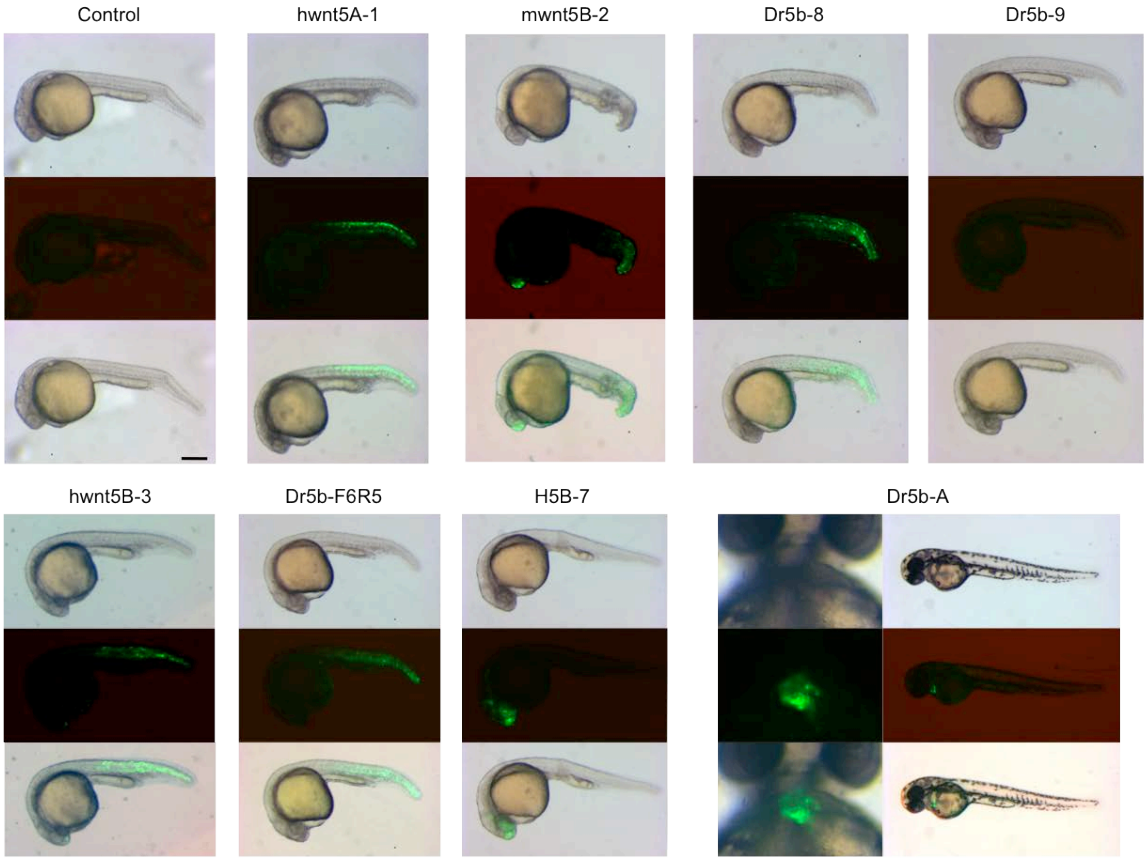

Figure 6: Conserved *cis*-regulatory elements from human, mouse and zebrafish genome drive tissue-specific expression shown by multiple transgenic lines.

Line	Origin	Primer 1	Primer 2	Ori.[#]	n	G	Expression
WNT5A-ERC2 *	*human WNT5A*	ACAACAGCAG CAAGCAGAAA	GCCACAAAGC ACCATTGACT	+: L -: T	4	-11312 ~ -9595	Tail; Adult caudal fin
LRTM1-WNT5A*	*human WNT5A*	TAGTTTCCCTG AGGCCAAGA	TGACACACTTC CAACCTTAGAC A	+: T -: T		+496387 ~ +497472	YSL; Random
hwnt5A-1 / h5A	*human WNT5A*	TCATGTTCGAC AGACCTCCA	AGTGGCAGCA CAAAGAGATG	-: L	2	-11052 ~ -10397	Tail
mwnt5B-2 / m5B	*mouse Wnt5b*	ACACCAGGCA GTATGGCTTC	CACAAACACCA GCAGACACA	+: L	3	-5536 ~ -3542	Forebrain; Tail tip
mwnt5B-1	*mouse Wnt5b*	CCTTGAACCTT CTCTTGGCA	GAATCTTTAAA GGCTGGCCC	N		-20504 ~ -19023	
Ze5b1	*zebrafish wnt5b*	AACCCAGCAG TTCCATGTTC	CCTGAGCTTTA GCCAGGTTG	N		-4184 ~ -2892	
Ze5b2	*zebrafish wnt5b*	GCTGCAGACA TAAACAGCCA	GAACATGGAA CTGCTGGGTT	+: T		-2911 ~ -956	YSL; Random
Ze5b3+4	*zebrafish wnt5b*	CAGGGTAAATA GGCACGTCG	CCCTTCGCTGT ACTGGAAAA	+: L	1	-16665 ~ -14577	to be determined
h5b3	*human WNT5B*	GCTTGGGACT CACTGAGAGG	GGGTAGGGAA AGAGGTCTGG	+: L	1	+1795 ~ +2545	Tail
h5b4	*human WNT5B*	TCTTGGCTGTC TCCCAGTCT	AGGATTAGGC ACCAGGCTTT	-: P		+10851 ~ +11912	to be determined
h5b5	*human WNT5B*	TTGAATTCAGG GAAGGATGG	ACACCATCCAT TTGTGAGCA	N		+12530 ~ +13664	
h5b6	*human WNT5B*	TCGATGCTGAA ATGGAATGA	CCCATTAAAGG ACTCCAGCA	N		-51500 ~ -50162	
Ze5b5	*zebrafish wnt5b*	TTGGCAGTTAT ATGGGGAGC	ACAAACGCTTT CTGATTGCC	N		+3103 ~ +4481	
Ze5b6	*zebrafish wnt5b*	AAGACATCGG AACGAATTGC	ACCCACATGC ACTCAAAACA	N		+2560 ~ +4026	
Ze5b7	*zebrafish wnt5b*	TTCAGTTATGG CGTCATGGT	ATCGGTTTAGC CTTGGTGGT	N		+20586 ~ +22071	
Dr5bF6R5 / Ze5bF6R5	*zebrafish wnt5b*	AAGACATCGG AACGAATTGC	ACAAACGCTTT CTGATTGCC	+: L	1	+3103 ~ +4026	Tail
H5B-7	*human WNT5B*	CGTGGACATTT GCTCAGTGT	TGGCCACACA TAACAGCAAT	+: L	2	-51258 ~ -50273	Forebrain
Dr5b-8 / Ze5b8	*zebrafish wnt5b*	CGGTTTCATCA CACCAAAAC	GCTTTCCCACA GAAGACAGC	+: L	2	+3464 ~ +3973	Tail
Dr5b-9 / Ze5b9	*zebrafish wnt5b*	CATGGGATTTT GATCTCTTGG	TGCAGGTACA CACCCGTTTA	-: L	1	+3759 ~ +4734	Not in embryos
Dr5b-A / Ze5b-A	*zebrafish wnt5b*	TTGGCCAAAAT TCAGGATTC	ATCGGTTTAGC CTTGGTGGT	+: L	2	+20586 ~ +21346	Heart ventricle
Dr5b-B / Ze5b-B	*zebrafish wnt5b*	AGGCGTTGGT ATCAAACAGG	CCCCTAAACC CACCCATACT	+: L -: L	1 1	-115032 ~ -114376	Heart ventricle
Fbxl14-M	*zebrafish wnt5b*	GTTTGTTTTCT TGAGCGCGT	CCCCAAGTTTC ACCTCACTT	-: T		-28623 ~ -27385	Not in embryos

#: L: permanent line generated; T: tested in transient transgenic lines; P: plasmid made. N: PCR products not obtained; +: plus strand in the same orientation as the coding sequence; -: minus strand; n: independent lines; G: genomic locus relative to the translational start site A (+1)UG (for zebrafish sequences, *wnt5b.1* was used).

*: Sequences information derived from http://enhancer.lbl.gov/ (Pennacchio et al., 2006)

Table 1. List of transgenic lines with *cis*-regulatory elements driving EGFP expression.

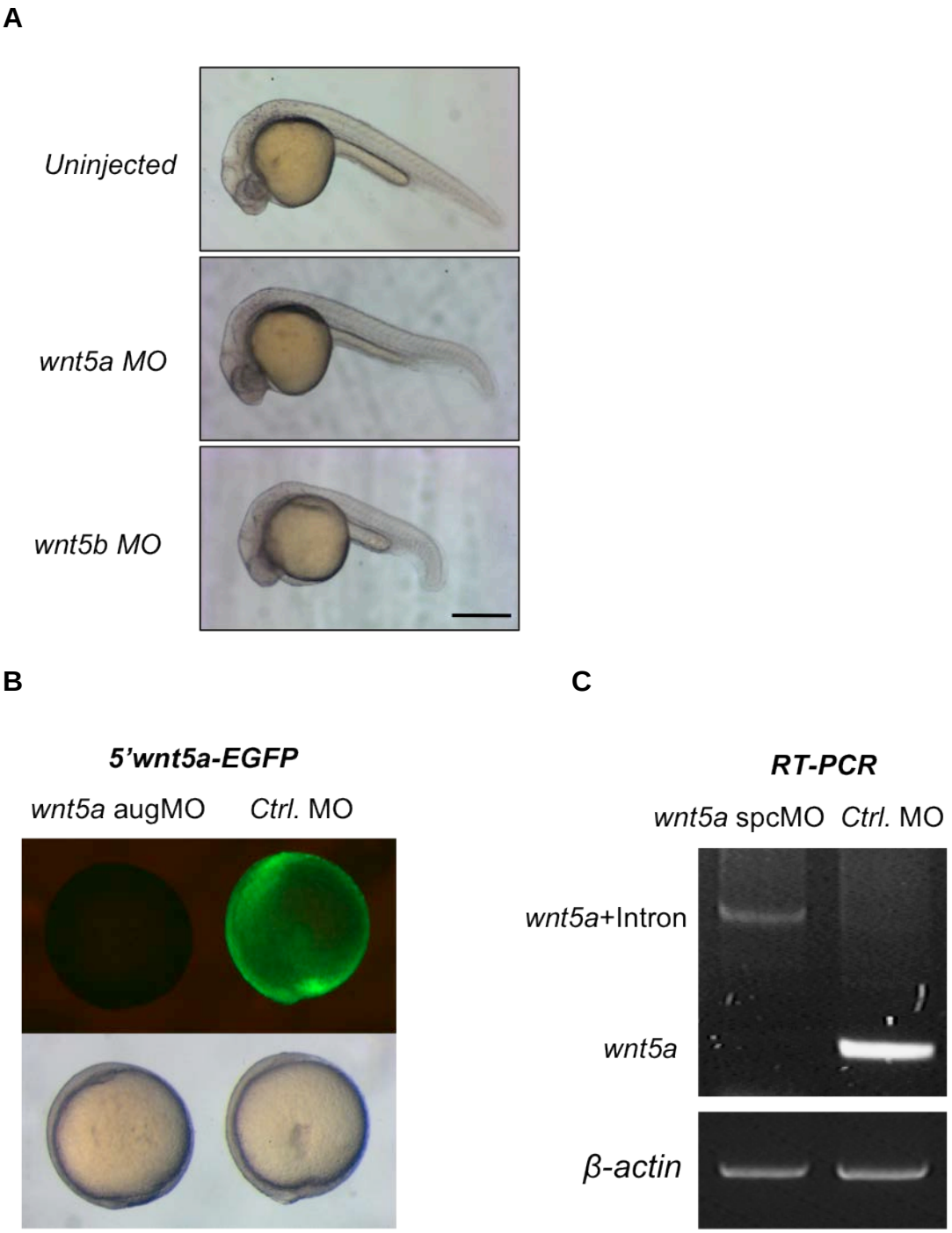

Figure 7: Knock-down of zebrafish *wnt5a*. (A) Gross morphology of *wnt5a* and *wnt5b* knock-down embryos at 24hpf with dorsal to the up and anterior to the left. (B) Translational blocker for *wnt5a* efficiently suppressed the expression of EGFP conjugated with MO targeting sequence in tailbud stage embryos. (C) Splicing MO efficiently eliminated *wnt5a* mRNA, resulting in aberrant RNA products with intron inclusion in 24hpf embryos.

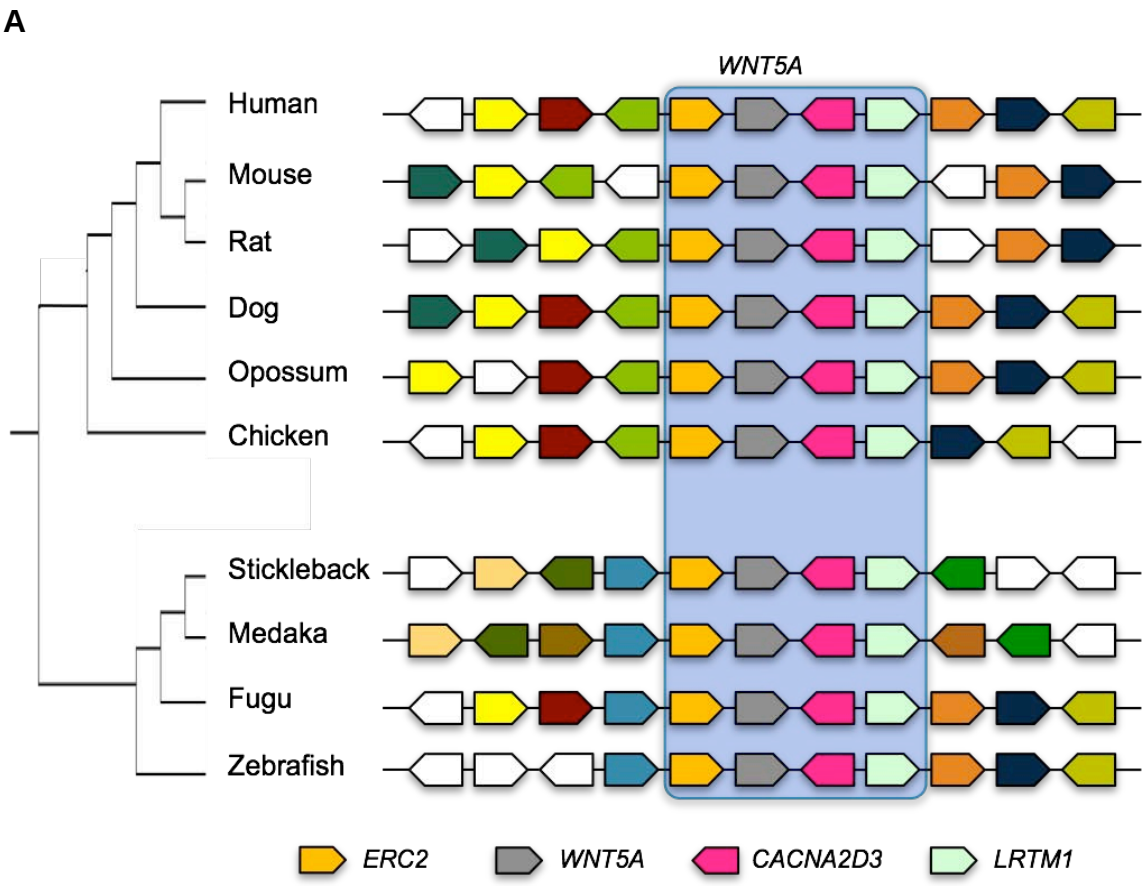

Figure 8: Loss of enhancer driving tail expression in zebrafish *wnt5a* locus. (A) Syntenty of *wnt5a* containing gene clusters in *tetrapoda* and *teleostei*. Pentagons note individual genes and their orientations. (B) The enhancer (hwnt5A-1/h5A) driving caudal *WNT5A* expression is conserved in *tetrapoda*; the syntenic *teleostei* enhancer sequence is conserved in stickleback, fugu, and puffer fish, but not zebrafish. (C) Injecting *cdx1a* RNA increases EGFP expression driven by the hwnt5A-1 enhancer. Arrowhead indicates the EGFP expression domain in control.

Figure 8 continued

B

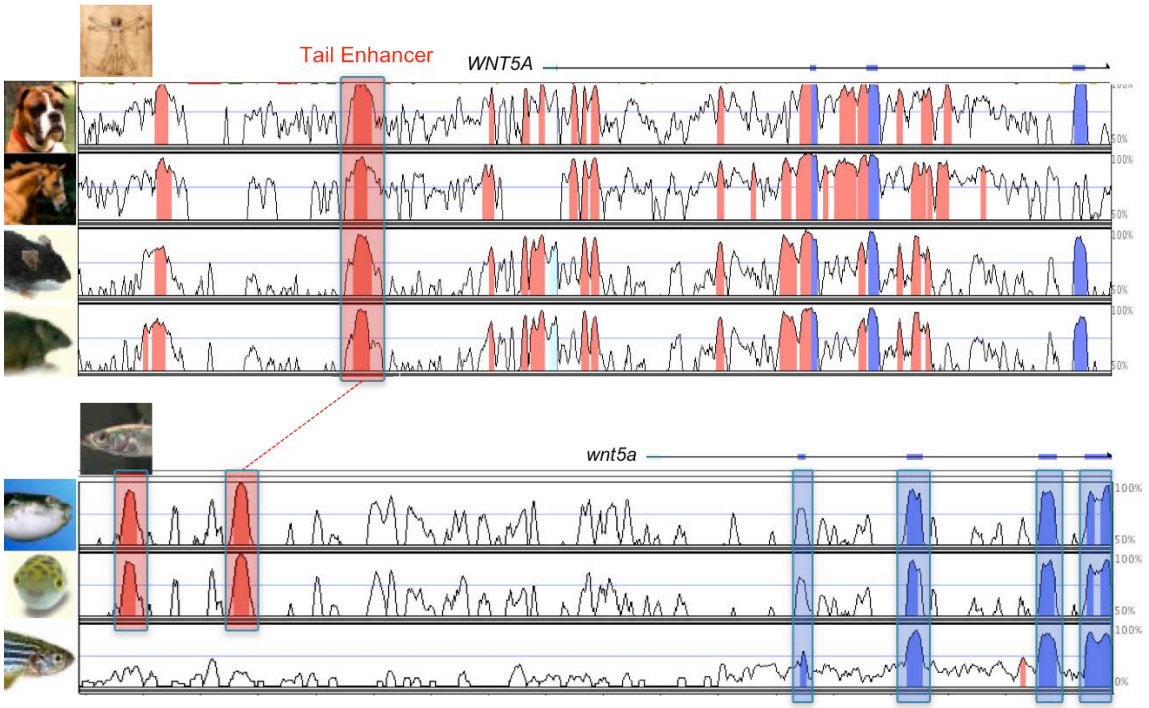

C

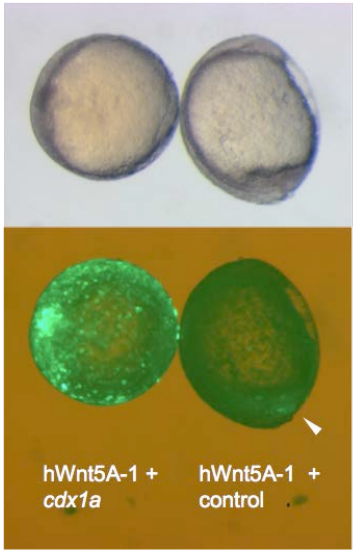

CHAPTER III
WNT5B FUNCTIONS IN EMBRYONIC DEVELOPMENT

Introduction

wnt5b/pipetail plays important roles during embryogenesis. In zebrafish, Wnt5b triggers multiple signaling pathways including the Wnt/Ca^{2+} pathway (Westfall et al., 2003a; Westfall et al., 2003b), Wnt/PCP pathway (Kilian et al., 2003) and Wnt/Ryk pathway (Lin et al., 2010). The molecular signaling processes are implicated in various developmental events: 1) Maternal Wnt5b regulates dorsal-ventral body axis by antagonizing Wnt/β-catenin signaling (Westfall et al., 2003b); 2) Zygotic Wnt5b regulates gastrulation movement and tail extension by both Wnt/PCP and Wnt/Ryk signaling pathways (Kilian et al., 2003; Lin et al., 2010; Rauch et al., 1997b); 3) Wnt5b/PCP pathways regulates endothelial cell differentiation and angiogenesis at multiple locations of the zebrafish embryos (Cirone et al., 2008; Ju et al., 2010).

As discussed above, ligand presentation and receptor selectivity underlie the diversity of Wnt5 signaling. Our discovery that embryonic *wnt5b/pipetail* is present in forms of *wnt5b.1* and *wnt5b.2*, suggests that the functional diversity of *wnt5b/pipetail* can be partially explained by the genetic separation of *wnt5b.1* and *wnt5b.2*. To better understand *wnt5b/pipetail*'s roles in development, we characterized *wnt5b*'s role in three embryonic developmental processes: DV patterning, tail extension and angiogenesis, with special emphasis on the correlation between the expression and function of various *wnt5* transcripts.

Expression of *wnt5b.1* and *wnt5b.2* correlates with functional dichotomy of zebrafish *wnt5b* in early development

Initiation of zygotic *wnt5b.1* and *wnt5b.2* transcription

By 5'RACE, we identified two transcripts from the *wnt5b* locus (Figure 2 A). We termed the shorter and previously known transcript *wnt5b.1*, and the novel transcript *wnt5b.2*. Since they differ in the transcription start site, these two transcripts can be distinguished by RT-PCR using specific primers. We designed a splicing blocker MO (sp MO) targeting an intron donor site shared by *wnt5b.1* and *wnt5b.2*. We reasoned that splicing blockers do not affect maternal mRNAs, and therefore aberrant RNA products resulted from splicing-blocking MO injection, such as intron included RNAs and exon deleted RNAs, must originate from zygotic transcripts. By comparison, RNA products of normal size are originated from maternal transcripts (Figure 9 A). We next injected embryos at one-cell stage with sp MO, collected wild-type and MO injected embryos at key developmental stages to generate cDNAs and then performed RT-PCR with primers specific to *wnt5b.1* and *wnt5b.2* (Figure 9 B). For *wnt5b.1*, PCR products from both wild-type and MO injected embryos were present in normal size prior the 6hpf, suggesting that *wnt5b.1* is maternally expressed; and PCR products resulted from intron inclusion do not appear until 12hpf, suggesting that the zygotic transcription of *wnt5b.1* initiates between 6-12hpf. For *wnt5b.2*, all PCR products from MO injected embryos were present in the form of intron-included bands, suggesting the expression of *wnt5b.2* is strictly zygotic; and all PCR products from both wild-type and MO injected embryos are present in embryos beyond 3.5hpf, suggesting that the zygotic transcription of *wnt5b.2* initiates between 3.5-6hpf.

Specific knockdown of *wnt5b.1* and *wnt5b.2*

RT-PCR results suggest efficient knock-down of both *wnt5b.1* and *wnt5b.2* by the splicing-blocker (sp MO). To study individual function of *wnt5b.1* and *wnt5b.2*, we

designed translational blockers specific to the two transcripts. To validate the potency as well as specificity of *wnt5b.1* MO and *wnt5b.2* MO, we cloned 5' regions of *wnt5b.1* and *wnt5b.2* transcripts containing the MO target sequences, and then conjugate these two sequences to GFP to make the reporter constructs 5'wnt5b.1-GFP and 5'wnt5b.2-GFP. We found that *wnt5b.1* MO injection is sufficient to eliminate the expression of 5'wnt5b.1-GFP, but not 5'wnt5b.2-GFP (Figure 10 A). Conversely, *wnt5b.2* MO injection eliminates the expression of 5'wnt5b.2-GFP, but not 5'wnt5b.1-GFP (Figure 10 B). We concluded that *wnt5b.1* MO and *wnt5b.2* MO are potent and specific to their targets.

Differential contribution of *wnt5 transcripts* to tail extension

We have shown that *wnt5a* knock-down does not lead to defects with regard to embryonic tail extension (Figure 7). To examine roles of *wnt5b.1* and *wnt5b.2* transcripts on tail extension, we performed a series of knock-down and rescue experiments with MOs and *wnt5b* coding RNA. We found that individual knock-down of the *wnt5b.2* transcript resembles the zygotic *pipetail*$^{-/-}$ embryos (Figure 10 C, D and F). Similar to the zygotic mutant, *wnt5b.2* knock-down cannot be suppressed by injecting *wnt5b* RNA (Figure 10 H). In contrast, knockdown of the *wnt5b.1* transcript leads to severely reduced growth of the whole embryos (Figure 10 E). Interestingly, this phenotype can be suppressed by injecting low-dose (5-10 pg) *wnt5b* RNA (Figure 10 G). To rule out that these phenotypes resulted from off-target effects which often lead to apoptosis (Robu et al., 2007), we performed acridine orange (AO) labeling, which marks apoptotic cells in living animals, on knock-down and rescued embryos (Figure 11). We found that distribution of apoptotic cells are similar in *wnt5b.2* knock-down and zygotic *pipetail* embryos, characterized by dense concentration in forebrain and developing tail. *wnt5b.1* knock-down embryos rescued by RNA injection show similar apoptosis pattern to uninjected wild-type controls. By contrast, *wnt5b.1* knock-down embryos possess

markedly increased apoptotic cells compared to the control. We concluded that *wnt5b.2* is the predominant transcript regulating developing tail extension.

Differential contribution of *wnt5* transcripts to DV axis

It has been reported that maternal loss of *wnt5b* function leads to dorsalization of embryos, as a result of lacking antagonism to canonical Wnt signaling (Westfall et al., 2003a; Westfall et al., 2003b). However, it is unknown which *wnt5* transcript(s) contribute to the establishment of DV axis. Based on the expression profile of *wnt5a*, *wnt5b.1* and *wnt5b.2* (Figure 3 A), we predicted that maternally expressed *wnt5b.1* is the predominant transcript during early DV patterning. To test this hypothesis, we examined subcellular localization of β-catenin, as well as the expression of nuclear β-catenin target gene *bozozok*, in *wnt5b.1* knock-down embryos. We found ectopic cytosolic and nuclear β-catenin at the animal pole of in *wnt5b.1* MO injected embryos at 3.5hpf (Figure 12 A, arrowheads), compared to uninjected wild-type control. Whole mount *in situ* hybridization to detect *bozozok* in embryos at 4hpf demonstrates the typical dorsal domain of *bozozok* expression in uninjected wild-type controls and *wnt5b.2* knock-down embryos (Figure 12 B, brackets). Ectopic *bozozok* expression was observed in *wnt5b.1* MO injected embryos (Figure 12 B, arrowheads). Consistently, injection of *wnt5b.1* MO, but not *wnt5b.2* MO, depresses intracellular Ca^{2+} release events in zebrafish embryos at 3-4hpf (data not shown).

A role of Wnt5b/PCP pathway in angiogenesis

Characterization of vascular defects in *wnt5b/pipetail*

Perturbation of PCP signaling disrupts endothelial polarity, growth, migration and network formation in cell culture assays. To study the effect of PCP inhibition on *in vivo* angiogenesis, we characterized vascular defects in *wnt5b* deficient embryos.

A transgenic zebrafish line expressing the Fli1-promoter (endothelial cell specific) driven GFP strain [Tg(fli:EGFP)] (Lawson and Weinstein, 2002) was crossed into the *wnt5b* mutant, *pipetail* genetic background. Homozygous *pipetail* embryos display shortened body length with head cartilage and tail defects (Rauch et al., 1997b). Wildtype-like (*wnt5b*$^{+/-}$ or *wnt5b*$^{+/+}$) Tg(fli:EGFP) animals displayed ordered angiogenesis throughout the animal including formation of well defined intersegmental (IS) vessels (Figure 13 A and E, arrows), a robust meshwork of the dorsal aorta (DA) and posterior cardinal vein (PCV) (Figure 13 A and E) in the trunk (Isogai et al., 2001). *wnt5b/pipetail* mutants displayed loss or disorganization of IS vessels (Figure 13 B and F, arrows), reduced DA and PCV (Figure 13 B, arrowhead) as well as a shortened yolk extension. In addition, *pipetail* animals showed a disruption of the dorsal vasculature including the Duct of Cuvier (DC), which will become the future common cardinal vein (CCV) (Figure 13 C and D). The vascular defects are not due to developmental delay as the defect persists through 48 hpf (Figure 13 E and F) and is consistent with the endothelial migration defects caused by diminished PCP regulation. We therefore conclude that the coordination of vascular networks has been compromised in this mutant model.

Activation of DAAM1 inhibits endothelial growth

Recently, binding of the formin Dishevelled-associated activator of morphogenesis 1 (DAAM1) to Dvl and the small GTPase Rho has been shown to coordinate Wnt signaling cues (Habas et al., 2001). To address the role of DAAM1 in angiogenesis *in vivo*, we analyzed Tg(fli:EGFP) transgenic zebrafish. First, we investigated whether manipulation of DAAM1 activity by CDAAM1 encoding RNA microinjection induced gastrulation defects as readout for reduced PCP signaling in zebrafish. Compared with wild-type (Figure 14 A), *CDAAM1* RNA injection at a low dose (0.2 ng of RNA) generated moderate defects with obvious tail kinks and shorter

anterior-posterior (A-P) length (Figure 14 C), although at a higher injection dose (0.4 ng), more severe convergence extension (CE) defects were observed (Figure 14 E). These results indicated that overactivation of DAAM1 affects the vascularization of these embryos in a manner consistent with non-canonical Wnt signaling inhibition such as in *pipetail* zebrafish (Cirone et al., 2008). Analysis of a fli-1-driven vascular endothelial cell marker in the injected embryos revealed clear vascular defects to the trunk and tail in CDAAM1-injected zebrafish (Figure 14 C and D). In a lateral view of a control 28hpf embryo, normal vasculature in the trunk displayed a dorsal aorta (DA) and posterior cardinal vein (PCV) with intersegmental vessels (IS's) extending dorsally (Figure 14 B). In CDAAM1-injected embryos with moderate tail kink defects, the IS's were thinner and more diffuse, and some even disappeared (Figure 14 D). Moreover, CDAAM1-injected embryos with more severe defects lacked SE outgrowth and had gaps in the DA and PCV (Figure 14 E and F).

To rule out the possibility that the CE defects contributed to the vascular disruptions, we performed transplantation of CDAAM-1- expressing cells into wild-type hosts. A majority of the host embryos (12 of 13) had transplanted cells outside of the somite/intersegmental region and showed normal vascularization (Figure 14 G). Of the host embryos with CDAAM-1 expression in the somite/intersegmental region, all (5 of 5) showed dramatic alterations to vascularization (Figure 14 H). Because the vascular disruptions observed in the transplant model were limited to the region of transplanted cells, the predominant effect of CDAAM on angiogenesis is within endothelial cells in an autonomous manner. CDAAM1-induced phenotypes are also highly penetrant compared with control injections (Table 2). Taken together, the data indicate that overactivation of DAAM1 signaling disrupts AP extension of the embryo and angiogenesis *in vivo*.

Materials and methods

MultiSite-Gateway cloning

Vectors for multiSite-Gateway cloning was obtained from the Tol2kit (Kwan et al., 2007) and Dr. Nathan Lawson's lab. Middle entry clones were created by TA-cloning PCR products into the pCR-GW8 vector (Invitrogen), and sequencing for clones with the sense strand of insert preceded by attL1site and proceeding to attL2 site. 5' entry clones were flanked by attL4 site and attR1 site. 3' entry clones were flanked by attR2 site and attL3 site. Destination vectors with attR4 and attR3 sites were used to incorporate 5', middle, and 3' entry clones. Destination vectors with attR1 and attR3 sites were used to incorporate middle and 3' entry clones. LR recombination was performed using LR clonase II or LR clonase II plus (Invitrogen).

Fura-2 calcium imaging

Ca^{2+} activity images were acquired by a Zeiss axiovert 100 inverted epifluorescence microscope with coverslip bottomed heating chamber at 30°C, filters for epifluorescence (Chroma Technology Corporation), dual filter wheel and 10X / NA 0.50 Plan-Neofluar objective, and slow-scan CCD camera at high spatial resolution and high bit depth (12-bit gray scale) (Photometrics Quantix). Data were collected at 15 second intervals as image pairs at 340 and 380-nm excitation wavelengths. Ratio images were calculated by the Ratio Tool software (Inovision). TxR distribution was determined by collecting a reference exposure at 540-nm excitation. The high-resolution images used for the subtractive algorithm were converted to 8-bit images and exported into Quicktime for generation of the supplemental movies.

Antibody staining

Embryos were fixed 12 hrs in 4% PFA/PBS at 4°C, washed for multiple times in PBS, and then incubated with mouse monoclonal anti–myc antibody (1:1,500; Cell

Signaling Technology), followed by goat-anti-mouse Alexa488 conjugated secondary antibody (1:400; Molecular Probes). Embryos were mounted in an animal pole orientation in bridged coverslips and optically sectioned using a scanning laser confocal microscope (Leica TCS SP2).

Apoptosis assays by Acridine Orange (AO)

Embryos were dechorionated at the appropriate developmental stages prior to Acridine Orange labeling. Acridine orange (Molecular Probes) is diluted to 5 μg/mL in culture medium. Embryos were incubated with Acridine orange solution in dark for 30 min, followed by five washes in embryo medium. Embryos were anesthetized in 5% tricaine and subjected to fluorescent imaging with an epifluorescent microscope equipped with FITC filter.

Discussion

In this study, we characterized zebrafish *wnt5*'s roles during tail extension, DV patterning and angiogenesis, with emphasis on differential contribution from individual transcripts. Our finding is consistent with previous finding that maternal Wnt5b counteracts canonical Wnt signaling and plays a role in the establishment of early dorsal-ventral axis (Westfall et al., 2003a). However, injecting *wnt5b.1* MO into one-cell stage embryos does not reproduce the dorsalized phenotype seen in maternal *wnt5b/pipetail* mutants (Westfall et al., 2003a). We hypothesized that this discrepancy was due to the presence of residual maternal Wnt5b proteins and *wnt5b.1* transcripts. Injecting MO prior to fertilization has been demonstrated to be effective to knock down residual maternal products (Gore et al., 2005). To recapitulate maternal *wnt5b/pipetail* mutant phenotype, we will target *wnt5b.1* transcript prior to fertilization by injecting oocytes with *wnt5b.1* MO and then perform *in vitro* fertilization on injected oocytes. Fertilized

oocytes will be allowed to develop to different developmental stages and analyzed by morphology and molecular marker.

We and other groups have shown that zygotic *wnt5b/pipetail* mutants could not be rescued by RNA injection at one-cell stage (Kilian et al., 2003; Westfall et al., 2003a). Similarly, RNA injection at one-cell stage does not rescue *wnt5b.2* knock-down. We cannot rule out slight attenuation of CE defects in *wnt5b.2* knock-down embryos by RNA injection, which would imply *wnt5b.2* functions in both permissive and instructive manner. However, severe tail defects in *wnt5b.2* knock-down embryos, which is characteristic of the zygotic *wnt5b/pipetail* mutants, were not rescued. This indicates that the zygotic function of *wnt5b/pipetail* mostly depends on *wnt5b.2*, but not *wnt5b.1*. We reason that the inefficiency of rescuing *wnt5b.2* knock-down embryos is due to the fact that exogenous Wnt5b does not recapitulate endogenous Wnt5b expression. To rescue zygotic *wnt5b/pipetail* mutants, we will restore temporal and spatial control of exogenous Wnt5b expression by introducing *wnt5b* transgenes driven by proper enhancer elements. We will conjugate functionally tested enhancer elements that drive gene expression in ventral-posterior region, proximal promoter of *wnt5b.2*, and Wnt5b protein coding sequence. The resulting DNA sequence will be cloned into a Tol2 site flanking transgene vector and delivered to the *pipetail* mutants and/or *wnt5b* knock-down embryos.

We also demonstrated that *wnt5b*, via PCP pathway, plays important roles in angiogenesis. The Wnt5b signals through DAAM1 to regulate vessel outgrowth. Since Wnt5b and DAAM1 are also involved in the development of somites, which is a source of various angiogenic signals, we performed a transplantation experiment to demonstrate that the vascular defects we observed are not due to defects in somitogenesis. We did not, however, differentiate *wnt5b.1* and *wnt5b.2*'s roles in angiogenesis. Future studies will address whether *wnt5b.1* and *wnt5b.2* contribute differently to angiogenesis by individually knocking down *wnt5b.1* and *wnt5b.2* transcripts.

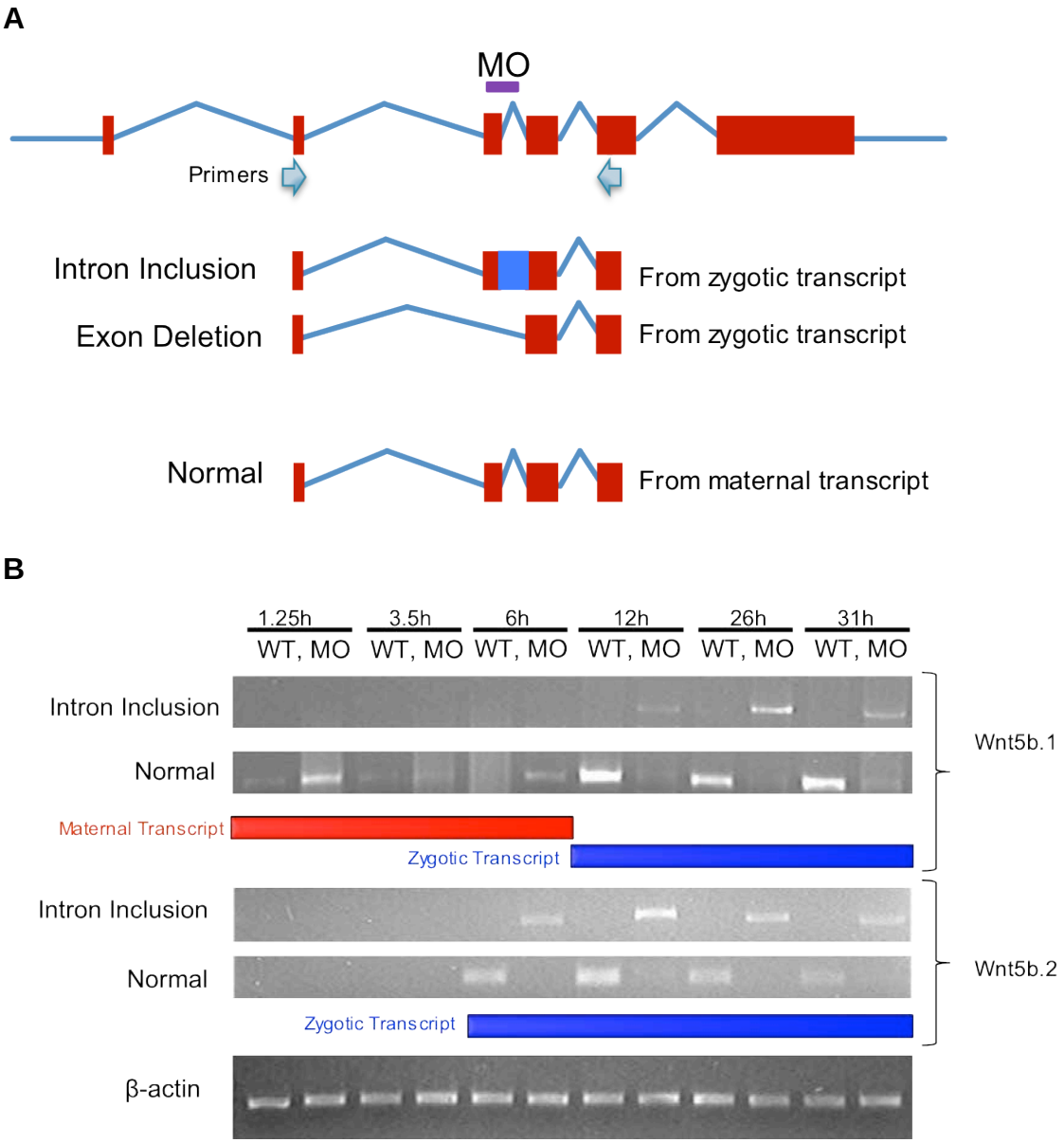

Figure 9: Zygotic transcription of zebrafish *wnt5b.1* and *wnt5b.2* are initiated at different stages. (A) A schematic diagram of experimental design. Since splicing blocker does not affect maternal mRNAs, aberrant RNA products resulted from splicing-blocking MO, such as intron included RNAs and exon deleted RNAs, originate from zygotic transcripts; while RNA products of normal size originate from maternal transcripts. (B) RT-PCR showing distinct zygotic initiation of *wnt5b.1* and *wnt5b.2*. A splicing MO targets both *wnt5b.1* and *wnt5b.2* was injected into embryos at one-cell stage. cDNAs derived from uninjected wild-type (WT) embryos and MO injected embryos were generated for RT-PCR using primers specific to either *wnt5b.1* or *wnt5b.2*.

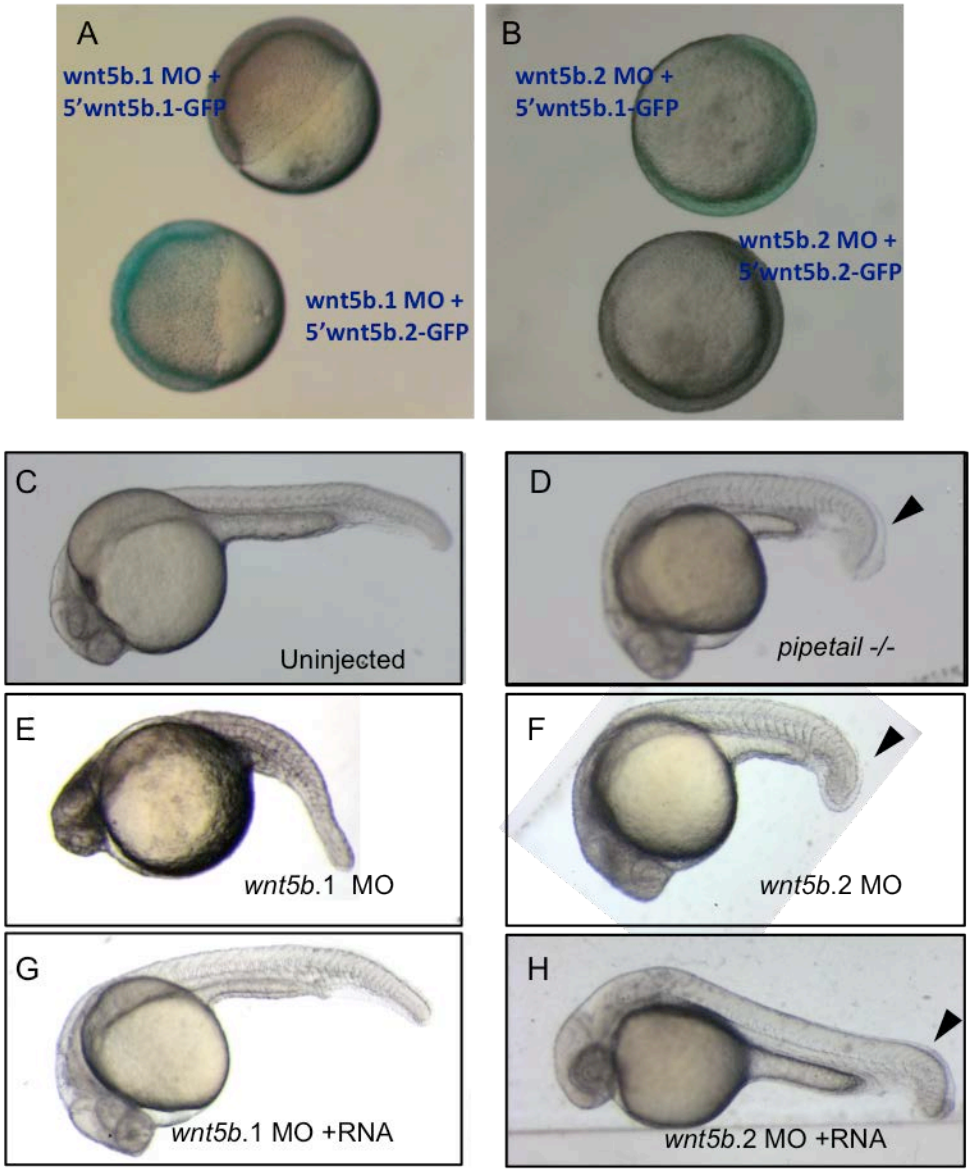

Figure 10: Individual knock-downs of *wnt5b.1* and *wnt5b.2* lead to distinct phenotypes. (A-B) *wnt5b.1* MO and *wnt5b.2* MO are potent and specific to their targets. *wnt5b.1* MO injection is sufficient to eliminate the expression of EGFP conjugated with *wnt5b.1* MO targeting sequence at N-terminus, but not that of a similar construct with *wnt5b.2* MO targeting sequence (A). Conversely, *wnt5b.2* MO injection eliminates the expression of EGFP 3' to *wnt5b.2* MO target, but not *wnt5b.1* MO target (B). (C-H) Distinct phenotypes from *wnt5b.1* and *wnt5b.2* knock-down and rescue. *wnt5b.1* knock-down leads to severely reduced growth of the whole embryos (E), and this phenotype can be suppressed by injecting low-dose (5-10 pg) RNA with *wnt5b* coding sequence (G). *wnt5b.2* knock-down leads to defects in the developing tail (F), similar to the zygotic *wnt5b/pipetail* mutant (D); and this phenotype cannot be suppressed by injecting *wnt5b* RNA (H).

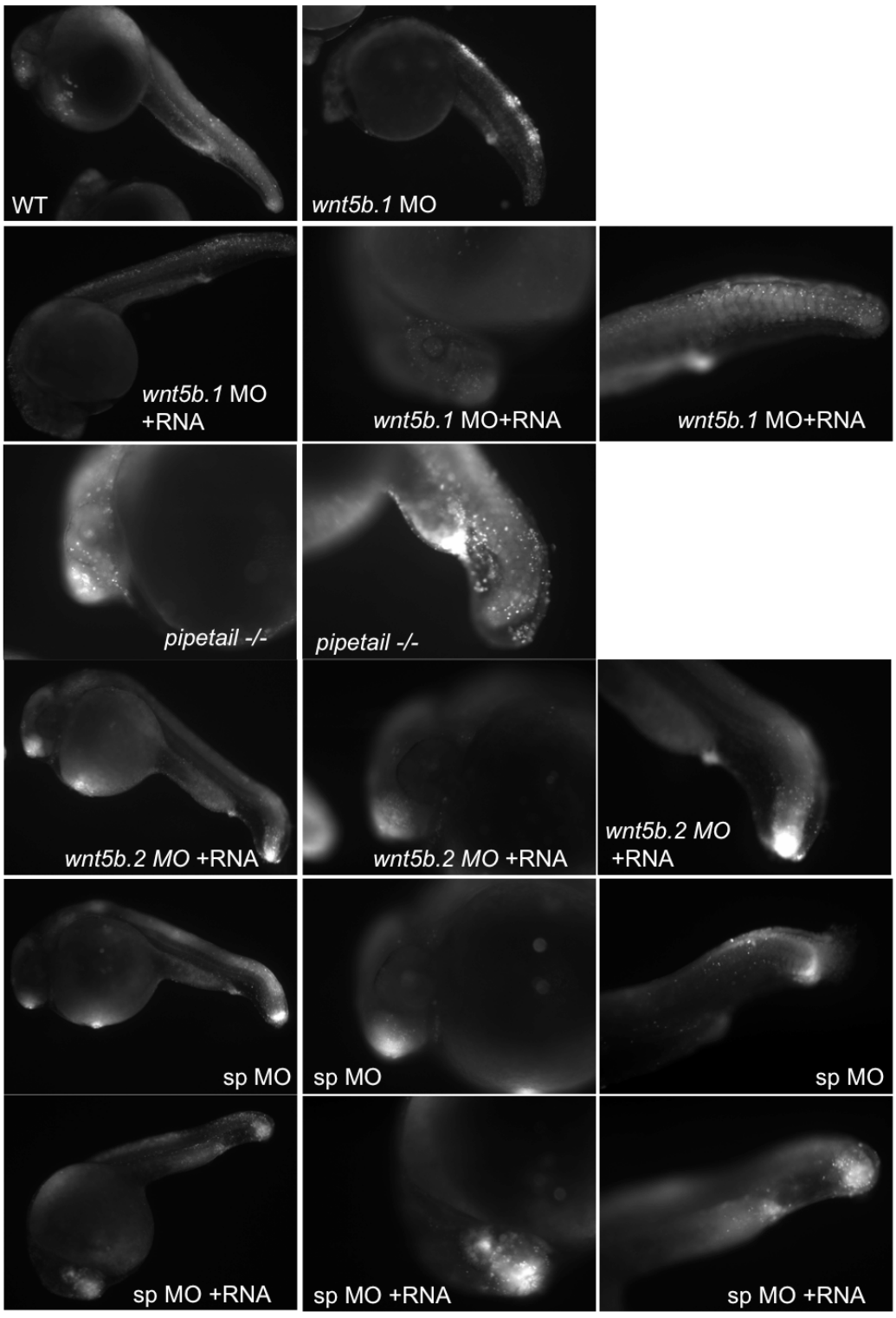

Figure 11: Acridine Orange (AO) staining reveals apoptotic cells in uninjected wild-type control, *pipetail* homozygotes, *wnt5b.1* MO injected, *wnt5b.1* MO with *wnt5b* RNA rescue, *wnt5b.2* MO injected, *wnt5b.2* MO with *wnt5b* RNA rescue, splicing blocker (sp MO) injected, and splicing blocker (sp MO) with *wnt5b* RNA rescue.

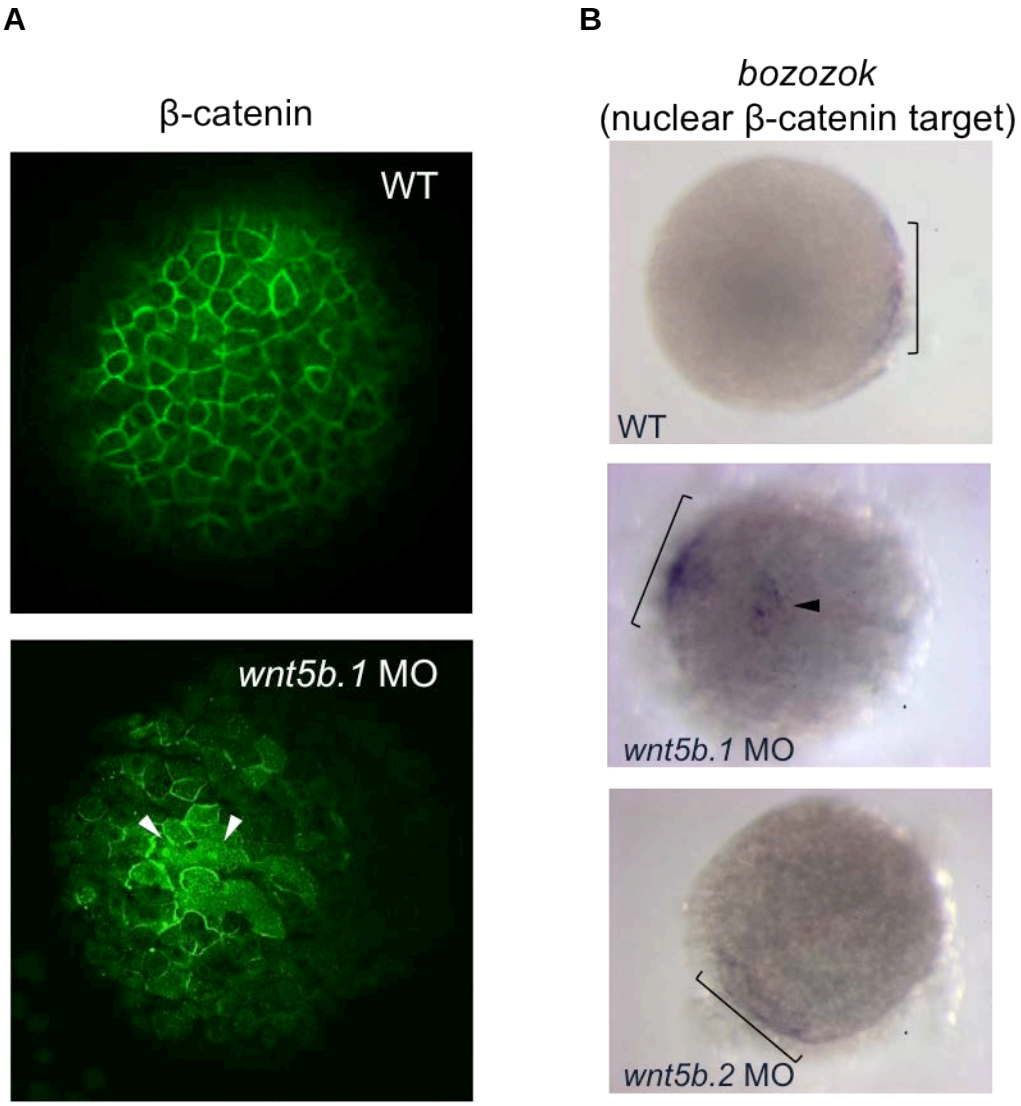

Figure 12: Knock-down of zebrafish *wnt5b.1* results in elevation of β-catenin signaling. (A) Ectopic cytosolic and nuclear β-catenin at the animal pole was observed in *wnt5b.1* MO injected embryos at 3.5hpf (arrowheads), but not in uninjected wild-type control. (B) Whole mount *in situ* hybridization revealed that nuclear β-catenin target gene *bozozok* was expressed in ectopic loci (arrowheads) in *wnt5b.1* MO injected embryos at 4hpf, but not in uninjected wild-type control or *wnt5b.2* MO injected embryos. Brackets mark normal *bozozok* domains.

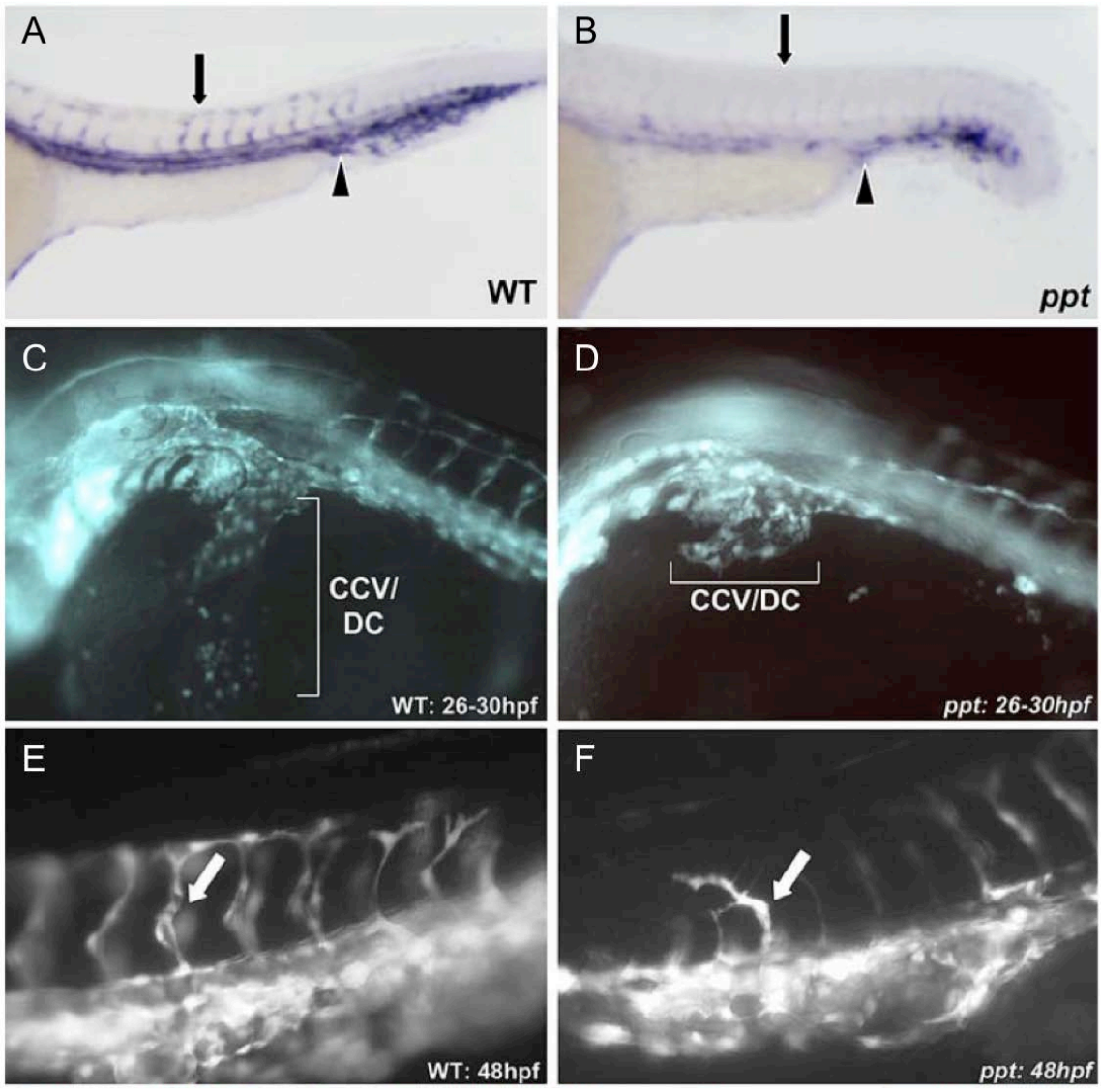

Figure 13: Wnt5b-deficient zebrafish display aberrant angiogenesis *in vivo*. (A-B) Fli-1 expression (28– 30 hpf) as detected by whole mount *in situ* hybridization. A Fli probe shows ordered intersegmental vessel (IS) development in wild-type embryos (A, arrow) as well as proper development of the dorsal aorta (DA), and posterior cardinal vein (PCV) (arrowhead). (B) Similarly staged *wnt5b* mutants display disrupted angiogenesis with defective IS vessel formation (arrow) and reduced DA/PCV expression (arrowhead). (C–D) Fli-GFP expression in Tg(fli:EGFP) transgenic zebrafish with wild-type (C) and *pipetail* (D) backgrounds. Loss of Wnt5b results in disruption of the Duct of Cuvier/CCV. (E–F) Live *in vivo* Fli-GFP images of 48 hpf embryos. Irregular vessel formation is seen in *wnt5b* mutants.

Source: Cirone, P., Lin, S., Griesbach, H.L., Zhang, Y., Slusarski, D.C., and Crews, C.M. (2008). A role for planar cell polarity signaling in angiogenesis. Agiogenesis. *11*, 347-360.

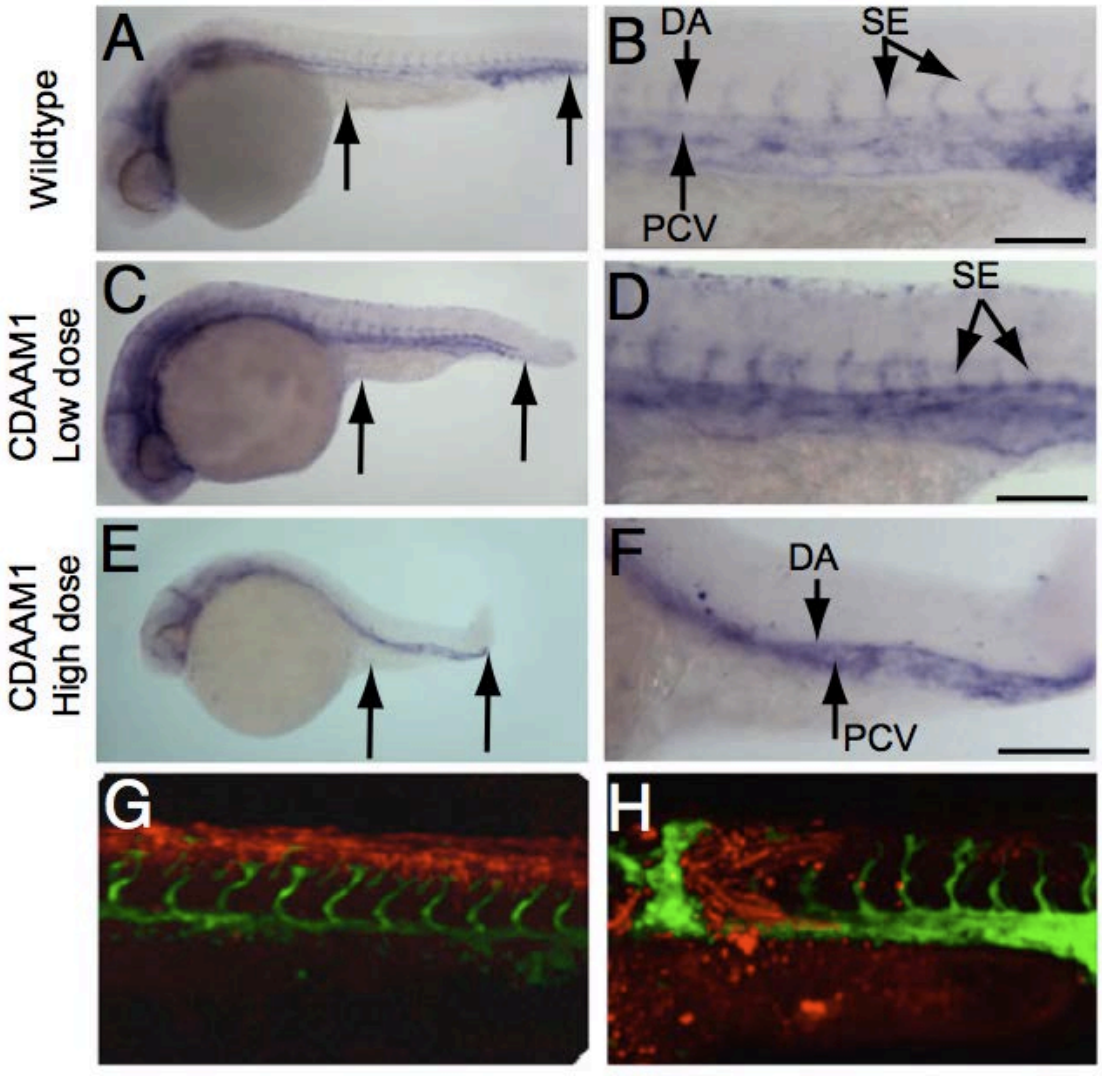

Figure 14: CDAAM1 inhibits angiogenesis in zebrafish. (A-B) Wild-type embryos demonstrating normal Fli-1 expression. (C-D) Embryos injected with 2 ng of *CDAAM1* RNA. (E-F) Embryos injected with 4 ng of *CDAAM1* RNA. A, C, and E (arrows) reveal the A-P length as readout for the PCP pathway. B, D, and F display vascular endothelial cell staining in the somite region. (G-H) Confocal images with Fli1-EGFP expression overlaid on lineage tracer identifying transplant location (red). Scale bars represents 100 μm.

Source: Ju, R., Cirone, P., Lin, S., Griesbach, H.L., Slusarski, D.C., and Crews, C.M. (2010). Activation of the planar cell polarity formin DAAM1 leads to inhibition of endothelial cell proliferation, migration, and angiogenesis. Proc Natl Acad Sci U S A *107*, 6906-6911.

RNA	Normal	Mild-moderate defects	Severe defects	% Defects
GFP, 0.5ng	32	--	--	0
CDAAM1, 0.2ng	8	32	5	82
CDAAM1, 0.4ng	9	17	6	72

Table 2. Statistical representation of defects caused by CDAAM1.

Source: Ju, R., Cirone, P., Lin, S., Griesbach, H.L., Slusarski, D.C., and Crews, C.M. (2010). Activation of the planar cell polarity formin DAAM1 leads to inhibition of endothelial cell proliferation, migration, and angiogenesis. Proc Natl Acad Sci U S A *107*, 6906-6911.

CHAPTER IV
WNT5B FUNCTIONS IN ZEBRAFISH DISEASE

Introduction

Mis-regulation of genes important for development has been implicated in diseases in adults, including various tumors. Growth factor signaling, such as proteins from the Wnt family, provides cues for cells proliferation, differentiation and apoptosis. Excessive and/or insufficient signaling can induce tumor formation. Multiple human tumor types demonstrate increased ß-catenin protein levels, and have been attributed to changes in ß-catenin levels or genes that encode proteins regulating the ß-catenin stability (Reviewed in (van Es et al., 2003; Wharton, 2003)). Mutations causing constitutive activation of ß-catenin can lead to cell fate changes during development and tumor formation in adult animals (Peifer and Polakis, 2000; van Es et al., 2003; Wodarz and Nusse, 1998). Due to its capacity to antagonize ß-catenin signaling, as well as triggering alternative signaling pathways during embryogenesis, *wnt5b* presents as a potential regulator of tumorigenesis.

It has been demonstrated that Wnt5 protein acts as a tumor suppressor gene in the adult gut (Topol et al., 2003a) and functions as an inhibitor of B cell proliferation in hematopoietic tissue (Liang et al., 2003). Consistent with these finding is the occurrence of spontaneous myeloid leukemia and B cell lymphoma in a subset of heterozygous Wnt5a mutant mice, as well as the loss of Wnt5A gene expression in human primary tumors isolated from patients with acute leukemia (Liang et al., 2003). The Wnt5b protein modulates Ca^{2+} releases that regulate axis formation and define a potential role for Wnt5 in promoting ß-catenin degradation in zebrafish embryos. Ca^{2+} treatment has chemopreventive properties in colon cancer (Lipkin, 1999; Wargovich et al., 2000) and parathyroid calcium sensing receptor (CaSR) promoted E-cadherin expression and suppressed ß-catenin/Tcf activation in human colon carcinoma cell lines (Chakrabarty et al., 2003). Given the profound implications in tumor formation, cell adhesion, metastasis

and invasion (Dejmek et al., 2003; Jonsson et al., 2002; Weeraratna et al., 2002), we expanded our knowledge of embryonic *wnt5b* function and explored the function of Wnt5b signaling in tumorigenesis using adult fish. Although spontaneous tumor formation is relatively rare in zebrafish, we have identified testis tumors in heterozygous *wnt5b*$^{Ti265/+}$ adult male zebrafish. We further characterized the pathological features of tumors, and analyzed changes in *wnt5b.1* and *wnt5b.2* expression.

Our preliminary data suggest that *wnt5b.2* expression is reduced in testis tumor from male *wnt5b*$^{Ti265/+}$ zebrafish, to a greater extent compared to *wnt5b.1* expression. We hypothesize that epigenetic changes underlie differential regulation of *wnt5b.1* and *wnt5b.2* expression in tumorgenesis. An important aspect of epigenetic regulation involves DNA methylation, which is the addition of a methyl group to the 5 position of the cytosine pyrimidine ring or the number 6 nitrogen of the adenine purine ring. Such modification can be inherited through cell divisions. Although DNA methylation occurs in regions other than CpG dinucleotide in embryonic stem cells, CpG methylation is most prevalent in adult somatic tissues (Dodge et al., 2002; Haines et al., 2001; Lister et al., 2009). Clustered CpG dinucleotides, called CpG islands are present in approximately 40% of promoters in mammalian genes (Fatemi et al., 2005). Methylation state of the CpG dinucleotides in promoters is correlated with downstream gene expression. In most instances, CpG islands of promoters are unmethylated in actively transcribed genes and methylated in silenced genes. Methylation is also intrinsically linked to imprinting and histone modifications (Feil and Berger, 2007). We found that CpG islands are present in zebrafish *wnt5b.2* promoter and homologous region of multiple species. Consistent with our hypothesis, *wnt5b.2* promoter methylation is correlated with tumorigenesis in male *wnt5b*$^{Ti265/+}$ zebrafish.

In addition, *wnt5* plays pivotal roles in regenerating zebrafish fins (Stoick-Cooper et al., 2007), suggesting that *wnt5* regulates tissue homeogenesis in adult fish. Notably, both *wnt5a* and *wnt5b* are upregulated in regenerating fins (Lee et al., 2009; Stoick-

Cooper et al., 2007). Surprisingly, we found that a human *WNT5A* enhancer driving gene expression in both embryonic and adult caudal fin does not drive gene expression in regenerating caudal fins post amputation, counterintuitive to the general speculation that regeneration is a repetition of embryonic development. This observation suggests that *wnt5*-expressing cells in caudal fin can be divided into sub-populations according to specific enhancers that are activated. We will take advantage of the transgenic lines we generated, which report the activity of individual *wnt5b* enhancers, to explore the role of *wnt5b/pipetail* in adult tissue homeogenesis.

Characterization of testis tumor from *wnt5b*$^{+/-}$ zebrafish

Tumor incidence and morphology

Tumor incidence and morphology was characterized by past effort of the Slusarski lab: Given the potential tumor-suppressor function of Wnt5b, we evaluated all the genetic strains in our facility for gross morphological defects, suggestive of spontaneous tumors. We noted > 11% frequency of zebrafish with distended abdomens or external growths (Figure 15 B, 3/27) in *wnt5b*$^{Ti265/+}$ zebrafish when compared to 0% in wild-type of a similar age and diet (Figure 15 A, 0/138). We previously determined a genetic interaction between Wnt5b and Wnt11 mutant alleles because *wnt5b/pipetail*;*wnt11/silberblick* double mutant combinations display a more severe phenotype than would be predicted from the single mutations alone (Westfall et al., 2003b). Consistent with a genetic interaction between *wnt5b* and *wnt11*, we also observed a higher frequency of spontaneous tumors in the double mutant genetic background (>20%). This is a significant frequency of spontaneous tumor formation as an ENU-mutagenesis screen designed to identify testicular tumors only identified 3 alleles out of ~125 mutagenized genomes (Bauer and Goetz, 2001). Dissection of zebrafish with distended abdomens revealed large masses of abnormally shaped tissue the

abdomen (Figure 15 D) when compared to the internal composition of wild-type (Figure 15 C). Genotype was determined by standard genetic crosses or by PCR.

In the mutant males with enlarged abdomens, the testis was the tissue that demonstrated the most morphological change. We could observe varying degrees of growth based on overall size of the testis compared to other organs and whether one or both testes were altered. The isolated testis tissue was processed for flow cytometry, using chick erythrocyte as an internal reference. We measured and compared the DNA content of normal zebrafish testis and mutant testis. The peak is shifted relative to control, indicating a differing DNA content. A quantitative method of expressing DNA content is by DNA index (DI), which takes the ratio of the mean tumor sample and the DNA content of control sample. Normal tissue would have a DI of 1.0, while the deviation of the DI from 1.0 indicates genomic instability, a feature observed in malignant cells. The heterozygous Wnt mutant testis cells in this example had a DI of 1.2. Indeed, a DI index of 1.15 was observed for clonal leukemic cells in zebrafish (Langenau et al., 2003), confirming that the tissue isolated from the Wnt heterozygous testis shares the aneupliody feature with other characterized zebrafish tumors.

Pathological features

The pathological features accessed by hematoxylin and eosin staining was characterized by past effort of the Slusarski lab and repeated recently in this study. To establish the nature of the enlarged testis, we studied tissue sections from several diseased mutant males and their wild-type-like siblings. Zebrafish testis is arranged in tubules that contain germ cells undergoing spermatogenesis. Spermatogenesis occurs synchronously within a tubule and can contain spermatogonia, spermatocytes, or spermatids (Figure 16 A). Each tubule is bounded by a basement membrane and a connective tissue sheet (Figure 16 A, star). Typically, one large spermatogonium type A cell can be discerned near the basement membrane. These are actively renewing germ cells and give rise to

spermatogonia type B cells. The type B cells typically occur in clusters of four or more cells. Cells from early spermatogenic stages do not stain as darkly (Figure 16 A, arrow). Testis tumor sections typically display a large amount of immature cells with few small pockets of mature spermatids (Figure 16 B). These features were confirmed by couter-staining sections form tumor and control samples with anti-β-catenin antibody and the nuclear marker Topro3 (Figure 16 C and D).

Male *wnt5b*$^{Ti265/+}$ zebrafish display various degrees of tumorgenesis. A majority of tumor-forming fish has one enlarged testis and swim normally. We grouped tumor-forming fish with both enlarged testes, which often exhibit abnormal behavior, as fish with more advanced tumor. Ratios of differentiating spermatocytes and spermatids to total cells including primordial germ cells are relatively constant among wild-type mature males, but are severely reduced in tumor tissues. We measured the percentage of spermatozoa area in total testis tissue in control testis, one-sided tumors and two sided (advanced) tumors and found that spermatozoa areas are reduced as tumors progress (Figure 16 E).

Epigenetic modifications of the *wnt5b.2* promoter correlates with increased testis tumor incidence

Expression of *wnt5b* is altered in testis tumors

To study the function of *wnt5b* in adult testes, we first examined the expression domain of *wnt5b* by performing whole mount *in situ* hybridization on sections. We found that in control testes, *wnt5b* is expressed in organized areas of undifferentiated cells (Figure 17 A and C). Tubular structures of spermatozoa are without detectable *wnt5b* expression. We next examined the expression pattern of *wnt5b* in testis tumor sections. It is noteworthy that *wnt5b*^{Ti265} allele varies from wild-type *wnt5b* allele by a single basepair close to the STOP codon (Rauch et al., 1997b), and in theory should be

detected by the same riboprobe. Indeed, expression patterns of *wnt5b* remain the same in wild-type, *wnt5b*$^{Ti265/+}$ and *wnt5b*$^{Ti265/Ti265}$ embryos (data not shown). Accompanying morphological changes in tumor testis, *wnt5b* expression pattern undergoes dramatic changes in tumor sections (Figure 17 C and D). Compared to age-matched control, *wnt5b* expression is restricted in a patched pattern in testis tumor from male *wnt5b*$^{Ti265/+}$ zebrafish, suggesting that the gene expression profiles in undifferentiated cells are different between wild-type and tumor background.

Since *wnt5b.1* and *wnt5b.2* shared a high degree of sequence similarity, we postulated that WMISH is insufficient to differentiate expression of the two transcripts. We therefore performed quantitative RT-PCR to investigate the expression level of *wnt5b.1* and *wnt5b.2* using primers specific to the two transcripts. Our preliminary data showed that *wnt5b.2* is reduced (Figure 17 E), suggesting that the expression of *wnt5b.2* is under additional regulation.

Increased DNA methylation in *wnt5b.2* promoter

Distinct transcription start sites of the two transcripts *wnt5b.1* and *wnt5b.2*, which differ from each other by several hundreds of bps in the 5'UTR region, suggest different promoter usage. We have demonstrated that the immediate ~1.2kb sequence upstream to *wnt5b.2* demonstrates orientation specific ability in driving gene expression (Figure 2 C), an activity that is common to promoter elements. We further found that the region contains CpG islands (with the criteria: island size > 100bp, GC content > 50.0%, and observed CpG/expected CpG > 0.60) and homologous sequence of this region is conserved in teleosts (Figure 18 B, grey shaded area). Putative conserved distal promoter elements are also found (Figure 18 B, green shaded area). To screen potential changes in the methylation pattern of this CpG island region, we used bisulfite conversion of genomic DNAs and methylation PCR to study methylation in a ~1kb CpG island (Figure 18 C). Methylation-specific primers (forward: 5'-AAG TTT AAA ACG CGT TTT TGT

GTA C-3'; reverse: 5'-TTT CTA TCT CTA CCG AAT CTC TCG A-3') detect methylation products in tumor samples, but not wild-type like controls. By contrast, unmethylation-specific primers (forward: 5'-GTT TAA AAT GTG TTT TTG TGT ATG G-3'; reverse: 5'-TTC TAT CTC TAC CAA ATC TCT CAA T-3') detect DNAs in both tumor and wild-type samples. The data is consistent with sequencing data from a pair of non-selective primers (forward: 5'-GTA AAT TAT AGT GTT AAG GAG AAT GAG A-3'; reverse: 5'-AAA TAC AAA CAT AAT CCA AAC TCT CTC C-3')(data not shown). Our data is consistent with the hypothesis that hypermethylation of *wnt5b.2* promoter further reduces *wnt5b* expression in tumors from male *wnt5b*$^{Ti265/+}$ zebrafish. We therefore propose a model of tumor progression in male *wnt5b*$^{Ti265/+}$ zebrafish (Figure 19). In this model, both genetic (Ti265 mutation) and epigenetic (methylation of the *wnt5b.2* promoter) contribute to reduction of Wnt5b expression and thereby relieve growth control on undifferentiated cells, which leads to tumor formation.

Preliminary results and future directions

Additional characterization of testis tumor

DNA methylation is linked to imprinting and histone modifications (Feil and Berger, 2007). To understand the role of histone modification in *wnt5b* expression, we will perform chromatin-IP with antibodies against modified histones associated with gene repression, such as trimethylation of H3K9 and H3K27, to detect if histone modification plays a role in *wnt5b* repression during tumorigenesis.

Additionally, we will design PCR arrays for detecting expression levels of targets of canonical signaling pathway such as *cyclinD* and *bozozok*. We hypothesize that reduction of *wnt5b* expression relieves antagonism of β-catenin signaling and hence leads to upregulation of growth-promoting genes that are targets of the canonical Wnt pathway.

Successful completion of these experiments will provide detailed mechanism of tumorigenesis in *wnt5b* deficient cells.

We have demonstrated that *wnt5b* plays important roles in regulating angiogenesis in zebrafish embryos. This raises the possibility that mis-regulation of vasculature contributes to the tumor progression from *wnt5b*$^{Ti265/+}$ zebrafish. Although our preliminary data suggest that overall vessel growth remains roughly unchanged in testis tumor (not shown), a more careful examination of vessel invasion and routing is required to address this proposition.

The roles of Wnt5 in fin regeneration

Upregulation of both *wnt5a* and *wnt5b* are seen in regenerating fins following blastema formation (Lee et al., 2009; Stoick-Cooper et al., 2007). Taking advantage of the transgenic lines we generated to screen *wnt5* enhancers (Figure 6), we carried out pilot experiments to assess the roles of Wnt5 in fin regeneration and tissue homeostasis. We have demonstrated that a human *WNT5A* enhancer drives gene expression in both embryonic (Figure 6 and Table 1) and adult caudal fin (Figure 20). Surprisingly, this enhancer does not drive gene expression in regenerating caudal fins (Figure 21) at three days post amputation, a time point when *wnt5a* and *wnt5b* are clearly upregulated in regeneration (Lee et al., 2009; Stoick-Cooper et al., 2007).

This observation raises the question whether adult fin regeneration repeats the developmental program of embryonic development. We will perform fin amputation of other transgenic lines and use the sequence information to deduct possible transcription factors responsible for driving *wnt5* expression during fin regeneration. We also noticed that the human *WNT5A* enhancer drives EGFP expression only in a subset of pigmented cells (Figure 20, C-F). Since pigmented cells appear after the initial regeneration which restores gross morphology of amputated fins, our observation is indicative of a role for *wnt5* to guide cell migration at later stages of fin regeneration, which is different from,

but not mutually exclusive with earlier study showing *wnt5b* plays roles in restricting growth at initial stages of fin regeneration (Stoick-Cooper et al., 2007).

Materials and methods

Hematoxylin and eosin staining

Testis tissues were fixed with 4% paraformaldehyde in PBS for 12 hours, and then infiltrated at 4°C in 15% sucrose, 30% sucrose, and over-night in 100% OCT. The tissues were then oriented in freezing molds and sectioned at -25°C at 12μm. Sections for general histology were stained with hematoxylin and eosin.

Image analysis

Measurement of the spermatozoa area versus total tissue area was performed on β-catenin/Topro3 stained sections. Spermatozoa areas were defined by tubular areas with tightly-packed nuclear staining surrounded by basement membrane and a connective tissue sheet. Confocal images were taken and areas of interest were measured by ImageJ software.

Bisulfite conversion and methylation-specific PCR

Bisulfite conversion of genomic DNAs from testes samples was performed using DNA purification columns and sodium bisulfite (Zymo Research). PCR reactions were carried using the converted DNAs as templates. For each CpG island region, methylation-specific primers, unmethylation primers, and non-selective primers were designed. Methylation-specific primers and unmethylation primers were complement to CpG dinucleotide containing sequences. Methylation-specific primers were designed on sequences with all non-CpG cytosines (C's) converted to T's. Unmethylation specific primers were designed on sequences with all C's converted to T's. Non-selective primers were complement to sequences without CpG dinucleotides and designed on sequences

with all C's converted to T's. Sequencing data of PCR products were analyzed using the BISMA package (Rohde et al., 2010).

Zebrafish fin amputation

Zebrafish ~6 months of age were used for fin amputation studies. Before amputation, zebrafish were anesthetized in 5% tricaine. One-half of the caudal fin was amputated using a razor blade. After amputation, zebrafish were returned to recirculating water at 30°C.

Disscussion

Genes important for development are often implicated in disease. We characterized the higher frequency of *wnt5b*$^{Ti265/+}$ zebrafish with testis tumor in zebrafish The pathological features includes markedly increased proliferation of the undifferentiated cells and accompanying reduction of the differentiated cells, which comprise the spermatozoa.

We further found correlation between increased tumor incidence and hypermethylation if *wnt5b.2* promoter region, suggesting that both the point mutation in Ti265 allele and the epigenetic changes in *wnt5b.2* might contribute to tumorigenesis.

Tumorigenesis may be resulted from elevation of β-catenin signaling and excessive cell growth due to lack of antagonism from Wnt5b, but may also be resulted from misregulated angiogenesis. Future studies will include PCR array for detecting expression levels of β-catenin signaling or β-catenin target genes, and vessel markers staining for mis-routing or uncontrolled growth.

Lastly, we developed transgenic zebrafish expressing EGFP under the control of conserved *cis*-elements for *wnt5* homologs. Even though we have not identified testis EGFP expression yet, we already identified *cis*-elements driving gene expression in various adult tissue, which sets the foundation for studies on regeneration in adult fish.

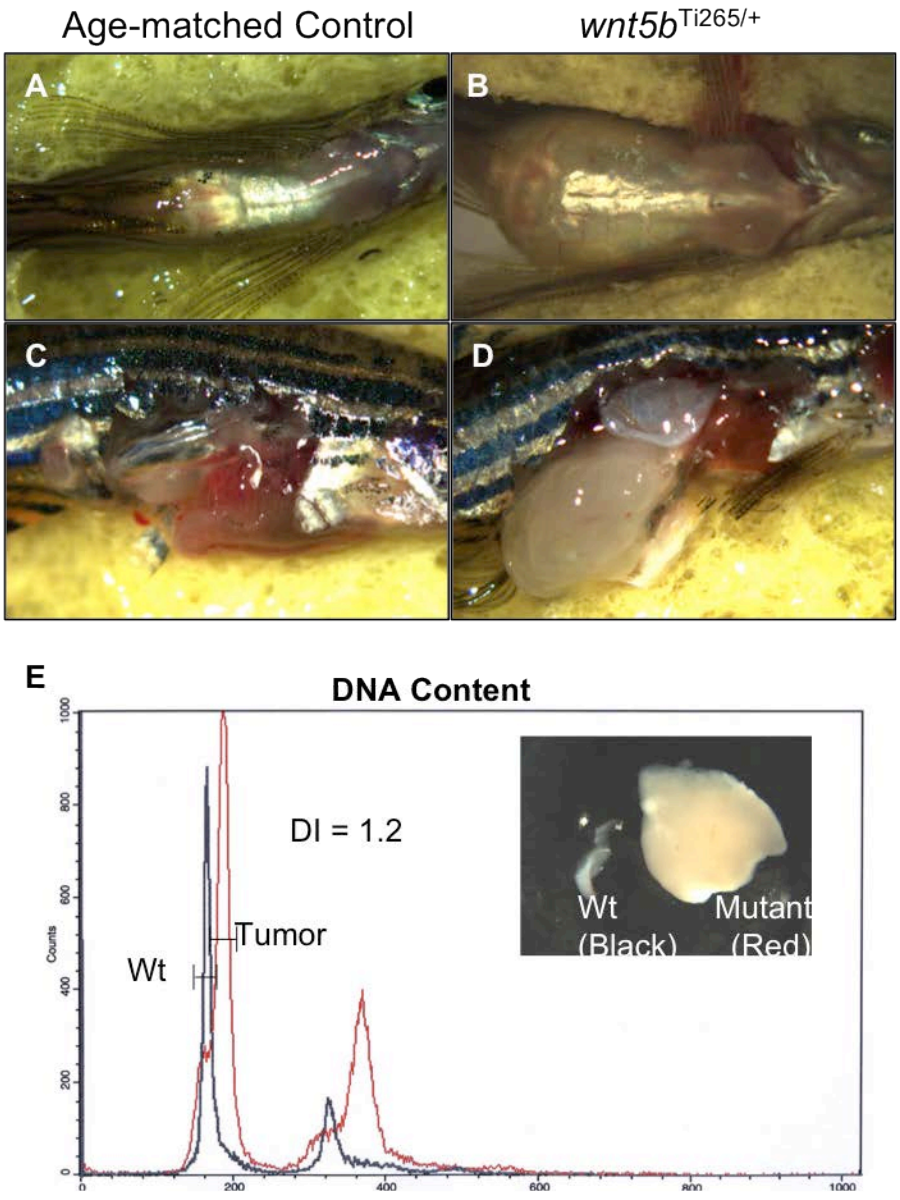

Figure 15: Testis tumor in male *wnt5b*$^{Ti265/+}$ zebrafish. (A-D) Ventral external view of adult male morphology. Age-matched control before (A) and after dissection (C), and *wnt5b*$^{Ti265/+}$ male before (B) and after dissection (D) are shown. (E) DNA content measured by flow cytometry. DNA content of the tumor cells in red and wild-type control in black. Inset shows relative size of a wild-type testis and a mutant testis.

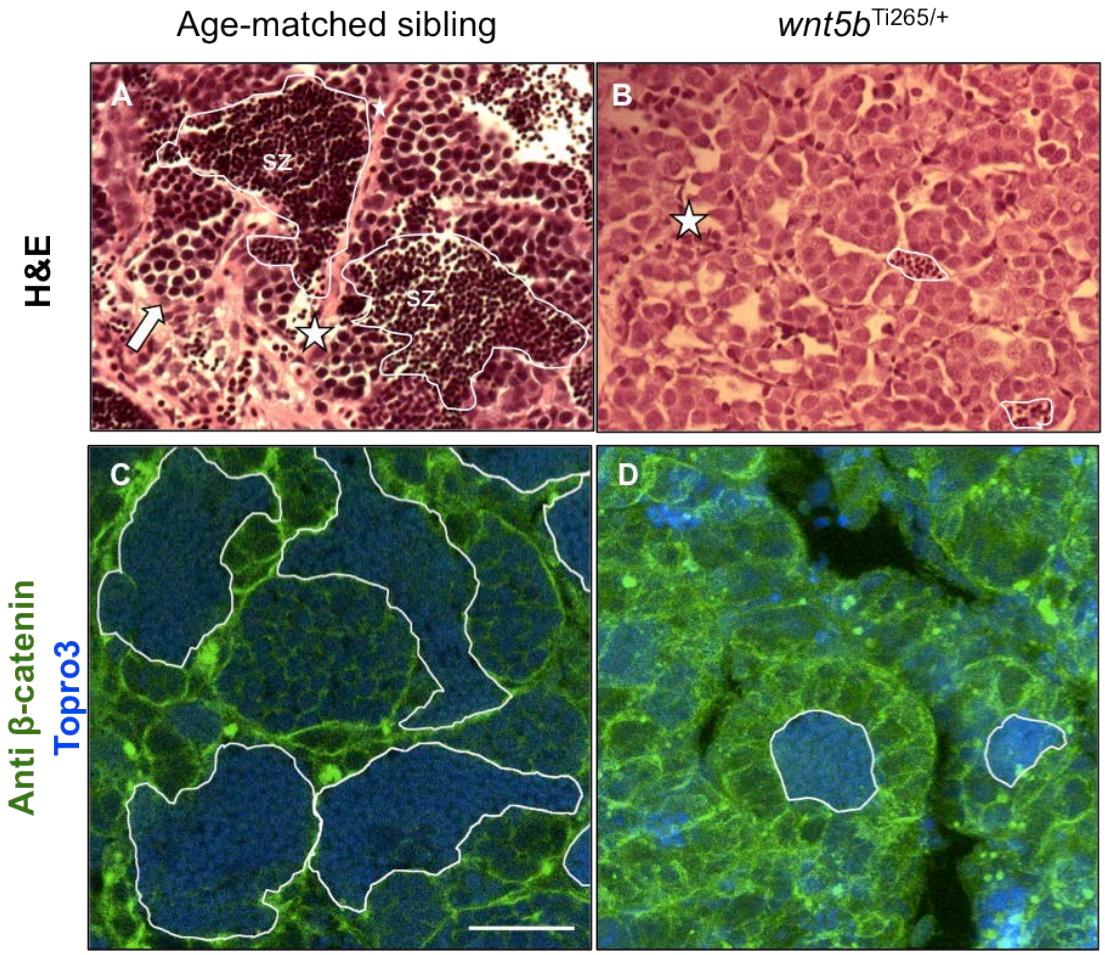

Figure 16: Pathological features of testis tumor in male *wnt5b*$^{Ti265/+}$ zebrafish. (A-B) Zebrafish testis histology. Hematoxylin and Eosin staining of testis sections in wild-type (A) and tumor-forming male *wnt5b*$^{Ti265/+}$ zebrafish (B). Note the reduced mature spermatozoa (sz, outlined with white lines), changes in immature spermatogonia (arrow) and connective tissue (white star). (C-D) Zebrafish testis immunohistochemistry. Anti-β-catenin and nuclear staining by Topro3 in wild-type (C) and tumor-forming male *wnt5b*$^{Ti265/+}$ zebrafish (D) shows reduced spermatozoa area in testis tumor. (E) Quantification of spermatozoa area in total testis tissue in control testis, one-sided tumors and two sided (advanced) tumors.

Figure 16 continued

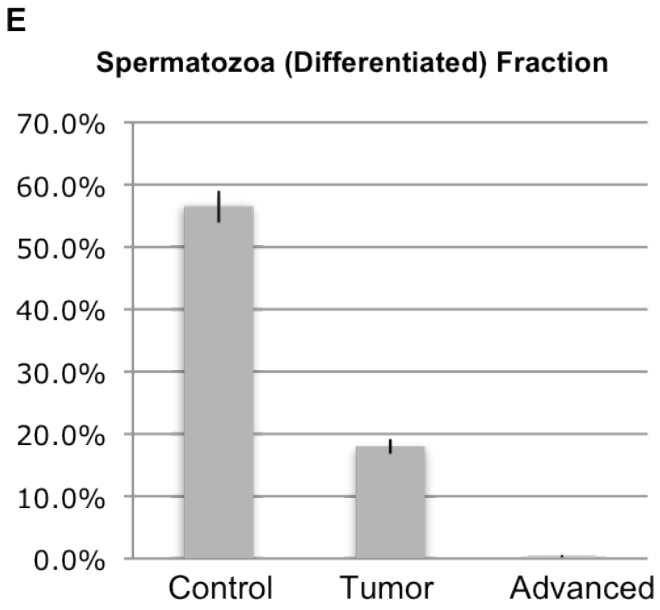

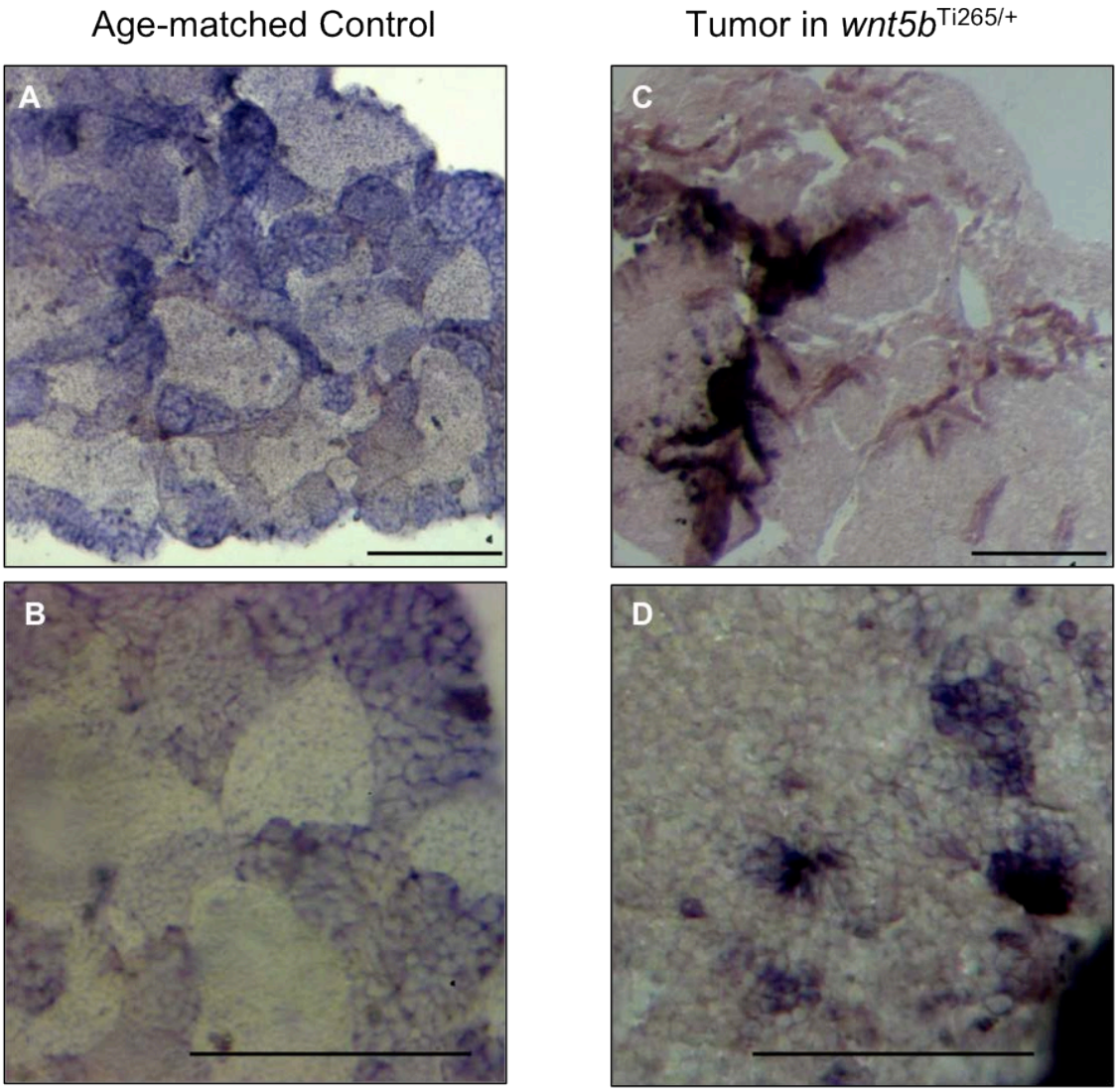

Figure 17: *wnt5b* expression in zebrafish testis. (A-D) Whole mount *in situ* hybridization with a generic *wnt5b* probe. In age-matched control, *wnt5b* is expressed in organized areas of undifferentiated cells (A, B). In testis tumor from male *wnt5b*$^{Ti265/+}$ zebrafish, *wnt5b* is expressed in restricted in patches (C, D). (E) Quantitative RT-PCR shows that the *wnt5b.2* transcript, to a more extent than the *wnt5b.1* transcript, is reduced in tumor samples.

Figure 17 continued

E

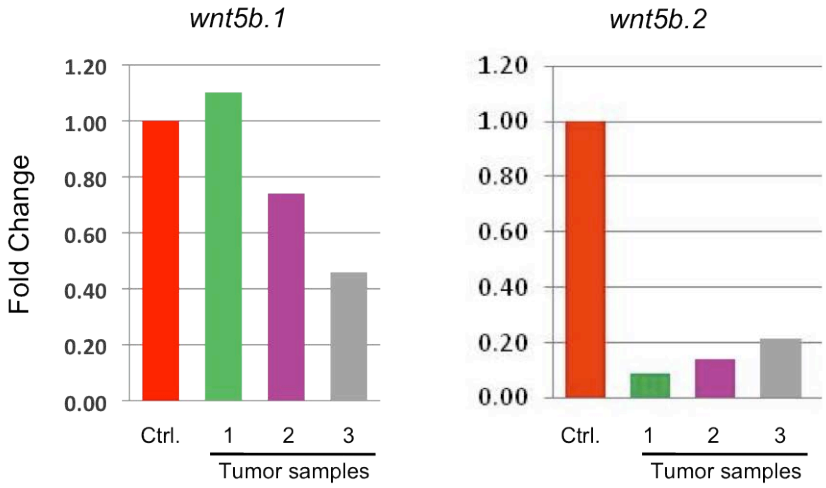

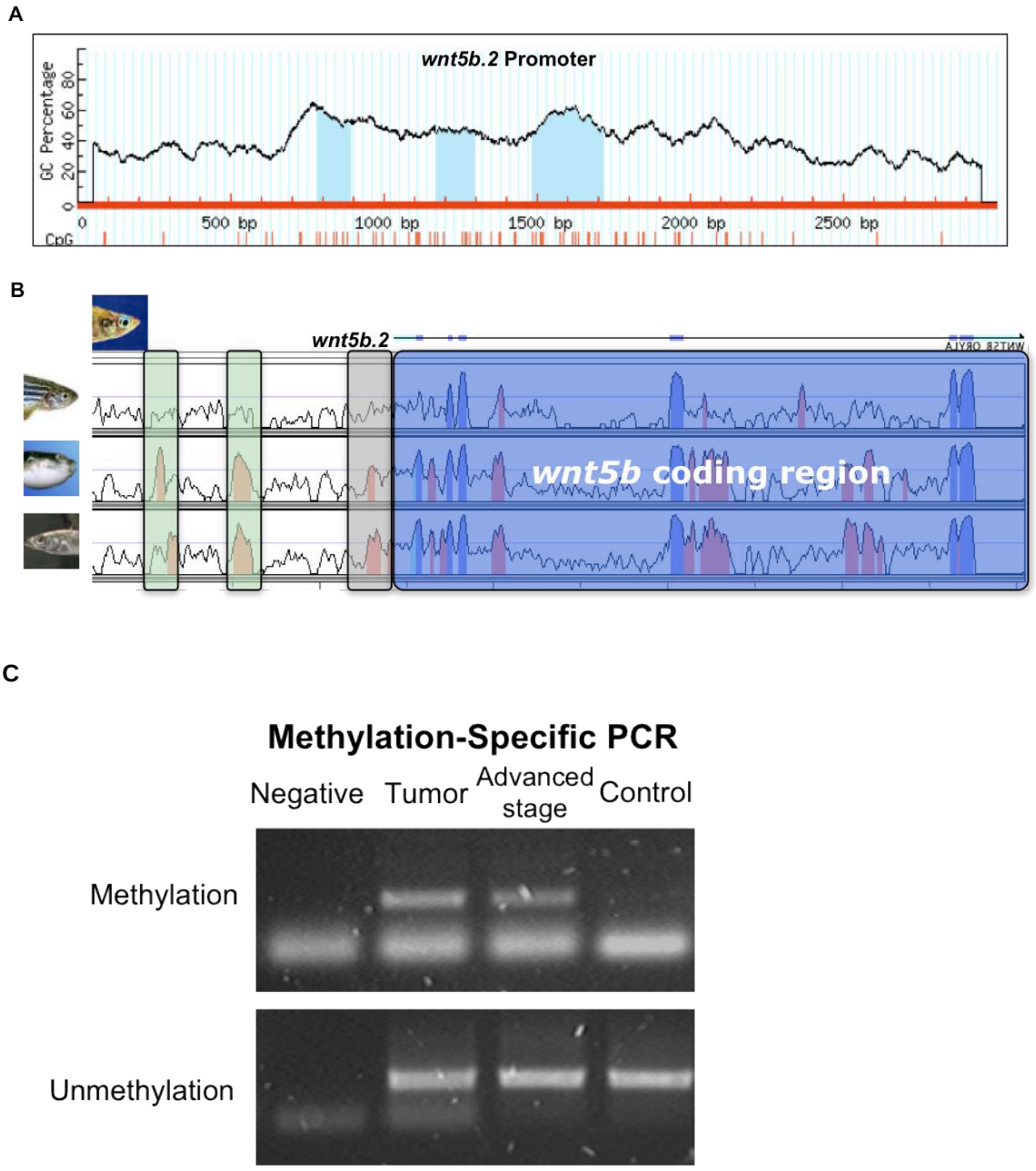

Figure 18: Increased DNA methylation of *wnt5b.2* promoter in tumor-forming male *wnt5b*$^{Ti265/+}$ zebrafish. (A) CpG islands are present in *wnt5b.2* promoter. (B) *wnt5b.2* promoter is conserved in teleosts. *wnt5b.2* coding region is shaded in blue; proximal promoter with CpG island is shaded in grey; and putative distal promoter is shaded in green. (C) Methylation-specific PCR detects methylated DNA in tumor samples, but not control. Unmethylated DNA are present in both tumor and control testes.

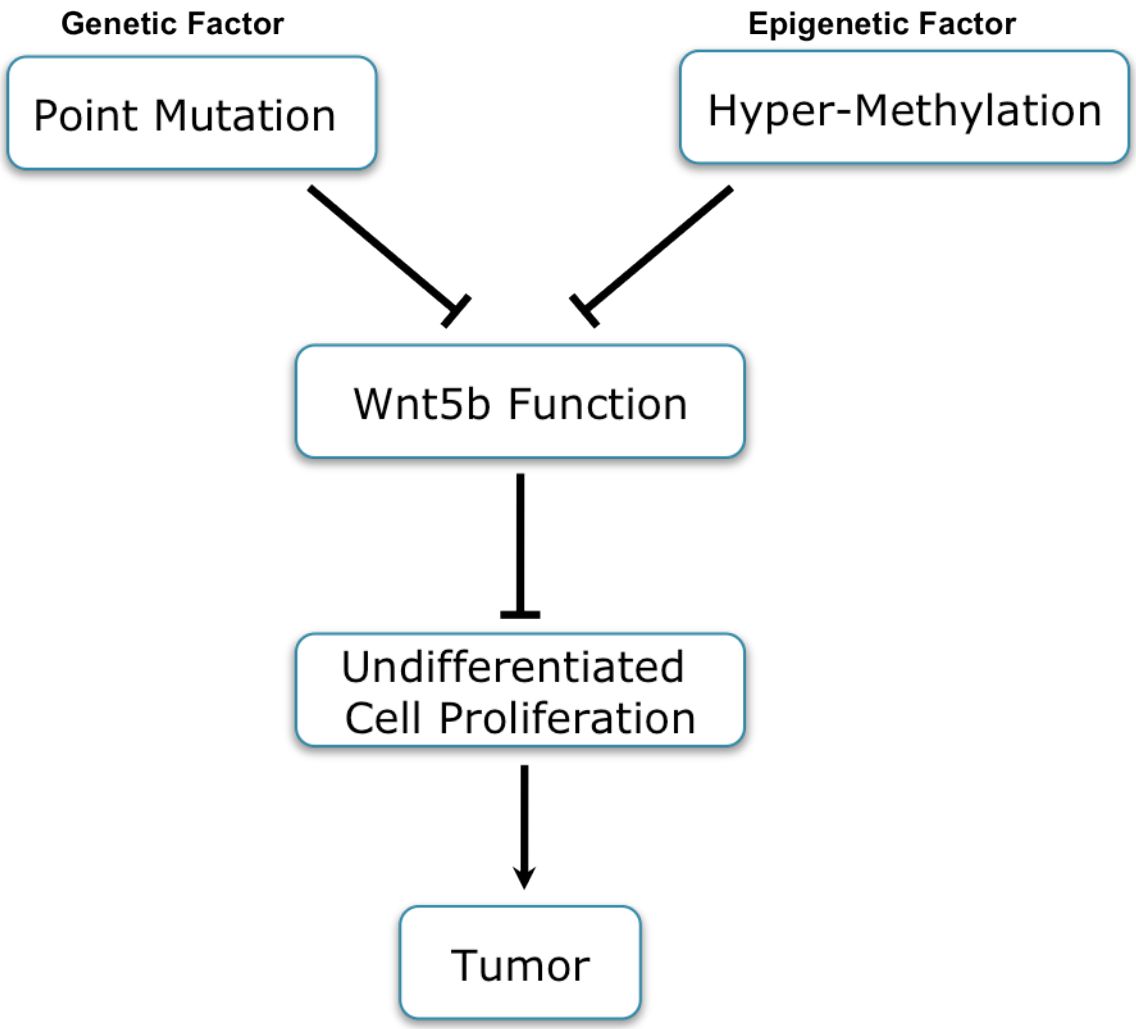

Figure 19: A model of tumor progression in male *wnt5b*$^{Ti265/+}$ zebrafish.

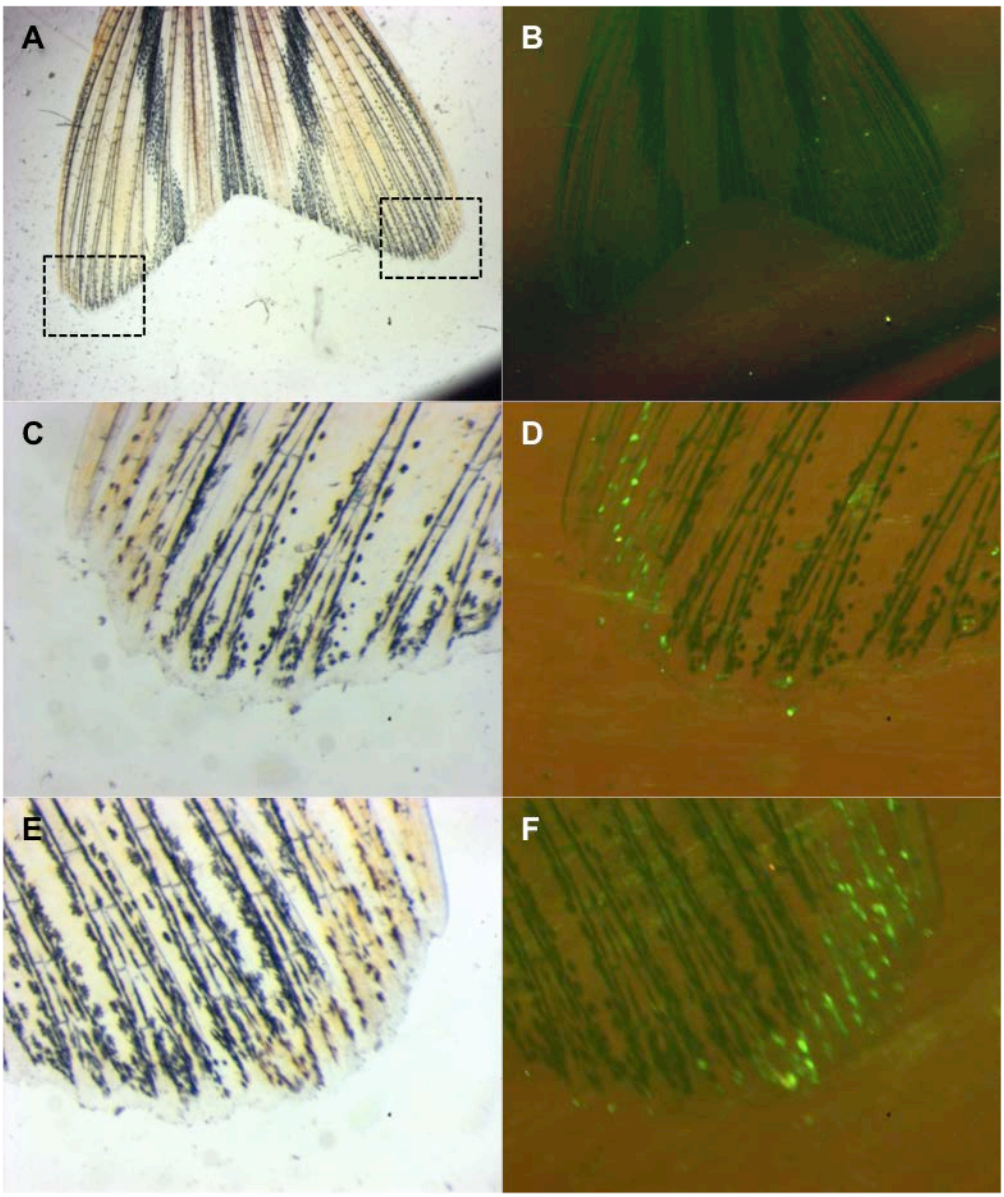

Figure 20: A subset of *wnt5b* expressing cells are present in adult zebrafish caudal fin. (A-B) A reporter transgenic line with EGFP driven by a human *WNT5A* enhancer demonstrates *wnt5b* expression in a population of pigmented cells located in the extende posterior edges of the caudal fin (boxed). (C-F) Higher magnification of areas with the subset of *wnt5b* expressing cells.

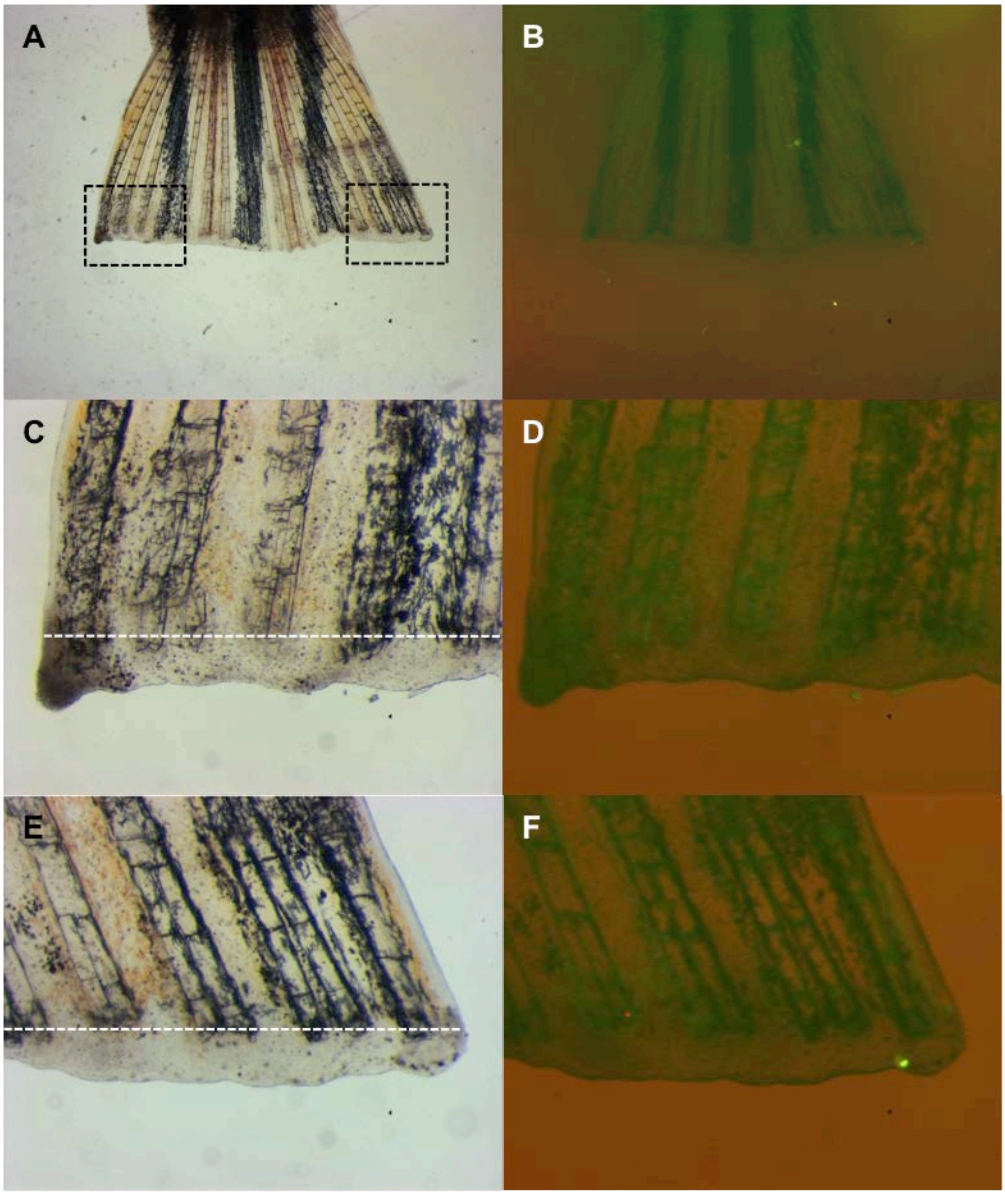

Figure 21: Lack of transgenic EGFP expression during early stages of fin regeneration. (A-B) An amputated caudal fin from the human *WNT5A* enhancer transgenic line at 3 days post amputation. Note the lack of EGFP expression. (C-F) Higher magnification of regenerating areas (corresponding areas in A outlined by boxes) in the caudal fin. White dashed lines indicate the amputation plane.

CHAPTER V
RYK RECEPTOR TRANSDUCES WNT5B SIGNALS DURING GASTRULATION

Introduction

In addition to Fz, Wnt ligands are known to regulate neurite outgrowth through an alternative receptor Related to Tyrosine Kinase (Ryk). However, Wnt-Ryk signaling during embryogenesis is less well characterized. Here we report a role of Ryk to transduce Wnt5b signals during gastrulation movements. We cloned zebrafish Ryk, characterized its interaction with Wnt5b, and combined genetic, biochemical, and physiological tools to show that Ryk deficiency impairs Wnt5b-induced calcium activity and directional cell movement.

Ryk knock-out in homozygous mice is embryonic lethal, characterized by truncated body, craniofacial defects and significant shortening of the limbs (Halford et al., 2000). In human patients, a *RYK* mutation was associated with a nonsyndromic cleft lip and palate defect (Watanabe et al., 2006). In addition, Ryk function has been implicated in polarizing vulval cells in *C. elegans* (Green et al., 2008; Inoue et al., 2004) and in Drosophila it plays a role in the selection of muscle attachment sites in the epidermis (Callahan et al., 1996) as well as salivary gland migration (Harris and Beckendorf, 2007). Although Ryk activities outside the nervous system have been reported, the mechanism of Wnt-Ryk signaling during vertebrate embryogenesis is not well defined. Diverse molecular events downstream of Ryk include heterodimerization with other RTKs (Halford et al., 2000), src kinase activation (Wouda et al., 2008), Fz binding (Kim et al., 2008; Lu et al., 2004) and additionally, Wnt induces the nuclear translocation of the Ryk intracellular domain (ICD) to promote neuronal differentiation (Lyu et al., 2008).

We report that Ryk deficiency in zebrafish leads to gastrulation defects. Consistent with these observations, we show that Wnt5b binds to Ryk and Ryk function

is necessary to modulate Wnt5b induced calcium (Ca^{2+}) dynamics. We also show that Wnt5b and Ryk knockdown embryos (morphants) share similar defects relative to cell movement and neuronal migration. Ryk is internalized and Ryk-expressing cells show increased cellular protrusions in a Wnt5b dependent manner.

Identification of the *ryk* gene in zebrafish

Genomic locus, conservation and splicing variants

Zebrafish *ryk* exists as a single-copy gene (Ensembl assembly release 55, Zv8) and the ~1Mb flanking sequences show synteny with the corresponding region in the human genome (Figure 22 A). We isolated two splicing variants from 24hpf zebrafish embryo cDNAs. The two proteins encoded by these two transcripts differ by 28 amino acids in between the trans-membrane (TM) domain and the intracellular tyrosine kinase domain. Interestingly, the two splicing variants of human *RYK* gene are distinguished from each other by three amino acids (SLG) in the homologous region. To date, there are no existing reports that identify the functional differences between alternatively spliced *ryk* transcripts (Figure 22 B). We based our analysis on the shorter transcript *ryk.1* in this thesis study, unless specified otherwise.

Protein domains, structural features and expression constructs

Zebrafish Ryk protein (Ryk.1) is 604aa in length and 76% identical to its human homolog (Figure 22 B). Ryk protein is composed of an extracellular domain (ECD) similar to the secreted Wnt inhibitory factor-1 (Wif-1), a transmembrane (TM) domain and a "kinase-dead" tyrosine kinase domain (Halford and Stacker, 2001) and can bind to Wnt5a protein (Keeble et al., 2006; Kim et al., 2008; Liu et al., 2005; Yoshikawa et al., 2003). Alignment of vertebrate Ryk protein sequences reveals interesting features that characterize Ryk proteins. Figure 22 shows aligned sequences of human and zebrafish Ryk protein sequences with key conserved amino acids boxed. Cystine155 and

Cystine188 in the extracellular domain (ECD) are conserved in all Ryk and Wif homologs, and based on structural analysis of human Wif1 protein, are likely to form a disulfide bond, (Liepinsh et al., 2006). The TM domain shows an unusually high degree of conservation in Ryk homologs. A previous report demonstrated that TM domain in Ryk is indespensible for proteolytic processing of the mature protein, as replacing Ryk TM domain with a counterpart in EGFR abolished cleavage of wildtype Ryk by γ-secretase (Lyu et al., 2008). The tyrosine kinase domain of Ryk is predicted to be "kinase-dead", as key subdomains conserved among all "kinase-active" RTKs are substituted by variant sequences (Halford and Stacker, 2001). These variant subdomains include the GXGXXG > QEGTFG motif, the VAVK > (V/A)FVK motif, and a key substitution of three amino acids (DFG >DNA) 3' to the catalytic loop (Figure 22 B). It is noteworthy that the aspartate residue chelating Mg^{2+} in phosphodonor complex is present in Ryk, and substituting the "DNA" residues with "DFG" motif of the TrkA-Ryk chimera restores the kinase activity (Katso et al., 1999). Various tyrosine residues are present in Ryk tyrosine kinase domain as potential phosphorylation sites (Figure 22 B). We created a series of Ryk and Wnt5b expression constructs to study their functions in zebrafish (Figure 23 and Table 3)

Expression pattern of Ryk in early development

RT-PCR and whole mount in situ hybridization demonstrate zebrafish *ryk* expression at maternal and zygotic stages (Figure 24 A). During somite stages, *ryk* is enriched in the developing somites and central nervous system (Figure 24 D and E). After 30 hpf, *ryk* is highly expressed in the brain, heart, eyes and the posterior tail (Figure 24 F and G). At four days post fertilization (dpf), *ryk* shows enriched expression in the lining of the ventricular zones and in the notochord (Figure 24 H).

Interaction with Wnt5b and processing of Ryk receptor

Disulfide-bond formation and proteolytic cleavage of Ryk

To investigate the functional role of Ryk processing in zebrafish development, we generated a flag-Ryk-myc construct (Figure 25 A). First, we confirmed that Wnt5b reduces Ryk levels in a dose dependent manner (Figure 25 B). Most of the Ryk protein was found in a truncated form, with a size similar to the ICD of Ryk and suggestive that processing is important for Ryk function (Figure 25 B). In fact, a constitutive cleavage event within the ECD of Ryk was predicted (Halford and Stacker, 2001) and is consistent with our data. Additionally, the structurally related human WIF-1 protein is predicted to have disulfide bond formation between conserved cystines (Liepinsh et al., 2006). The conserved C155 and C188 amino acids in the Ryk WIF domain would allow cleavage products to remain bound to each other (Halford and Stacker, 2001) (Figure 25 F); however, it remains unclear if this binding occurs *in vivo* and its functional relevance. Therefore, we generated a point mutation in the conserved C155 (C155A) to disable disulfide bond formation. N-terminal flag-tag allows identification of full-length-size Ryk or processed ECD based on size. Under non-reducing conditions to maintain the disulfide bond, full-length-size Ryk is observed with no detectable ECD product (Figure 25 C). Conversely, expression of the Ryk-C155A point mutation resulted in accumulation of Ryk ECD (Figure 25 C), indicating that there is a cleavage site in the ECD and a disulfide bond formed between Ryk products requires C155.

Similar to mammalian Ryk protein (Lyu et al., 2008), zebrafish Ryk is cleaved by gamma-secretase at the TM and this Ryk processing is sensitive to γ-secretase inhibitor DAPT (Figure 25 E). Since most of the expressed flag-Ryk-myc protein was found in the ICD size by anti-myc, and the mammal processed ICD was shown to drive neuronal differentiation in cell culture (Lyu et al., 2008), we also cloned Ryk ICD and used it to induce non-directional Ryk signaling for functional assays.

Ryk protein interacts with Wnt5b

To determine if Wnt5b binds Ryk and if such interaction depends upon the disulfide bond formation, we performed co-immunoprecipitation (co-IP) using myc-tagged Wnt5b and EGFP-tagged Ryk constructs (Figure 25 D). Since Wnt5b induces significant turnover of Ryk (Figure 25 B), we generated an ECD-TM-EGFP construct for co-IP (Figure 23 and Table3). Anti-GFP antibody precipitated Wnt5b-myc when it was co-expressed with ECD-TM-EGFP; however, little Wnt5b-myc was co-immunoprecipitated with ECD-TM-EGFP point mutant (C155A) (Figure 25 D). Thus, we demonstrate that the cleaved ECD is bound to the remaining Ryk product, and that this structural feature is critical for Wnt5b binding.

Ryk-expressing cells respond to external Wnt5b

To define a role for Ryk function and address the impact of Wnt5b-Ryk interaction on migrating cells, we created tagged constructs of Ryk and Wnt5b (Figure 23, Table 3). mCherry tagged Ryk (Ryk-mCherry) showed ubiquitous membrane localization at 90% epiboly (Figure 26 A). Donor embryos were also injected with Wnt5b MO to reduce effects due to autocrine signaling and did not alter cell shape or the membrane localization in Ryk-mCherry expressing cells (Figure 27 A). Wnt5b-expressing cells were traced by membrane EGFP driven by an internal ribosome entry site (IRES) in a Wnt5b-IRES-EGFP-CAAX construct (Figure 27 B). Ryk-mCherry donor cells transplanted into a Wnt5b-IRES-EGFP-CAAX host display redistribution of mCherry signals away from the membrane (Figure 27 C and F). Co-localization of Ryk-mCherry with Caveolin1-EGFP indicates that Ryk redistribution is due to internalization (Figure 26 B and C). Moreover, Wnt5b induces Ryk-mCherry cells to undergo significant shape changes with increased filopodia and lamellipodia-like protrusions (Figure 27 C and F). To determine if these changes require Wnt5b, Ryk-mCherry donor cells were transplanted into Wnt5b MO+EGFP-CAAX injected host embryos and no obvious morphological change in Ryk-expressing cells was observed (Figure 27 D). In

addition, donor cells expressing a dominant-negative Ryk (lacking the ICD, dnRyk-mCherry) demonstrate no morphological changes when transplanted into Wnt5b-IRES-EGFP-CAAX-expressing host (Figure 27 E).

Quantification of cell shape changes was used to demonstrate increased cell roundness in *wnt5b/pipetail* mutants (Kilian et al., 2003). Measuring transplanted cells revealed that dnRyk-expressing cells in Wnt5b-expressing host (0.77±0.01, group 1), Ryk-expressing cells in Wnt5b-depleted host (0.76±0.02, group 2) and control cells in Wnt5b-depleted host (0.73±0.02, group 3) all show similar cell roundness (Figure 27 G-I). In contrast, Ryk-expressing cells, transplanted into a Wnt5b-expressing host show significantly reduced average cell roundness (0.53±0.03, group 4) in a wide distribution (Figure 27 G-I). Taken together, our data indicate that Wnt5b stimulates the protrusive activity of Ryk-expressing cells in zebrafish gastrula.

Ryk mediates gastrulation movement in a Wnt5b-dependent manner

Overlapping phenotypes with Ryk and Wnt5b knockdown

To evaluate the developmental role of *ryk*, gene knockdown was performed with translation-blocking antisense morpholino oligonucleotides (MOs). Ryk MO injection resulted in shortened Anterior-Posterior (A-P) body axis. Compared to control (Figure 28 A and D), Ryk MO injected embryos have reduced distance between rhombomeres 3 and 5 of the hindbrain (*krox20*) and the somites of the trunk (*myoD*) show lateral expansion (Figure 28 B and E). A-P extension can be represented by the length to width ratio of the *myoD* domain as a CE index value for analysis (Angers et al., 2006). Wild-type embryos show a CE index above 2.5 (Figure 28 G). Embryos with a CE index smaller than 2.1 are considered CE-defective. Using this parameter, Ryk knockdown resulted in greater than 80% CE-defective embryos. Co-injection of Ryk MO and MO-

resistant *ryk* RNA, at a subphenotypic dose (50ng, Figure 29 C) is sufficient to suppress the CE defect (Figure 28 C and F) to only 38% (Figure 28 G). MO specificity was confirmed by co-injection of Ryk MO with a reporter construct (*ryk* 5'UTR containing the MO target sequence fused to EGFP) resulting in diminished EGFP expression (Figure 29 A) and also by generating similar phenotypes with a second Ryk MO (Figure 29 B).

Consistent with the hypothesis that Ryk functions as a Wnt5b receptor, is the strikingly similar phenotypes of Ryk and Wnt5b morphants. Morphological analysis shows a characteristic reduced posterior extension and tightly-packed somites (Figure 28 I and J), compared to control (Figure 28 H). Both *ryk* (Figure 24 F, inset) and *wnt5b* (data not shown) are expressed the retina. The huc:GFP transgenic line (Park et al., 2000), in which cytoplasmic GFP highlights ganglion and amacrine cell neurite outgrowth and lamina formation, was used to determine if Wnt5b and Ryk have overlapping function in the retina. The inner plexiform layer (IPL) of the retina harbors synaptic connections between the ganglion, amacrine and bipolar cells. At 3dpf, huc:GFP transgenic embryos have two distinct sublamina within the IPL (Figure 28 K, arrows); however, in Wnt5b MO (Figure 28 M) and Ryk MO (Figure 28 L) injected embryos, these sublamina are not well defined, suggesting a disruption in neurite outgrowth. This phenotype can be partially rescued by co-injection of *ryk* RNA with Ryk MO (Figure 28 N). Thus Ryk and Wnt5b knockdown show overlapping defects relative to CE and retina structure.

To evaluate genetic interaction between Wnt5b and Ryk, we performed double knockdown and determined the length to width ratio, CE index (Figure 30). At the 13-14 somite stage, normal CE has an index of 2.8 and higher. Mild CE defects have an index between 2.1 to 2.8 and severe phenotypes have a CE index smaller than 2.1. Controls show normal A-P axis extension with a CE index greater than 2.8 (Figure 30 A and E). Individually, low dose Wnt5b MO (0.5 pmol) or low dose Ryk MO (1.0 pmol) generate mild CE defects (89% and 93% of embryos, respectively) (Figure 30 B, C and E). For

co-injection, MO doses were reduced by half (0.25 pmol Wnt5b MO + 0.5 pmol Ryk MO). All embryos injected with combined MOs present CE defects with the majority (84%) showing severe CE defects and only 16% showing mild CE defects comparable to single knockdown (Figure 30 D and E). We thereby conclude that Wnt5b and Ryk function synergistically to regulate zebrafish CE movement.

Ryk is partially responsible for Wnt5b-induced Ca^{2+} releases

Wnt5 is sufficient to activate Ca^{2+} release and zygotic *wnt5b/pipetail* embryos show reduced Ca^{2+} release (Freisinger et al., 2008b; Slusarski et al., 1997b; Westfall et al., 2003a). Using Ca^{2+} release as a physiological readout for Wnt5b activity, we tested the impact of Ryk function on endogenous and Wnt5b-induced Ca^{2+} release dynamics in vivo. Embryos injected with Fura-2 ratiometric Ca^{2+} sensor and imaged at early stages of epiboly demonstrate the most notable endogenous Ca^{2+} release dynamics in the enveloping layer (EVL) and yolk syncytial layer (YSL) (Figure 31 A, EVL, arrowheads and YSL, arrows) (Westfall et al., 2003a). A time course of ratio images was collected, aligned and subjected to a subtractive algorithm to identify changes in free Ca^{2+} levels at 15-second intervals (Figure 31 A). Changes in Ca^{2+} release dynamics are represented as a color scale surface plot showing the total number of events relative to the location in the embryo (Figure 31 B-G) (Freisinger et al., 2008b; Slusarski and Corces, 2000). In wild-type embryos, we observed a characteristic frequency and distribution of endogenous Ca^{2+} release (Figure 31 B). Unilateral injection of Ryk MO co-mixed with lineage tracer Texas Red (Figure 31 D) resulted in reduced endogenous activity on the injected side (Figure 31 C). Since expression of Wnt5b in zebrafish embryos is sufficient to activate Ca^{2+} release (Figure 31 E), we tested if Ryk activity is necessary for Wnt5b-induced Ca^{2+} release. Embryos were injected at one cell stage with *wnt5b* RNA and Fura-2 for uniform expression. At 16-32 cell stage, Ryk MO co-mixed with lineage tracer was injected unilaterally into a subset of cells (Figure 31 G). Knockdown of Ryk was sufficient to

suppress Wnt5b-induced Ca^{2+} release (Figure 31 F). This impact on Ca^{2+} dynamics indicates that Ryk functions downstream of Wnt5b.

Directional cell migration defects from Ryk knockdown

To define a role for Ryk function and address the impact of Wnt5b/Ryk interaction on gastrula cell migration, we performed a series of transplantation assays. Prior to transplantation, two donor embryos were injected with control MO combined with fluorescent lineage marker. At ~3 hpf, donor cells were mixed and transplanted into the lateral mesoderm at the germ ring margin of a shield-stage host (~6hpf) (Figure 32 A). Cells in this region of the embryo migrate in a ventral-to-dorsal direction and extend in both anterior and posterior directions. The distribution of transplanted cells was scored after host embryos completed gastrulation (~10hpf). Transplanted cells from two control MO injected donors (red and green) demonstrate similar convergent movement (Figure 32 B). In contrast, Ryk MO injected cells (red) demonstrate markedly reduced convergent movement compared to control MO injected cells (green) (Figure 32 C). When Ryk MO (red) and control MO (green) cells are transplanted into Wnt5b knockdown host embryos, both control MO and Ryk MO cells show reduced dorsal convergence (Figure 32 D). To quantify cell migration between the two populations of transplanted cells, the distance from the center of the embryo was averaged for red and green labeled cells (Figure 32 E). In wild-type hosts, the mean difference in average position of Ryk MO injected cells (red) compared to control MO injected cells (green) was 100μm, corresponding to 5-10 cells and is statistically different from the control group ($p<0.01$) (Figure 32 E). In contrast, there was no significant difference in average distance traveled by Ryk MO and control MO cells transplanted into Wnt5b knockdown hosts (Figure 32 E). These data indicate that dorsal convergence is compromised in the absence of Ryk and in the absence of the Wnt5b ligand, either with or without the Ryk receptor.

Materials and methods

Disulfide-bond detection

As gastrulation begins, morphogenetic movements such as involution, convergence and extension (CE), produce the primary germ layers and the embryonic axes. Ca^{2+}-release activity has been described during epiboly/gastrula stages in both zebrafish and *Xenopus* (Gilland et al., 1999; Wallingford et al., 2001; Webb and Miller, 2006). During epiboly, zebrafish embryos are staged by the extent to which cells have moved over the yolk. At 50% epiboly, the embryonic dorsal shield forms as a thickening on the future dorsal side (Kimmel et al., 1995). The DFCs lie just below the shield and migrate ahead of the shield during gastrulation. At the completion of gastrulation, the DFCs come to lie between the yolk and tailbud and will form the epithelial lining of the KV.

Western blot and co-immunoprecipitation

Injected embryos at 90% epiboly were lysed for analysis with mouse anti-myc antibody (9E10, Santa Cruz) in 1:2000 dilution, anti GFP antibody (Roche) in 1:1000 dilution, or mouse anti-flag antibody (M2, Sigma) in 1:1000 dilution. Anti β-actin antibodies (Sigma) in 1:2000 dilution were used for loading controls. Anti-oxidant reagents were omitted for non-reducing condition.

EGFP-tagged proteins were immunoprecipitated with anti GFP antibody (Roche) in 1:100 dilution and protein A/G agarose (Thermo Scientific). The immunoprecipitates were washed four times at 4 °C with buffer (50mM Tris at pH 7.5, 150mM NaCl, 0.8% Triton X-100, 0.5mM PMSF and leupeptin at 5μg/mL).

Cryosection

Embryos were processed for cryosectioning as previously described (Baye and Link, 2007). Briefly, embryos were infiltrated at 4°C in 15% sucrose, 30% sucrose, and

over-night in 100% OCT and then oriented in freezing molds and sectioned at -25°C. 12 μm cryosections were mounted on glass slides and coverslipped with Vectasheild mounting media (Vector Laboratories) for confocal imaging.

Transplantation

For assessing cell migration by transplantation, a group of donor embryos were microinjected with Ryk MO mixed with 20ng lineage marker (dextran-conjugated Texas Red, Molecular Probes) at one-cell stage. A second group of donor embryos were injected with FITC-conjugated control MO. A group of host embryos were injected with Wnt5MO at one-cell stage. Donor and host embryos were manually dechorionated prior to transplantation. Using a single needle, 10-20 cells were removed from each donor embryo at high-sphere stage, mixed and transplanted into the center of lateral mesoderm of a host embryo at shield stage. Embryos with grafted cells were allowed to grow to tailbud stage for imaging. For assessing ligand-receptor interaction by transplantation, donor and host embryos were injected with 100pg RNA. At sphere stage, ~20 cells were transplanted into the blastodermal margin of each host embryo. At shield stage, embryos with transplanted cells at lateral or ventral mesoderm were selected and allowed to grow to 90%~100% epiboly for imaging.

Image analysis

Cell roundness was measured by ImageJ software which outlines cell perimeter including lamellipodia and lobopodia-like protrusions, and was defined as $4\pi A/P2$ (possible roundness values are between 0~1), in which P is the perimeter of a cell and A is the area the cell occupied after the cytoplasmic region within the perimeter is filled with corresponding color.

For measuring fluorescent protein colocalization, Zebrafish embryos were injected at one cell stage into the yolk for global expression, at 16-32 cell stages into

individual blastomeres for mosaic expression. Dvl-EGFP, Fz2-mCherry or Ryk-mCherry positive domains are measured by the ImageJ software with the "Colocalization" plugin.

Bright/dark field and in situ hybridization images were acquired by a Zeiss Stereo Discovery.V12 microscope with AxioVision software and X-Cite 120 light system (EXFO Photonic Solution Inc.), using either an Achromat S 1.0X / NA 0.50 objective or a 10X / NA 0.45 air objective at 30°C. Fixed sample was mounted in 1XPBS. CE index was defined as length to width ratio of the myoD domain (Angers et al., 2006). The length was defined as the distance between the anterior edge of the most rostral somite and the posterior edge of the most caudal somite. The width was defined as the distance between the left and right edges of the widest pair of somites. At 10-11 somite stage, the average CE index for wild-type embryos is 2.8; at 13-14 somite stage, the average CE index for wild-type embryos is 3.5.

Mean difference between distance traveled by TxR and FITC cells were analyzed by ImageJ software (NIH Open Source). For individual embryos, the mean distance between green and red tracers was determined by $\Delta R = R_{red} - R_{green}$, in which R_{red} and R_{green} are the average distance traveled by all green and red cells from the center of the embryos, respectively. ΔR from ten embryos in the same experimental group were used to calculate the average $\overline{\Delta R}$ and standard deviation within each group.

Fluorescence resonance energy transfer (FRET)

FRET experiments were performed on fixed cells with a Leica SP2 confocal system. An acceptor bleaching protocol was used. Fluorescence of the acceptor was bleached to 50% of the original intensity before post-bleach imaging.

Discussion

Although Ryk's function has been explored in multiple systems, the exact mechanism by which Ryk signals downstream molecular events is still elusive. Much of

the debate in the field centers around whether Ryk is associated with other receptors such as Fz and kinase-active RTKs on the membrane. The answer to this question seems to be highly context-related. Hence we performed preliminary studies using fluorescent tracing of Ryk proteins in zebrafish cells at a stage when the active state of Ryk functions is supported by previous data. We injected RNAs coding Ryk ECD-TM-EGFP and Ryk-mCherry in one-cell stage embryos and fixed the injected embryos at 80% -100% epiboly stage. The embryos were subjected to FRET study using an acceptor-bleaching approach. We found that of EGFP and mCherry signals overlap in all compartments of the cells (Figure 33). However, FRET signals were only observed in plasma membrane, but not cytoplasm (Figure 33, box). This suggests that Ryk proteins cluster specifically on the membrane, possibly in a ligand-binding dependent manner.

Future studies will repeat the experiment with Ryk constructs tagged with more traditional FRET-pair, namely CFP and YFP. Although the excitation/emission spectra of EGFP and mCherry are within the theoretical limit of a FRET-pair, the efficiency of EGFP/mCherry FRET with an acceptor-bleaching approach is low, due to the exceptional photo-stability of mCherry fluorescence protein. Second, we will perform FRAP and FRET studies on membrane Ryk proteins to monitor the rate of Ryk receptor clustering. Third, we will compare the extent to which Ryk receptor cluster on the plasma membrane between the Wnt5b-bound state and the Wnt5b-free state.

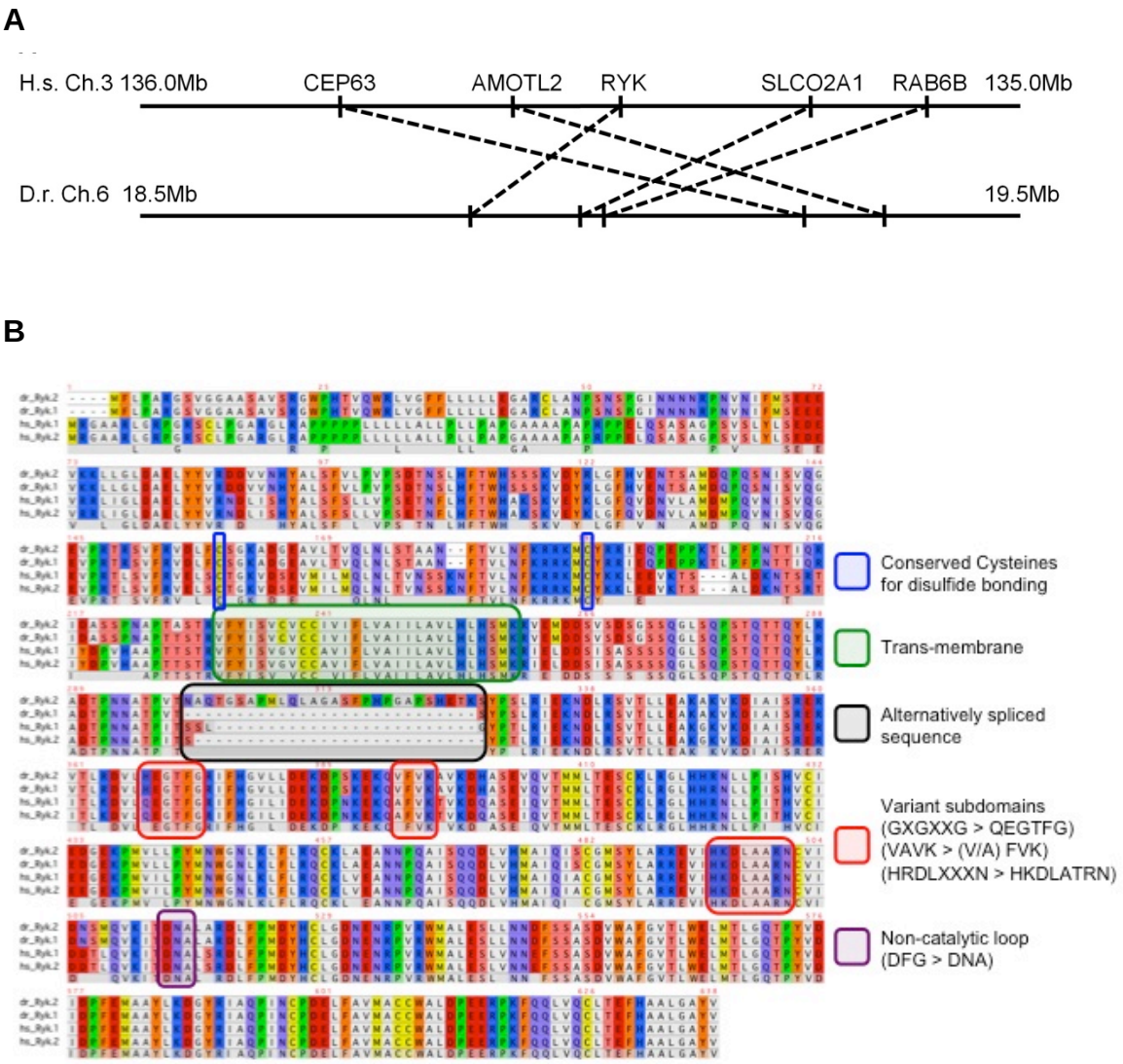

Figure 22: Ryk homologs in zebrafish and human. (A) Synteny of genomic sequences flanking zebrafish *ryk* and human *RYK* genes. (B) Alignment of zebrafish (Dr) and human (Hs) Ryk protein sequences.

Source: Lin, S., Baye, L.M., Westfall, T.A., and Slusarski, D.C. (2010). Wnt5b-Ryk pathway provides directional signals to regulate gastrulation movement. J Cell Biol *190*, 263-278.

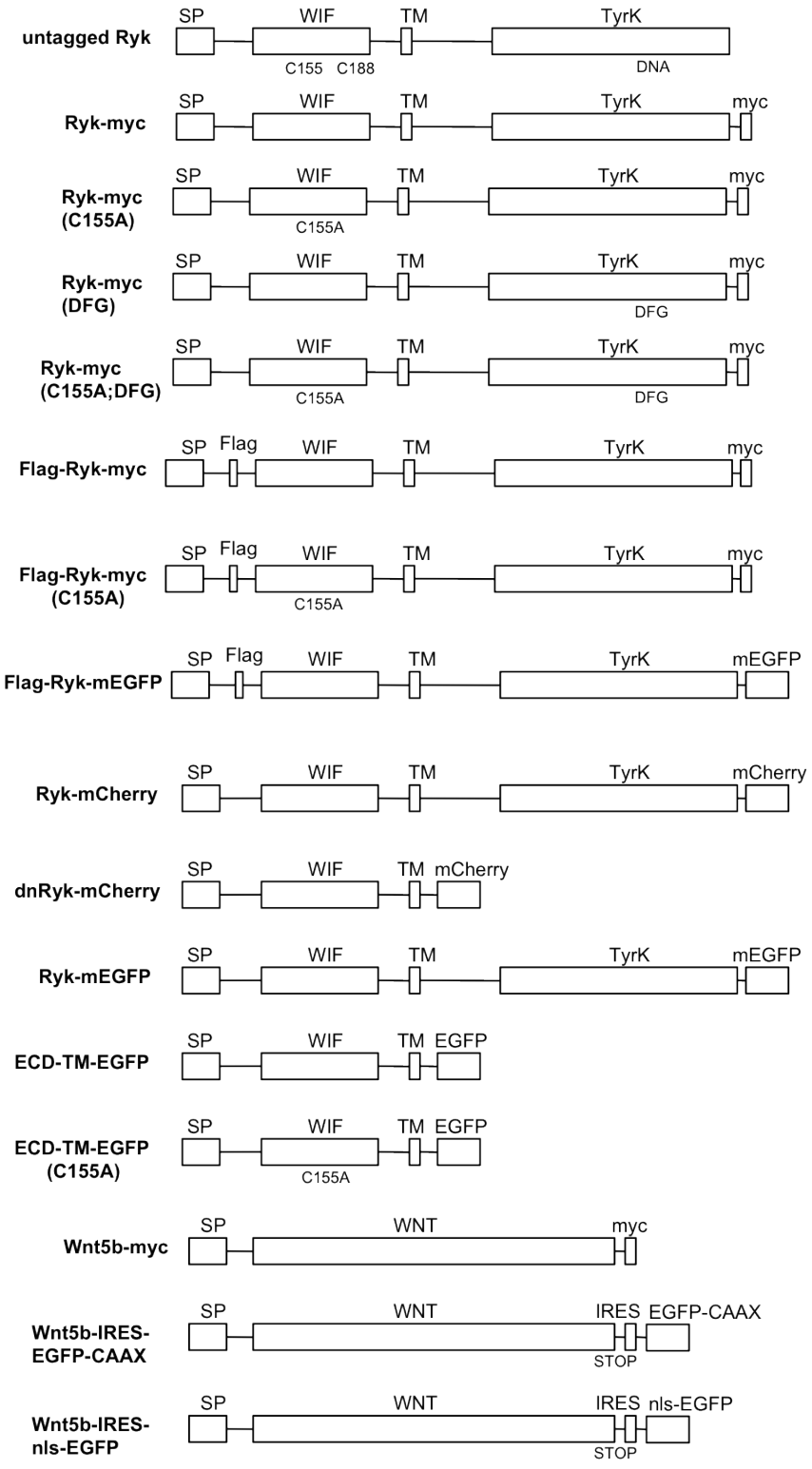

Figure 23: Expression constructs of Ryk and Wnt5b.

	Primers
Wnt5b with stop codon	Forward: 5'-CTG CTG TTT TGA GGG GAT TC-3' Reverse: 5'- CTG CTT AAT TGC TCA GTG CG -3'
Full-length Ryk with stop codon	Forward: 5'-ACT TTT TAA AGC GAC GGT GG-3' Reverse: 5'-ATC AAC AAC TCG GCT GGT TT-3'
Full-length Ryk without stop codon	Forward: 5'-TAA AGC GAC GGT GGG CTG TG-3' Reverse: 5'-CAC GTA GGC CCC CAA AGC TG-3'
dnRyk	Forward: 5'-GGT GGG CTG TGA TGT TTC TG-3' Reverse: 5'-CCT CTT CAT GCT GTG GAG GT-3'
ryk 5'UTR	Forward: 5'-GAG CGC GAG CTA ACA GAA GT-3' Reverse: 5'-GAG CAG CAG GAG GAG AAA GA-3'
Ryk ICD	Forward: 5'-GTG GAA ATG GAT GAC AGC GT-3' Reverse: 5'-CAC GTA GGC CCC CAA AGC TG-3'
β-actin	Forward: 5'-TCA GCC ATG GAT GAT GAA AT-3' Reverse: 5'-GGT CAG GAT CTT CAT GAG GT-3'
Fz2 without stop codon	Forward: 5'-GTT TGC CGG ACT CAT TTT GTA-3' Reverse: 5'-AAC AGT GGT TTC TCC TTG TCC-3'

Table 3. Primers for Wnt5b and Ryk constructs.

Source: Lin, S., Baye, L.M., Westfall, T.A., and Slusarski, D.C. (2010). Wnt5b-Ryk pathway provides directional signals to regulate gastrulation movement. J Cell Biol *190*, 263-278.

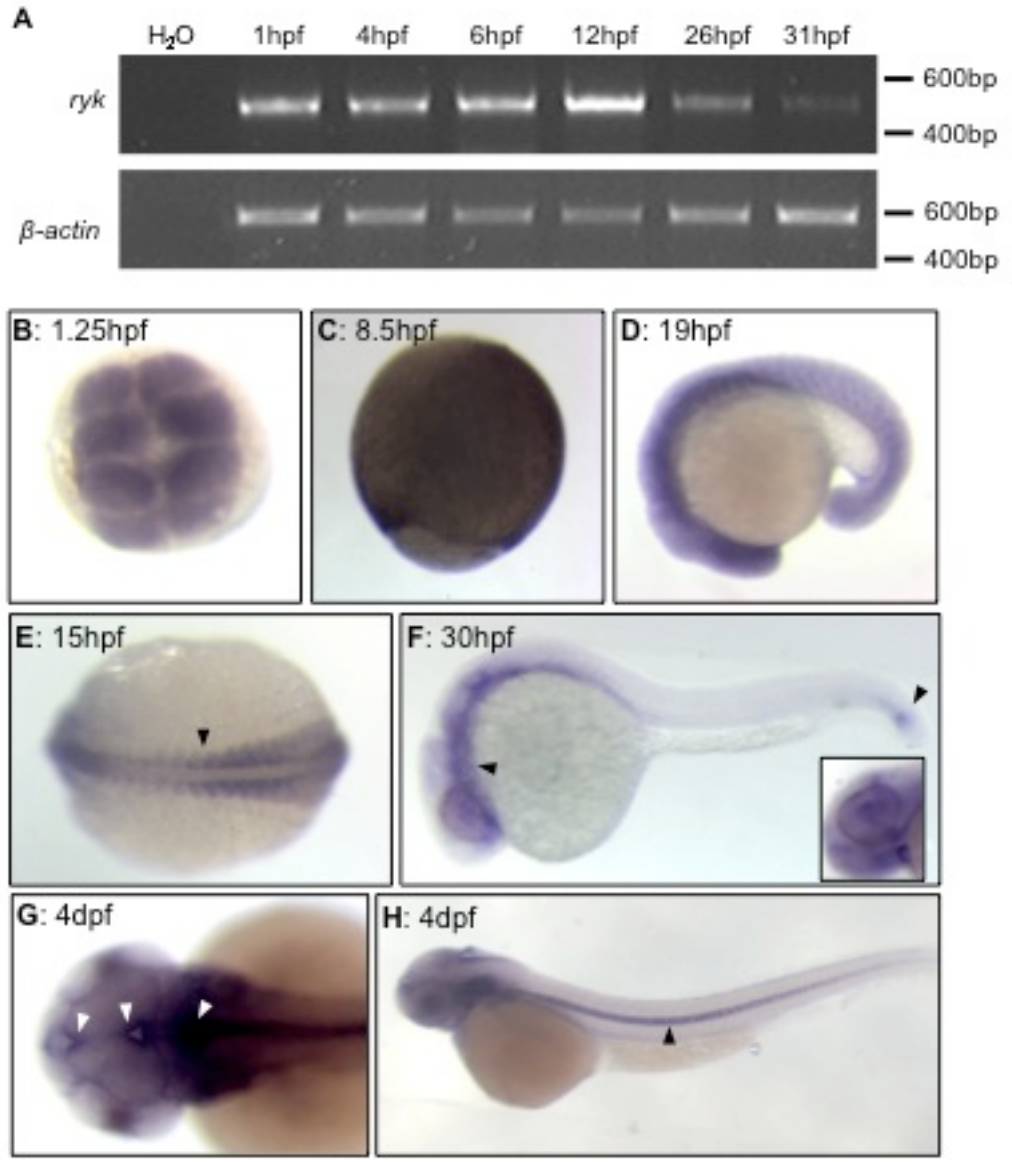

Figure 24: Zebrafish *ryk* expression profile. (A) Semi-quantitative RT-PCR showing temporal *ryk* expression. (B-E) Whole-mount in situ hybridization reveals ubiquitous *ryk* expression throughout maternal (B) and gastrula stages (C-E) with enrichment in somites (E, arrowhead) and the central nervous system. (F) At 30hpf, *ryk* is expressed in the brain and tail (arrowheads) and notably the eyes (inset). (G-H) At 4dpf, *ryk* is expressed in the lining of ventricular zones (G, arrowheads) and notochord (H, arrowhead). Stages and orientation: 1.25hpf, animal pole view; 8.5hpf, lateral view; 15hpf, dorsal view with anterior to the left; 19hpf and 30hpf, lateral view with anterior to the left; 4dpf, dorsal view of brain and lateral view of the whole body, anterior to the left.

Source: Lin, S., Baye, L.M., Westfall, T.A., and Slusarski, D.C. (2010). Wnt5b-Ryk pathway provides directional signals to regulate gastrulation movement. J Cell Biol *190*, 263-278.

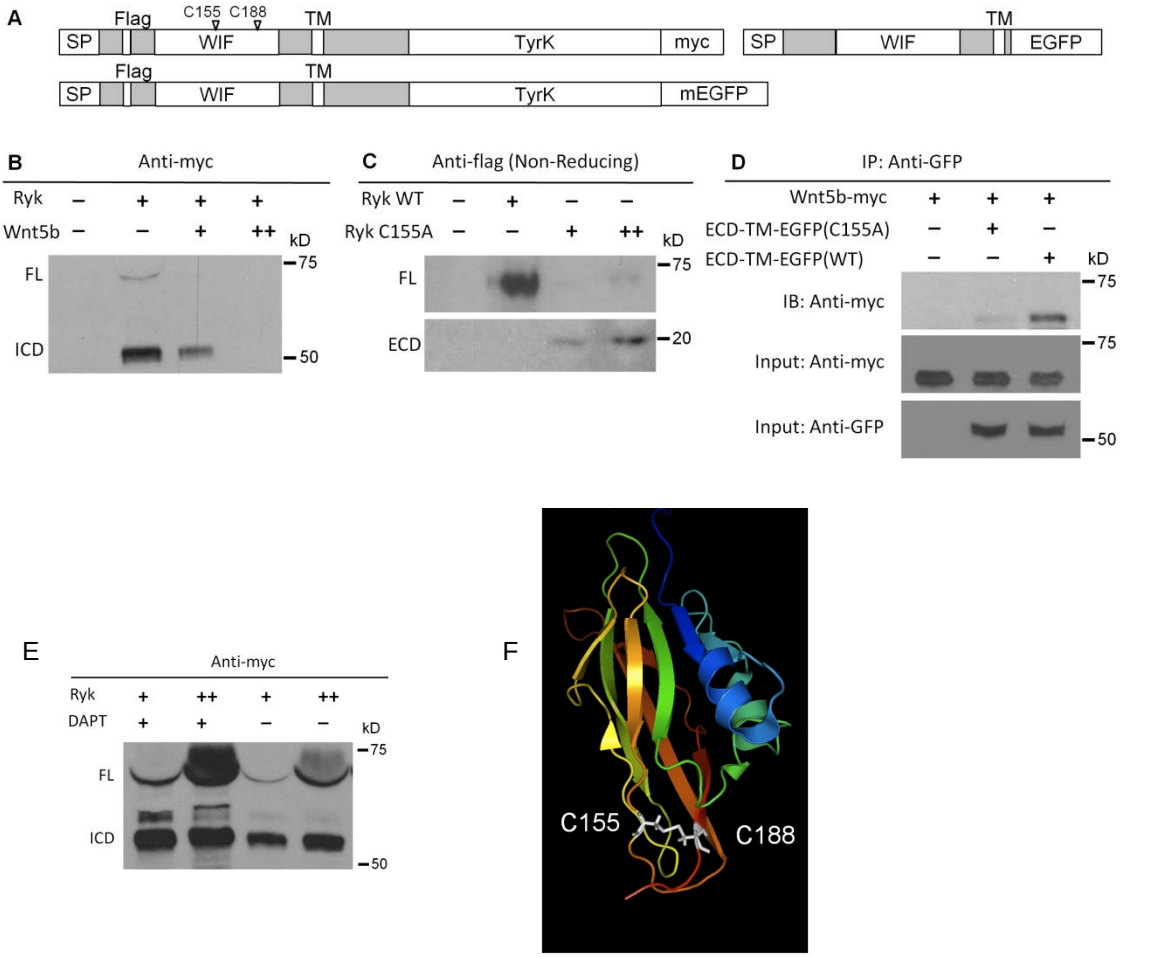

Figure 25: Ryk processing and domain localization. (A) Schematic of three different Ryk expression constructs. SP: signal peptide; WIF: Wnt-Inhibitory Factor domain; TM: Trans-Membrane domain; TyrK: Tyrosine Kinase domain. The positions of C155 and C188 are noted. (B) Western analysis of flag-Ryk-myc with increasing amounts of Wnt5b reveals Ryk cleavage with ICD and turnover. Tagged *ryk* RNA was injected at 20pg; *wnt5b* RNA was injected at 5pg (+) and 10pg (++). (C) Western analysis of flag-Ryk-myc under non-reducing conditions showing differential accumulation of Ryk full-length (FL) and ECD forms with wild-type and Ryk C155A ECD expression constructs. *ryk* RNA injected at 20pg; *ryk* C155A RNA injected at 20pg (+) and 50pg (++). (D) Co-immunoprecipitation analysis showing Wnt5b-myc interacts with Ryk ECD-TM-EGFP and not with Ryk C155A mutant. Wnt5b-myc injected at 10pg; WT and C155A ECD-TM-EGFP injected at 50pg. (E) Western-blot under reducing conditions. *ryk* RNA was injected at 20pg for low dose (+) and 35pg for high dose (++). DAPT in DMSO (25mM) was diluted to 100µM with egg water; mock treatment with the same concentration of DMSO was for control. (F) Disulfide bond-forming cystein residues (C155 and C188, shown in white sticks view) are present in the ECD of Ryk. The structure is derived from NMR structure of human WIF-1 (Liepinsh et al., 2006) and presented with PyMOL.

Source: Lin, S., Baye, L.M., Westfall, T.A., and Slusarski, D.C. (2010). Wnt5b-Ryk pathway provides directional signals to regulate gastrulation movement. J Cell Biol *190*, 263-278.

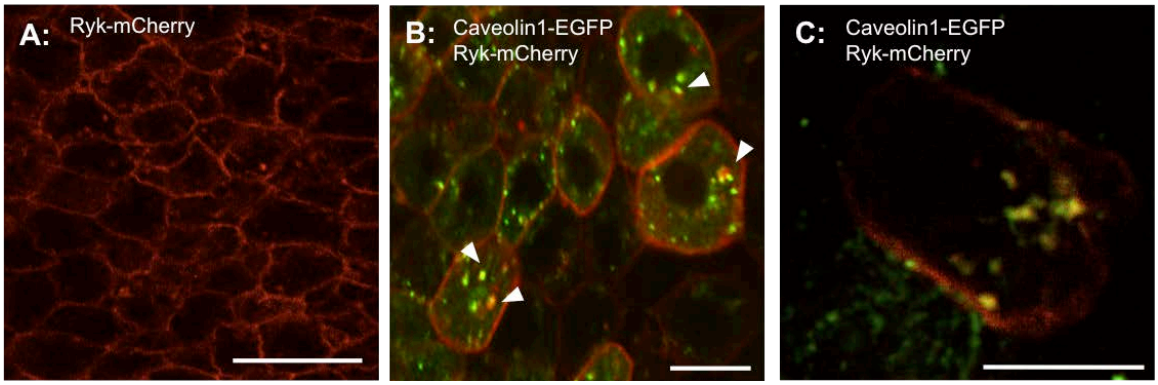

Figure 26: Localization of Ryk-mCherry in the absence of Wnt5b MO and colocalization of Caveolin1-EGFP and Ryk-mCherry. (A) Ryk-mCherry is expressed on the plasma membrane. (B-C) Caveolin1-EGFP and Ryk-mCherry co-localize when co-injected in embryos. EGFP and mCherry positive endocytic vesicles are indicated by arrowheads. Scale bars: 30μm in A, and 10μm in B-C.

Source: Lin, S., Baye, L.M., Westfall, T.A., and Slusarski, D.C. (2010). Wnt5b-Ryk pathway provides directional signals to regulate gastrulation movement. J Cell Biol *190*, 263-278.

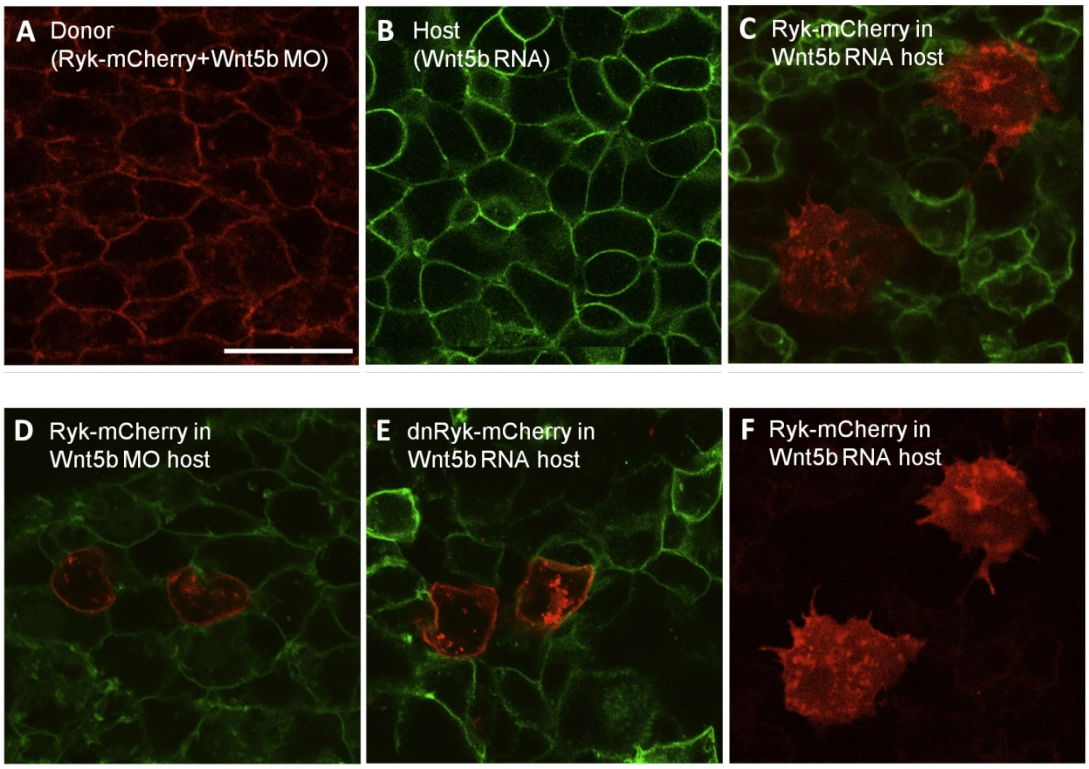

Figure 27: Ryk-expressing cells respond to Wnt5b stimulus by internalizing Ryk and protrusion formation. (A-F) Confocal images of hypoblast cells in 90% epiboly stage embryos, lateral view. Donor embryo with Ryk-mCherry and Wnt5b MO (A); host embryo with Wnt5b-IRES-EGFP-CAAX (B). Donor Ryk-mCherry+Wnt5bMO cells (red) transplanted into a Wnt5b-IRES-EGFP-CAAX host (green) (C). Red channel from (C) showing Ryk internalization and extensive protrusion formation in the transplanted cells (F). Donor Ryk-mCherry+Wnt5b MO cells transplanted into a EGFP-CAAX+Wnt5b MO host (D). Donor dnRyk-mCherry+Wnt5b MO cells transplanted into Wnt5b-IRES-EGFP-CAAX host (E). (G-I) Measurement of cell roundness frequency of transplanted cells. Donor and host combination and the color code for each transplantation experiment (group 1-4) are listed (G). A column chart shows the average roundness and standard error (H) and a cumulative frequency chart shows the distribution of roundness for each group (I). 50 cells were measured for each group. One-way ANOVA and Tukey HSD Test were applied, showing that group 4 is significantly different than group1-3 (asterisks, $p<0.01$). Scale bar: 30μm.

Source: Lin, S., Baye, L.M., Westfall, T.A., and Slusarski, D.C. (2010). Wnt5b-Ryk pathway provides directional signals to regulate gastrulation movement. J Cell Biol *190*, 263-278.

Figure 27 continued

G

		Donor	Host
1	◆	dnRyk-mCherry + Wnt5b MO	Wnt5b-IRES-EGFP-CAAX
2	■	Ryk-mCherry + Wnt5b MO	EGFP-CAAX + Wnt5b MO
3	▲	mCherry-CAAX + Wnt5b MO	EGFP-CAAX + Wnt5b MO
4	×	Ryk-mCherrry + Wnt5b MO	Wnt5b-IRES-EGFP-CAAX

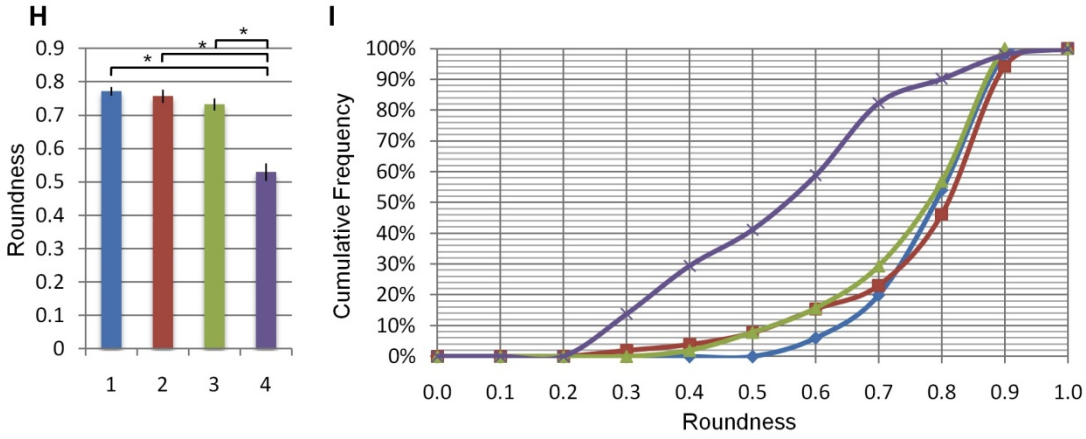

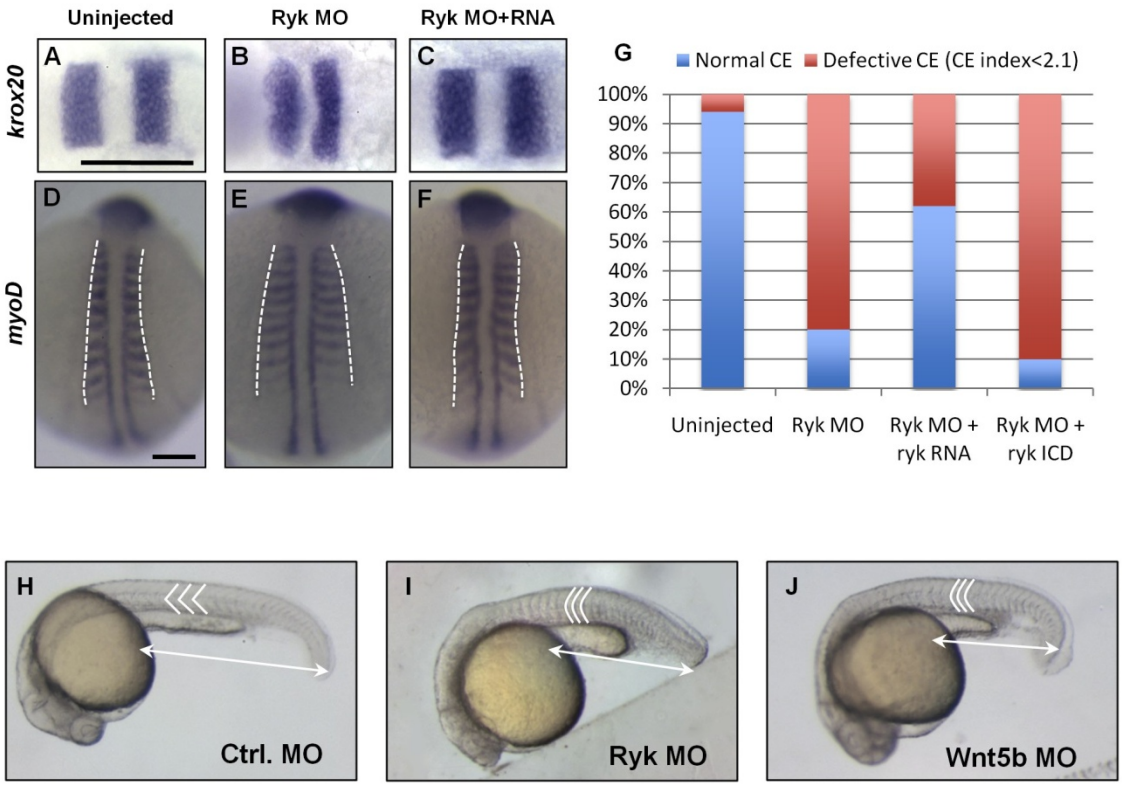

Figure 28: Zebrafish *ryk* loss-of-function phenotype. (A-F) Evaluating CE with markers. Dorsal view, anterior to the left of krox20 expression in uninjected (A), Ryk MO injected (B) and Ryk MO co-injected with *ryk* RNA (C) embryos. Dorsal view, anterior to the top of myoD expression in uninjected (D, n=32), Ryk MO injected (E, n=25), and Ryk MO coinjected with *ryk* RNA (F, n=29). (G) Quantification of the CE phenotype, incldluing embryos coinjected with Ryk MO and *ryk* ICD RNA (n=30). (Ryk MO, 2.0 pmol; *ryk* RNA, 50pg; *ryk* ICD RNA, 50pg). Columns display percentage of embryos at 10-11 somite stage with normal (blue) or defective (red) CE index. (H-J) Morphological phenotypes at 24hpf. Control MO injected (H) with even-spaced, V-shaped somites, Ryk MO (I) and Wnt5b MO injected (J) embryos with reduced posterior AP axis (double-head arrow), and curved, tightly-packed somites (white lines). Lateral view with anterior to the left. (K-N) Transverse central retina confocal images of 3dpf huc:GFP transgenic embryos. Control (K), Ryk MO (L), Wnt5b MO (M), and Ryk MO with *ryk* RNA (N) injected embryos. The two organized sublaminae in the wild-type Inner Plexiform Layer (IPL) (K, arrows) are less organized in both the Wnt5b (M, arrowhead) and Ryk (L, arrowhead) morphants. *ryk* RNA co-injection partially rescues Ryk MO-induced phenotype (N, arrows). Scale bars: 150 µm in A and D, 5µm in N.

Source: Lin, S., Baye, L.M., Westfall, T.A., and Slusarski, D.C. (2010). Wnt5b-Ryk pathway provides directional signals to regulate gastrulation movement. J Cell Biol *190*, 263-278.

Figure 28 continued

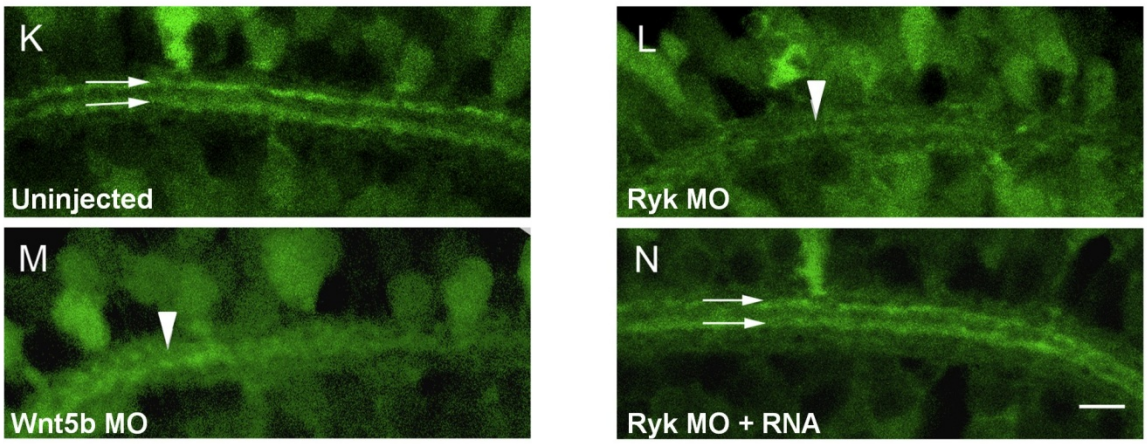

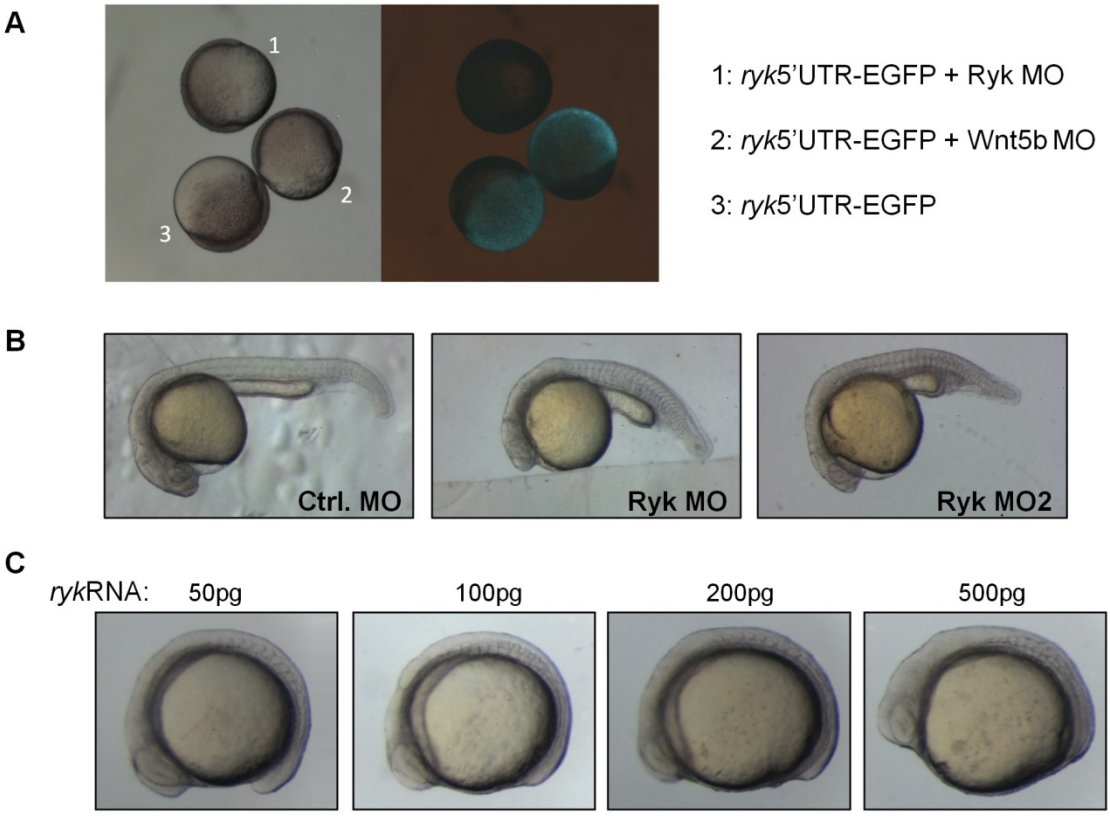

Figure 29: *ryk* knockdown and RNA injection. (A) Ryk MO efficacy evaluated with the 5'UTR-EGFP RNAs. Embryo 1: Ryk MO+*ryk*5'UTR-EGFP; embryo 2: Wnt5b MO+*ryk*5'UTR-EGFP; embryo 3: *ryk*5'UTR-EGFP. (B) Two non-overlapping Ryk MOs generate the same phenotype compared to the control embryo. (C) *ryk* RNA injection leads to CE defects in a dose-dependent manner. Lateral view shown with anterior to the left in B and C.

Source: Lin, S., Baye, L.M., Westfall, T.A., and Slusarski, D.C. (2010). Wnt5b-Ryk pathway provides directional signals to regulate gastrulation movement. J Cell Biol *190*, 263-278.

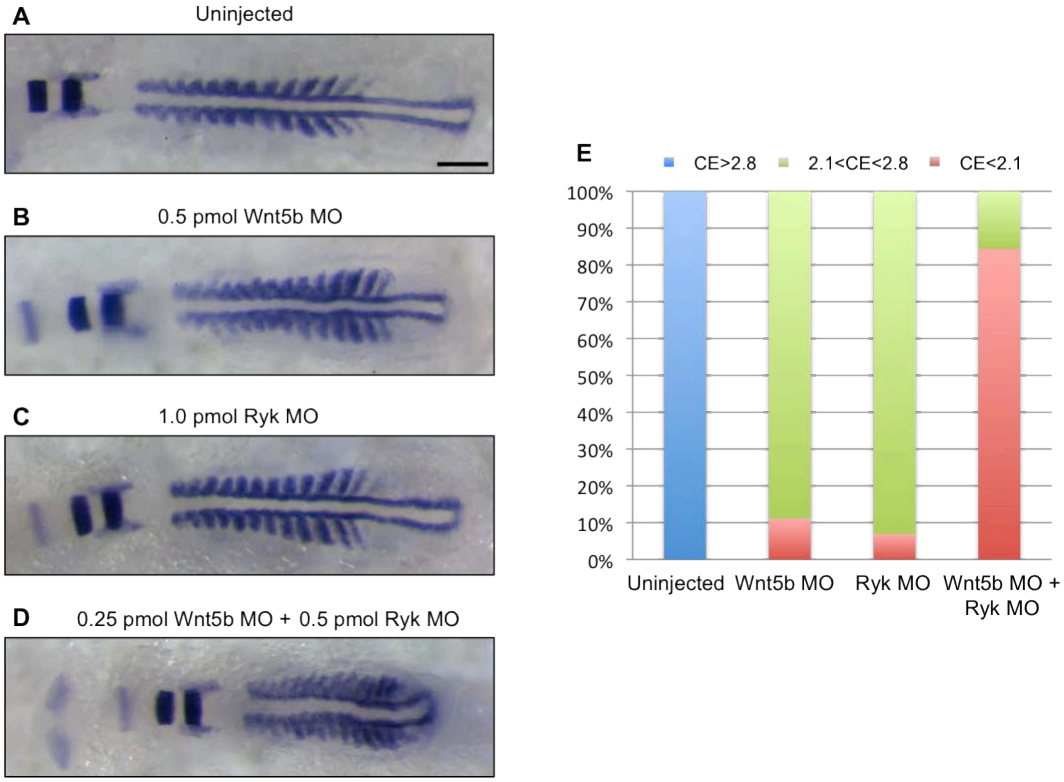

Figure 30: Wnt5b and Ryk show synergistic effects in zebrafish CE. (A-D) In situ hybridization with combined myoD, krox20 and pax2a probes. Dorsal view, anterior to the left of control (A), low-dose Wnt5b MO (0.5 pmol) (B), low-dose Ryk MO (1.0 pmol) (C), and combined Wnt5b MO (0.25 pmol) and Ryk MO (0.5 pmol) (D) injected embryos. (E) Quantification of CE index defects. Scale bar: 150 µm.

Source: Lin, S., Baye, L.M., Westfall, T.A., and Slusarski, D.C. (2010). Wnt5b-Ryk pathway provides directional signals to regulate gastrulation movement. J Cell Biol *190*, 263-278.

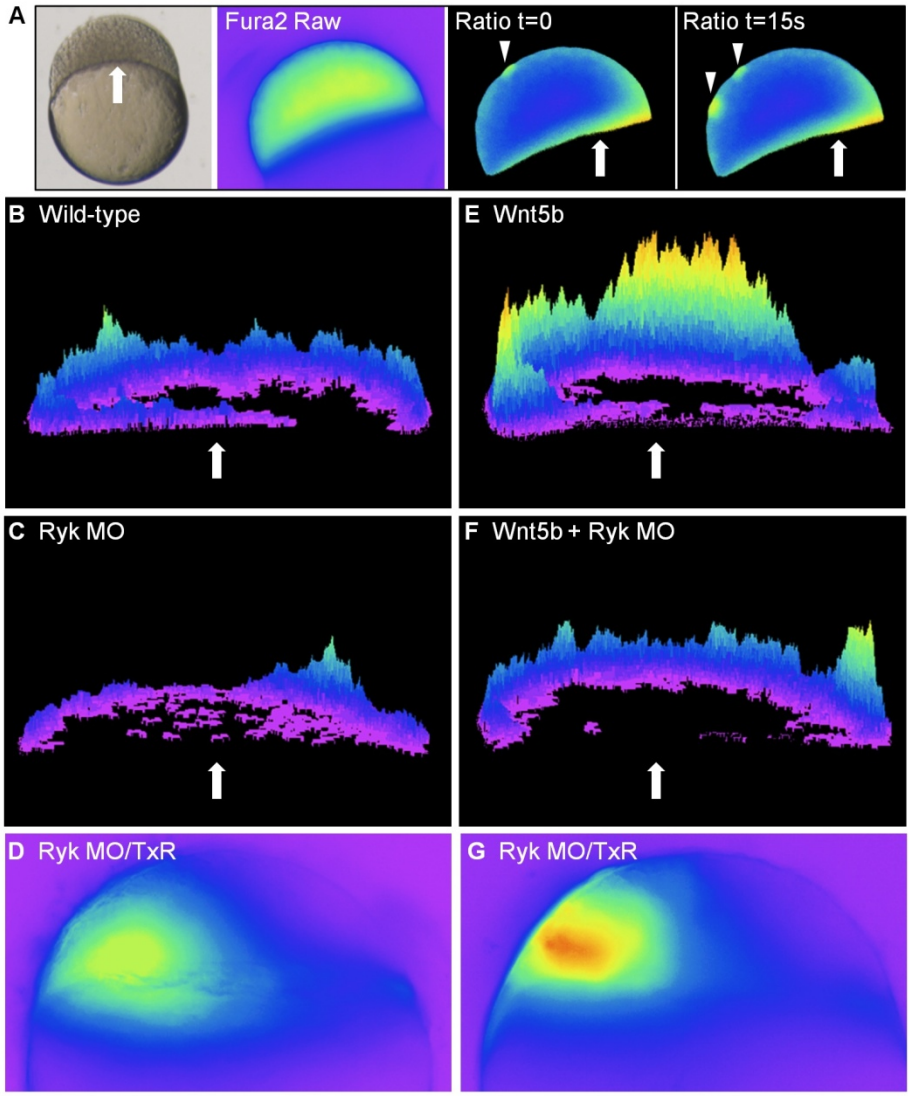

Figure 31: Wnt5b/Ryk modulation of calcium release. (A) Analyzing Ca2+ release in zebrafish blastula/epiboly stage embryos. Ca2+ detected by Fura2 ratiometric dye. Sample ratio images collected at 15s intervals with time t=0s compared to t=15s showing examples of Ca2+ release events in the EVL (arrowhead) and YSL (arrow). (B-D) Ryk knockdown blocks endogenous Ca2+ release. Endogenous Ca2+ release in control embryo (B). Unilateral injection of Ryk MO reduced endogenous Ca2+ activity (C); lineage tracer TexasRed co-mixed with Ryk MO reveals the injected side (D). (E-G) Ryk deficiency blocks Wnt5b-induced Ca2+ release. Wnt5b injection activates Ca2+ release (E). Unilateral injection of Ryk MO suppressed Wnt5b-induced activation (F); lineage tracer indicates the injected side (G). Arrows note the YSL.

Source: Lin, S., Baye, L.M., Westfall, T.A., and Slusarski, D.C. (2010). Wnt5b-Ryk pathway provides directional signals to regulate gastrulation movement. J Cell Biol *190*, 263-278.

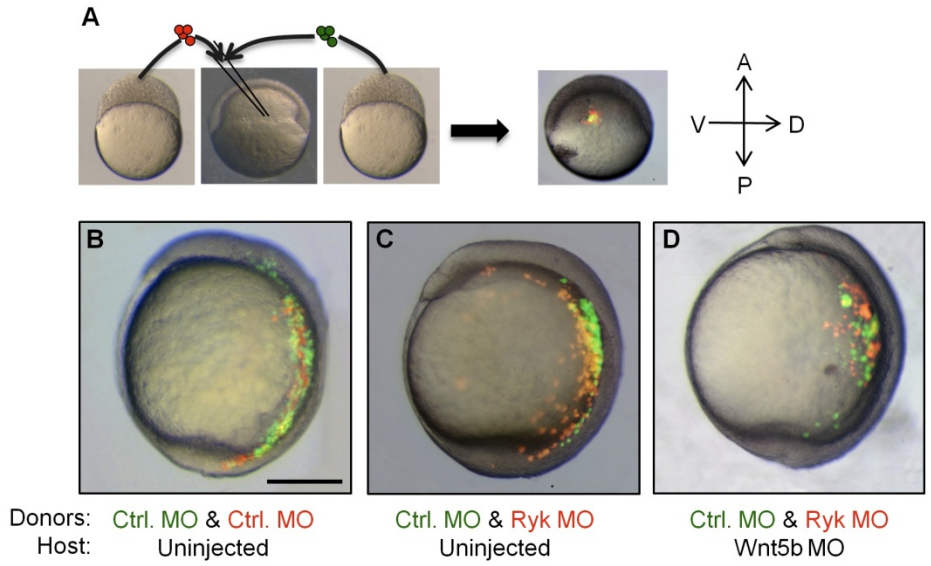

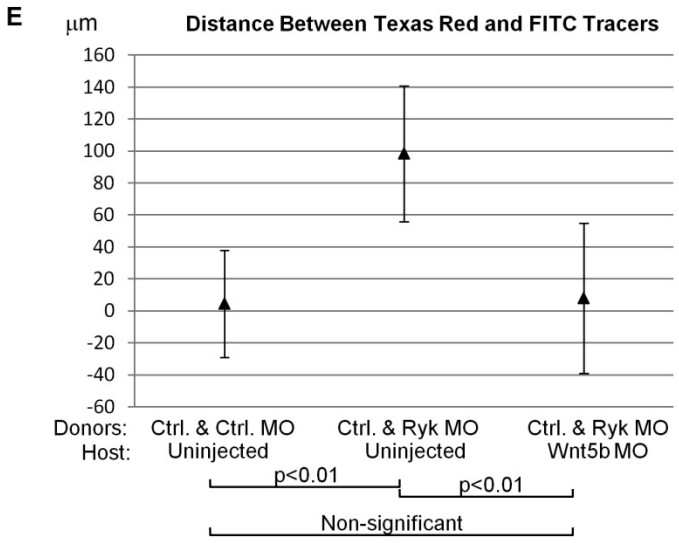

Figure 32: Ryk deficiency leads to directional cell migration defects in a Wnt5b-dependent manner. (A-D) Assessment of cell migration. Donor cells separately labeled with FITC (green) or TexasRed (red) were transplanted into the center of the lateral mesoderm at the germring margin (A). Uninjected host with control MO injected (red and green) donor cells (B); uninjected host with control MO injected (green) and Ryk MO injected (red) donor cells (C); Wnt5b MO injected host with control MO injected (green) and Ryk MO injected (red) donor cells (D). (E) Quantification of the average distance between green and red tracers. 10 embryos were scored for each group and error bars represent standard deviation. One-way ANOVA and Tukey HSD Test were used to determine statistical significance. Scale bar: 250 µm.

Source: Lin, S., Baye, L.M., Westfall, T.A., and Slusarski, D.C. (2010). Wnt5b-Ryk pathway provides directional signals to regulate gastrulation movement. J Cell Biol *190*, 263-278.

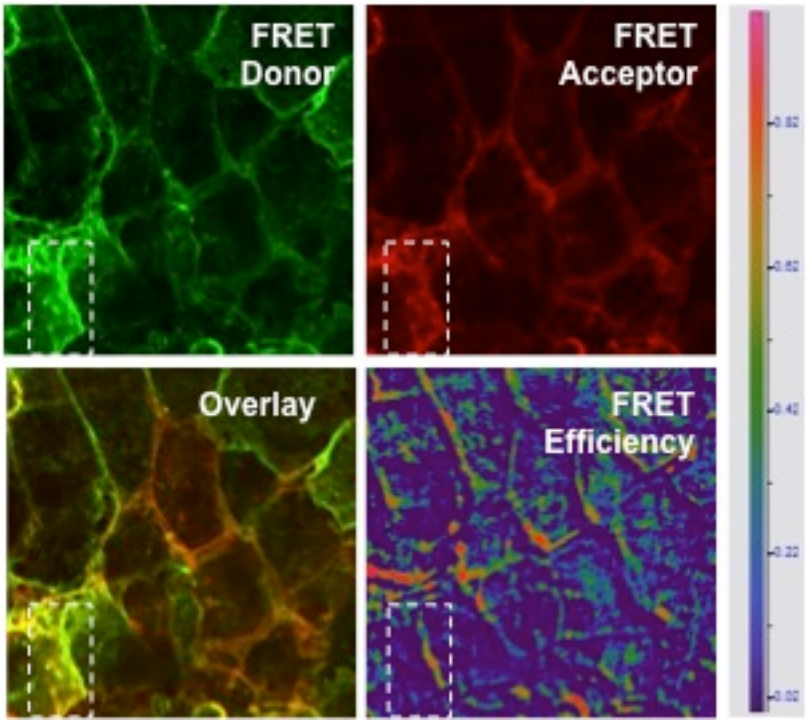

Figure 33: FRET experiments showing oligomerization of membrane Ryk proteins. White box outlines a region where FRET signals occurred in membrane, but not in cytoplasm even though donor and acceptor signals were colocalized.

CHAPTER VI
WNT5B-RYK PATHWAY PROVIDES DIRECTIONAL INFORMATION IN CELL MOVEMENT

Introduction

In the context of this study, we use the term "permissive" to describe a ligand-triggered event, in which the recipient cell's response is determined by the presence/absence of ligand (or whether the ligand reaches a threshold level); and the term "instructive role" to refer to a process, in which the recipient cells' response depends on their position relative to the ligand source or that the response is correlated with the direction of the morphogen/ligand gradient. Non-canonical Wnts are largely believed to act as permissive cues for vertebrate cell movement via Frizzled (Fz). Here we tested the hypothesis that Wnt5b can provide directional information in Ryk-mediated cell migration.

Directional cell migration in zebrafish gastrulation is manifested by coordinated locomotion of all cells in the germ layer. The resulting tissue movement toward the midline and the overall narrowing/lengthening of the tissue is known as convergent extension (CE) (Solnica-Krezel, 2005). β-catenin independent, or non-canonical, Wnt signaling is pivotal in vertebrate CE (Rohde and Heisenberg, 2007). In Drosophila, the Planar Cell Polarity (PCP) pathway establishes polarity in epithelial cells (Zallen, 2007). Despite shared core components (Zallen, 2007), non-canonical Wnt activities in vertebrates are not fully explained by the mechanisms of *Drosophila* PCP. Compared to *Drosophila* epithelia, vertebrate mesenchyme possess different physiological traits and dynamic cell behaviors such as directional migration, as well as planar and radial cell intercalations (Yin et al., 2008). Moreover, Drosophila Wnt mutants do not exhibit PCP phenotypes, whereas zebrafish Wnt mutants (*wnt5b/pipetail* and *wnt11/silberblick*) have cell movement defects (Solnica-Krezel, 2005). Since *wnt5b* and *wnt11* RNAs rescue the *wnt11* genetic mutant (Heisenberg et al., 2000; Kilian et al., 2003), non-canonical Wnts

are largely believed to have a permissive role in CE. However, zygotic loss of *wnt5b/pipetail* displays severe CE defects (Rauch et al., 1997a) and cannot be rescued by exogenous *wnt5b* RNA (Kilian et al., 2003; Westfall et al., 2003a), suggesting that Wnt5 signaling may be both permissive and instructive. Receptor tyrosine kinases (RTKs), including Related to Tyrosine Kinase (Ryk) are Wnt responsive (Cadigan and Liu, 2006; Nusse, 2008). In fact, both Drosophila Wnt5 and vertebrate Wnt5a act as repulsive cues to Ryk-expressing neurons (Keeble and Cooper, 2006; Keeble et al., 2006; Liu et al., 2005; Yoshikawa et al., 2001). We hypothesize that a Wnt-dependent mechanism is utilized in concert with the conserved PCP framework to coordinate precise vertebrate CE movements.

Ryk signaling has been shown to be independent of Fz, as well as facilitating Fz activity. In *C. elegans*, Ryk is necessary to polarize vulval cells and genetic analysis indicates that Ryk and Fz are involved in separate pathways (Green et al., 2008; Inoue et al., 2004). Ryk and Fz have opposing roles in Wnt5-mediated Drosophila salivary gland migration (Harris and Beckendorf, 2007), and Wnt3a-mediated retinal ganglion cell axon outgrowth in chick and mouse (Schmitt et al., 2006). In contrast, Ryk synergizes with Fz to facilitate Fz-dependent signaling in *Xenopus* (Kim et al., 2008) and 293T cells (Lu et al., 2004). Knockdown of *Xenopus* Ryk results in gastrulation defects with compromised Wnt11-induced Fz7 and Disheveled (Dvl) endocytosis (Kim et al., 2008). In zebrafish, Wnt11 does not induce Fz7/Dvl endocytosis, but rather stimulates Fz7/Dvl accumulation on the plasma membrane (Witzel et al., 2006), raising the possibility that Wnt/Ryk and Wnt/Fz signaling pathways are distinct.

We find that Ryk deficiency in zebrafish leads to gastrulation defects and that Ryk acts downstream of Wnt5b to regulate directional cell movement. Co-culture of zebrafish animal caps demonstrates that Wnt5b acts as an instructive cue. In this assay, Wnt5b expressing cells and Fz2 expressing cells show extensive intermingling; in contrast, Wnt5b-expressing and Ryk-expressing cells demonstrate restrictive

intermingling and Ryk cells show directed migration away from the Wnt5b source. We find that Fz2, but not Ryk, recruits Dvl to discrete domains on the plasma membrane, similar to previously reported Wnt11/Fz7 interactions (Witzel et al., 2006) and consistent with our working model that Wnt5/Ryk and Wnt5/Fz lead to distinct signaling outputs. Our findings demonstrate that non-canonical Wnt signaling modulates zebrafish cell movement via two separate mechanisms: activating the core PCP components to establish cellular polarity (Simons and Mlodzik, 2008), and Ryk-mediated signaling to regulate directional cell migration.

Intracellular signaling from Ryk cannot be uncoupled with its Wnt5b-sensing activity for gastrulation movement

We found that co-injection of Ryk MO and MO-resistant *ryk* RNA, at a subphenotypic dose (50ng, Figure 29 C) is sufficient to suppress the CE defects to only 38% (Figure 28 G). Since most of the exongenously expressed Ryk protein was found in the ICD size (Figure 25 B), and the mammallian processed ICD was shown to drive neuronal differentiation in cell culture (Lyu et al., 2008), we compared non-directional signaling by Ryk-ICD and directional signaling by full-length Ryk. We found that only full-length Ryk, but not Ryk ICD, suppresses Ryk-MO induced CE defects (Figure 28 G), suggesting that Ryk ICD alone is not sufficient to substitute for full-length Ryk.

To evaluate ECD and ICD distribution in response to Wnt5b, we performed cell transplantation assays. In donor embryos expressing flag-Ryk-EGFP, both ECD (flag) (Figure 34 A) and ICD (EGFP) (Figure 34 B) show membrane localization (Figure 34 C). When transplanted into a Wnt5b-expressing host, the flag-Ryk-EGFP expressing cells show increased protrusive activities (Figure F, arrowhead) and both the ECD and ICD are internalized with overlapping localization (Figure F, asterisk). These data coupled with the functional analyses suggest that cell shape changes in response to Wnt5b do not

require the separation of Ryk ECD and ICD and in fact, both portions of Ryk are required to properly convey directional Wnt5b signals.

Wnt5b-Ryk pathway is separated from Frizzled-mediated pathways

The impact of Ryk on canonical Wnt pathway

Ryk signaling has been shown to be independent of Fz, as well as facilitating Fz activity. Conflicting data from published sources exist, with regard to whether Ryk acts as co-receptors for Fz during canonical Wnt signaling (Lu et al., 2004; Lyu et al., 2008). It is noteworthy that LRP5/6 has been established as an essential co-receptor for canonical Wnt signaling (He et al., 2004). Should Ryk receptor indeed play a role as co-receptor in canonical Wnt signaling, it would demonstrate dynamic interaction of multiple membrane proteins composed of RTK, GPCR-like and LDL-related receptors. We postulate that Ryk is not an essential factor or core component of canonical Wnt signaling. We based this conjecture on previous knowledge: 1) regulators of canonical Wnt signaling are strongly associated with DV patterning in early embryonic development; and 2) neither Ryk-overexpression nor Ryk knockdown results in DV patterning defects (Figure 29).

To accurately test the impact of Ryk on canonical Wnt signaling, we utilized the dual luciferase TOP-FLASH reporter assay, which has been widely used in studies aiming at identification of novel regulators of canonical Wnt signaling (Angers et al., 2006). We found that neither Ryk-overexpression nor Ryk knockdown leads to changes in the luciferase activity at a level that is comparable to changes induced by a constitutively active β-catenin. Contrary to previous report suggesting Ryk as a positive component enhancing β-catenin signaling in 293T cells (Lu et al., 2004), manipulating Ryk expression level in zebrafish suggests that Ryk might negatively regulate β-catenin

signaling. Changes in the luciferase activity with Ryk overexpression is insignificant, while Ryk knockdown results in slight but statistically significant increase of TOP-FLASH luciferase activity (Figure 35).

We confirm that Ryk is not an essential component of canonical signaling and is not involved in the DV patterning of zebrafish gastrula. However, our experiments did not rule out the possibility that Ryk positively regulates β-catenin signaling in other contexts, as signaling intensity can be altered by intricate interplay of various membrane proteins/lipids.

Fz2 and Ryk demonstrate distinct responses to Wnt5b

Since Ryk signaling has been shown to both be distinct from Fz (Harris and Beckendorf, 2007; Inoue et al., 2004; Schmitt et al., 2006) as well as facilitate Fz signaling (Kim et al., 2008; Lu et al., 2004) in different models, we also evaluated Fz protein distribution in response to Wnt5b activation in zebrafish. *In vivo* imaging of Fz2-mCherry-expressing cells show predominantly membrane localization in donor embryos (Figure 36 A). When transplanted into Wnt5b-expressing hosts, Fz2-mCherry expressing cells demonstrate membrane localization (Figure 36 B, arrowheads) and overall cell shape does not change compared to controls.

Since Fz is known to recruit Dvl to the cell membrane (Zallen, 2007), we next determined the extent that Ryk and Fz influence Dvl membrane localization. We utilized mosaic injections to analyze receptor and Dvl distribution relative to Wnt5b stimulation. At 8-16 cell stage, one cell of an embryo was injected with Fz2-mCherry co-mixed with Dvl-EGFP and an adjacent cell was injected with Wnt5b-IRES-nls-EGFP (Figure 37 A) and imaged at 90% epiboly stage. When adjacent to Wnt5b expressing cells, Dvl-EGFP and Fz2-mCherry co-localize in discrete domains on the plasma membrane (Figure 37 B-D). A majority of Dvl-EGFP positive areas also show Fz2-mCherry localization (90 ± 3%; Figure 37 K). To determine if Ryk activity was necessary for Fz2 and Dvl co-

localization, Ryk MO was co-injected with Dvl-EGFP and Fz2-mCherry. Ryk deficiency did not compromise Dvl-EGFP and Fz2-mCherry co-localization (Figure 37 E-G), as 95 ± 2% of the Dvl-EGFP positive area also displayed Fz2-mCherry localization (Figure 37 K). Ryk-mCherry, in response to Wnt5b stimulus presents with only 18 ± 2% Dvl-EGFP co-localization (Figure 37 H-K) and internal Dvl-EGFP distribution instead of membrane (Figure 37 I). We conclude that Wnt5b/Ryk and Wnt5b/Fz2 interactions demonstrate distinguishable effects on Dvl localization and cellular protrusions, suggesting that the two pathways lead to distinct downstream events.

Ryk conveys directional Wnt5b signals in migrating cells

Create directional Wnt5b signals *ex vivo*

Wnts are a large family of secreted glycoproteins that act both as short- and long-range ligands to activate receptor-mediated signaling pathways. Measuring directional Wnt signaling *in vivo* is complicated by the presence of multiple ligands, heterogeneity of the cells, and mostly lack of defined signaling direction. *In vitro* assays based on cell culture system are often limited because matrix-based movement can be drastically different from cell movement inside tissues where cell-cell contact provides important feedback on migrating cells. To solve this problem, we developed an explant co-culturing assay to create directional Wnt5b signals *ex vivo*.

To test if Wnt5b-Ryk signaling provides directional cues for cell movement, we adapted an animal cap explant co-culture assay developed to monitor Eph/Ephrin mediated repulsion in zebrafish (Mellitzer et al., 1999). We generated Wnt5b directional signals by juxtaposing a *wnt5b* RNA injected explant with a Wnt5b MO injected explant, both of which were dissected from embryos at mid-blastrula transition stage (Figure 38 A and B). We verified that Wnt5b signals were propagated from *wnt5b* RNA injected moiety into the Wnt5b MO injected moiety of the explant aggregate by calcium imaging.

We then used two types of measurement to assess cell motility in this artificial Wnt5b gradient: 1) examining cell-intermingling at the interface of the fused animal caps/explants, similar to the method used in the previous study (Mellitzer et al., 1999); and 2) monitoring cell migration in the Wnt5b gradient by transplanted cells into Wnt5b MO injected moiety close to the interface. For cell-intermingling measurement, we used an over-night incubation protocol developed by the original application (Mellitzer et al., 1999). This raises the question whether the blastomeres in explants differentiate in cultures. We tested this question by dissecting explants from transgenic lines with fluorescent reporters and/or examining gene expression in the explant aggregates after prolonged incubation. We found that spontaneous differentiation occurs at an infrequent and stochastic manner. For example, endothelial differentiation only takes place with exogenous Vegfab expression, and only in a small population of cells after >30 hours incubation (data not shown).

Directional Wnt5b signals propagate Ca^{2+} release events

Wnts are a large family of secreted glycoproteins that act both as short- and long-range ligands to activate receptor-mediated signaling pathways. To determine if Wnt5b signals were propagated from *wnt5b* RNA injected moiety into the Wnt5b MO injected moiety of the explant aggregate, we used Ca^{2+} release events as the readout of Wnt5b signaling and performed calcium imaging on aggregates from a Wnt5b-expressing explant and a Wnt5b-depleted explant. We found that control aggregates from explants expressing endogenous Wnt5b demonstrates baseline calcium activity in the form of periodic transients on the perimeter and sustained level on the interface (Figure 38 C). In contrast, a Wnt5b-depleted explant when juxtaposed to a Wnt5b-expressing explant, exhibits significantly elevated Ca^{2+} release events (Figure 38 D). We concluded that co-cultured explants generate directional Wnt5b signals that are sufficient to activate physiological responsens in the adjacent explants.

Cellular responses at the interface of explant aggregates

A control mCherry-CAAX injected cap co-cultured with an EGFP-CAAX injected cap showed intermingling of EGFP and mCherry expressing cells (Figure 39 B and Table 4). Similarly, a Wnt5b-expressing cap co-cultured with a Fz2-mCherry/Wnt5bMO injected cap revealed intermingling of EGFP and mCherry cells (Figure 39 C and Table 4). In contrast, a Wnt5b-expressing cap co-cultured with a Ryk-mCherry/Wnt5b MO injected cap did not show cell intermingling (Figure 39 E and Table 4); rather, a border of reduced Ryk-mCherry signals, approximately 3-4 cells wide, was found at the interface of the two caps (Figure 39 E, asterisk). This gap was not due to cell loss (Figure 39 H and I) and indicates potential receptor turnover. Since *wnt11* mutants also demonstrate CE defects (Heisenberg et al., 2000), we evaluated Ryk response to a directional Wnt11 signal. A Wnt11-expressing cap co-cultured with a Ryk-mCherry expressing cap showed intermingling of cells (Figure 39 D and Table 4). Taken together, these data reveal that Wnt5b and Ryk expressing cells do not intermingle and suggests that Ryk is turned over in the presence of sustained Wnt5b signals.

Transplanted Ryk-expressing cells migrate away from Wnt5b

We noted that Ryk-mCherry expressing cells at the interface showed the leading edge oriented away from the Wnt5b source (Figure 39 F, arrowhead), we therefore performed time-lapse imaging to follow cell movement, as well as the direction of lamellipodia-like protrusions. To follow membrane dynamics, EGFP-CAAX was co-injected with *ryk* RNA or Ryk MO in donor embryos. Cells from these donor embryos were transplanted into the center of the animal cap aggregate generated from a *wnt5b*-RNA injected cap juxtaposed with a Wnt5b MO injected cap (Figure 40 A). Transplanted cells were imaged over time to evaluate active extension and retraction of lamellipodia-like protrusions (Figure 40 B). Lamellipodia-like protrusions from *ryk* RNA injected cells demonstrated polarized projection with 72% of the protrusions

directed away from the Wnt5b source (Figure 41); in contrast, protrusions from Ryk MO injected cells were random with 52% directed away from and 48% directed toward the Wnt5b source (Figure 42). Compared to Ryk MO injected cells (0.70±0.01), *ryk* RNA injected cells transplanted into the aggregate showed reduced roundness (0.57±0.01) reflective of increased protrusions and cell elongation (Figure 40 C). These results are consistent with previous transplantation experiments and suggest that a Wnt5b can be translated into directional cue by Ryk-expressing cells

Lateral mesoderm cells migrate at a total speed of ~70 μm/h (net dorsal speed at ~40 μm/h) in zebrafish embryos at 80-85% epiboly stage (von der Hardt et al., 2007). Tracking individual Ryk-expressing cells shows migration at a total speed of 105 ± 5 μm/h and net speed away from the Wnt5b source of 51 ± 7μm/h (Figure 40 D and E, Figure 41). On the other hand, Ryk-MO injected cells were relatively immobile (total speed at 40 ± 3 μm/h and net speed away from the Wnt5b source at 8 ± 4μm/h) (Figure 40 D and F, Figure 42).

Directional protrusions in Ryk-expressing cells

To monitor protrusive activity in epiboly stage embryos, Ryk-mCherry and Wnt5b-IRES-nls-EGFP RNAs were injected into individual cells to generate mosaic expression (Figure 43 A). Ryk-mCherry cells adjacent to a Wnt5b-producing cell demonstrated distinct cell shape changes with lamellipodia-like protrusions projected away from the Wnt5b source (Figure 43 B, arrowhead). To determine if Ryk activity was necessary for the directional projection of lamellipodia, RykMO was co-injected with mCherry-CAAX and when adjacent to a Wnt5-producing cell, showed random projections relative to the Wnt5b source (Figure 43 C, arrowhead). A majority of Ryk-expressing cells individually adjacent to one Wnt5b-expressing cell (77%, n=35) show protrusions opposite to the Wnt5b source while only 17% of Ryk-deficient cells (n= 36) show distinct protrusions opposite to the Wnt5b source. Taken together, these data

suggest that Wnt5b/Ryk signaling polarizes cellular projections and directional cell migration.

Materials and methods

Luciferase assay

Zebrafish embryos were injected with either TopFlash and indicated RNAs or MOs at one-cell stage, and allowed to develop into tailbud-stage embryos as previously described (Park and Moon, 2002). After three washes with embryo medium, excess medium was removed and embryos were flash frozen and kept in -80°C. Triplicate samples of 15 embryos each were used for TopFlash dual luciferase assays performed following manufacturer instructions (Promega); and luminescence was detected in a Turner Biosystems 20/20n Luminometer as previously described (Schneider et al., 2008).

Explants co-culture

Experiments were carried out as described previously (Mellitzer et al., 1999), with the exception that the aggregates were imaged alive in glass cover-slips without fixation. Briefly, embryos were injected at one-cell stages with 100pg RNAs. At 1000-cell stage, embryos were dechorionated and animal caps were dissected in L15 medium with 10% fetal calf serum. Animal caps were juxtaposed and heal for 10 min. Aggregate was mounted under a coverslip and cultured overnight. Fluorescent tracers were visualized with confocal microscopy. Non-intermingled aggregates show a clear boundary (of the EGFP moiety) and a dark gap (from the mCherry moiety) wider than 30μm in five non-overlapping 5.7×10^{-8} m^2 squares at the interface. Intermingled aggregates show skewed boundaries, uniform mCherry intensity, and at least five isolated mCherry-positive cell clusters per square in five non-overlapping 5.7×10^{-8} m^2 squares at the interface.

For cell transplantation in the aggregates, animal caps were allowed to heal for 30min in culture medium after juxtaposition. Cells from sphere/dome stage donor

embryos were transplanted to the center of the aggregates with a needle. The aggregates were healed in culture medium for one hour and then mounted under a coverslip and cultured for additional one hour before imaging.

Time-lapse imaging

Confocal images were acquired with a Leica TCS SP2 confocal microscope system, using either a 63X / NA 1.40 oil objective or a 20X / NA 0.70 air objective on a heating stage at 30°C at 30 second intervals. Live samples were mounted in 1% low-melting point agarose and/or corresponding culture medium using bridged coverslips. A string of fiber wick connected the bridged coverslips and a chamber of culture medium to prevent samples from drying. Movies were generated and annotated using ImageJ software.

Discussion

Non-canonical Wnts are speculated to function as permissive cues that do not provide positional signals to components of the PCP pathway (Rohde and Heisenberg, 2007b; Simons and Mlodzik, 2008). Zygotic wnt5b expression is localized in the ventral-posterior region (Kilian et al., 2003), with a graded expression pattern resembling that of mammalian Wnt5a (Yamaguchi et al., 1999). We tested the hypothesis that a Wnt5b gradient could be conveyed to Ryk-expressing cells by co-culturing explants expressing Wnt5b and Ryk, respectively. We found that Wnt5b/Ryk interaction restricted cells intermingling, while Wnt11/Ryk cells freely intermingled. Moreover, lamellipodia-like protrusions of Ryk-expressing cells are projected away from the Wnt5b source, which may underlie repulsive migration. Our data supports a model in which Wnt5b can act as both a permissive cue through Fz and core PCP components, and as an instructive cue through Ryk to regulate directional cell migration during gastrulation.

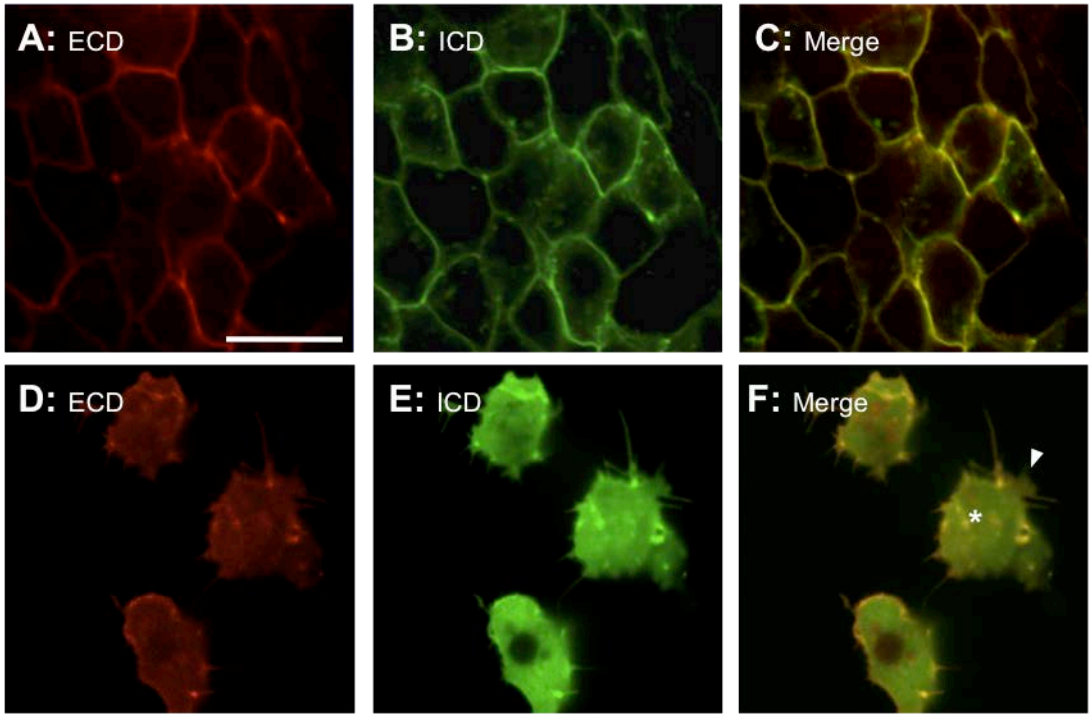

Figure 34: Ryk domain localization. In donor embryos, Flag-tag detects ECD (A); and C-terminal monomeric EGFP detects ICD (B) at 80-90% epiboly; merged images shown (C). After transplantation into a Wnt5b-expressing host, both ECD (D) and the ICD (E) show internalization; merged images shown in (F) and coarse co-localization (asterisk). Note increased protrusive activity of the transplanted cell (F, arrowhead). Scale bar: 20μm.

Source: Lin, S., Baye, L.M., Westfall, T.A., and Slusarski, D.C. (2010). Wnt5b-Ryk pathway provides directional signals to regulate gastrulation movement. J Cell Biol *190*, 263-278.

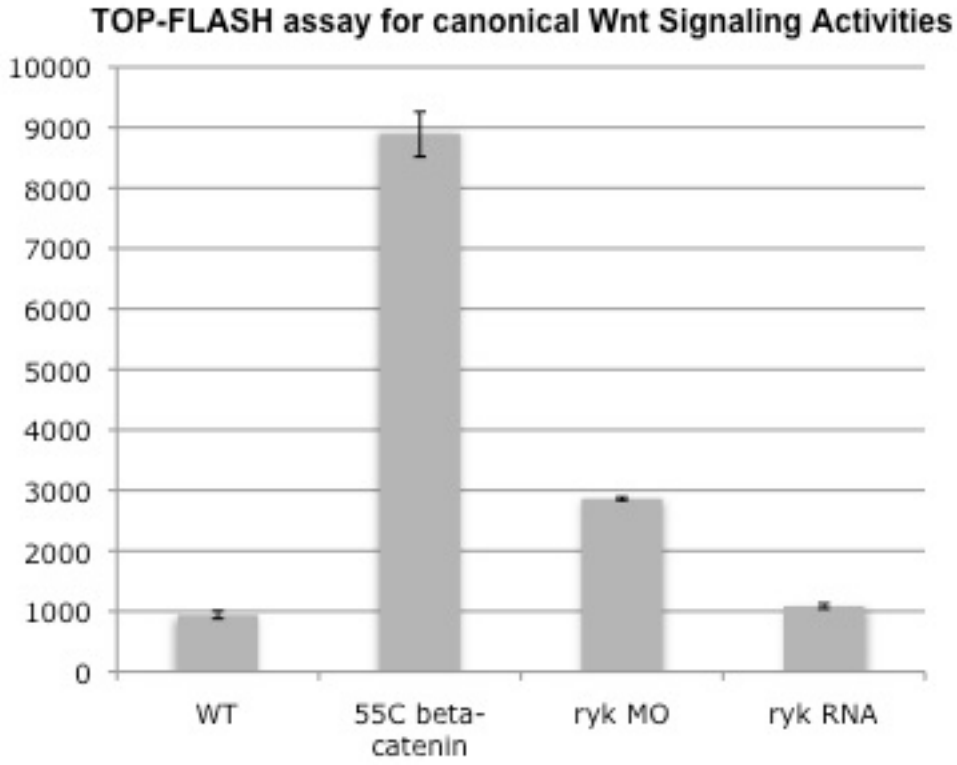

Figure 35: TOP-FLASH assay for canonical Wnt signaling activities in 80% epiboly stage zebrafish embryos. RNA coding for a constitutively active β-catenin (55C β-catenin, with an N-terminal truncation) was injected as a positive control. Ryk MO injection leads to slight increase of TOP-FLASH luciferase activity. *ryk* RNA overexpression leads to a level of TOP-FLASH luciferase activity comparable to that in WT control.

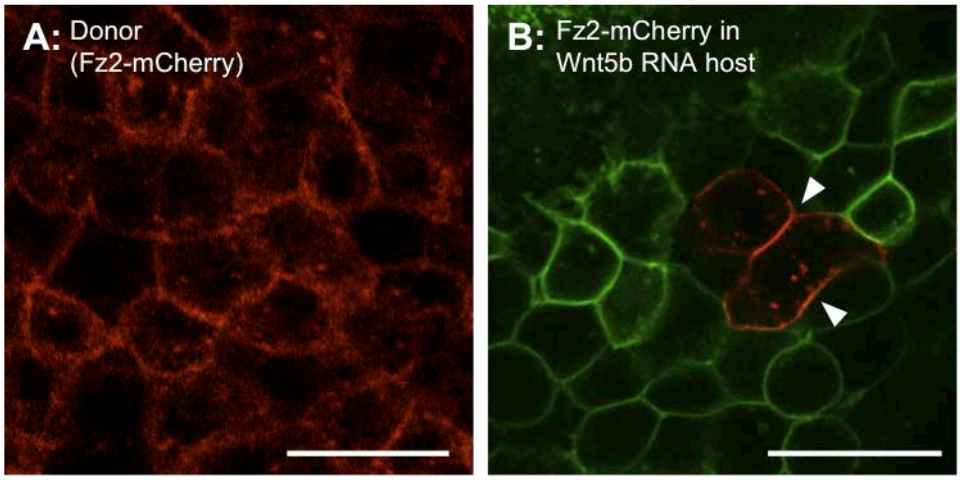

Figure 36: Localization of Fz2-mCherry cells transplanted into Wnt5b-expressing host Cells from donor embryos injected with Fz2-mCherry and Wnt5b MO (A) were transplanted into Wnt5b-expressing host. Fz2-mCherry transplanted cells do not undergo significant morphological changes and Fz2-mCherry is concentrated in discontinuous membrane areas (B, arrowheads). Scale bars: 10μm.

Source: Lin, S., Baye, L.M., Westfall, T.A., and Slusarski, D.C. (2010). Wnt5b-Ryk pathway provides directional signals to regulate gastrulation movement. J Cell Biol *190*, 263-278.

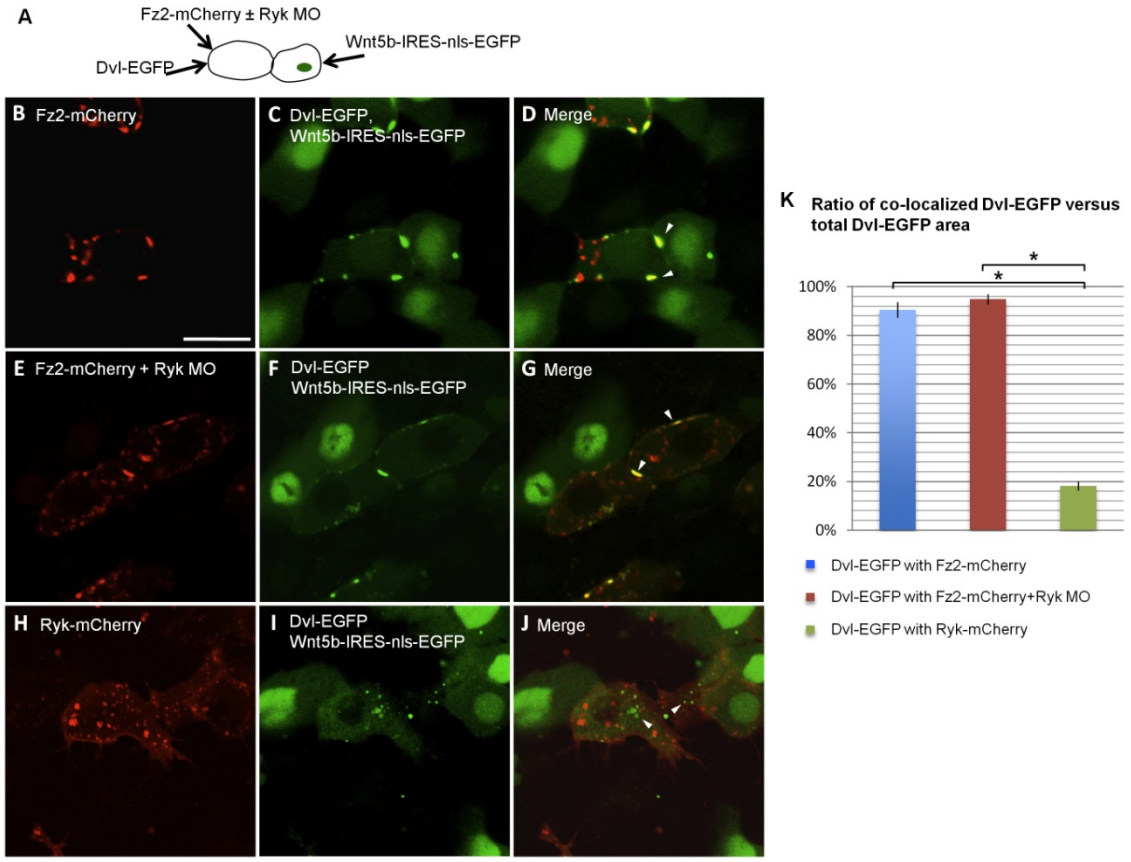

Figure 37: Fz2, but not Ryk, recruits Dvl. (A) schematic of mosaic injection approach. At 8-16 cell stage, one cell was injected with Wnt5b-IRES-nls-EGFP encoding RNA while an adjacent cell was injected with Dvl-EGFP encoding RNA alone or combined with: Fz2-mCherry encoding RNA, Fz2-mCherry encoding RNA + Ryk MO, or Ryk-mCherry encoding RNA. (B-D) Fz-mCherry (B) when co-injected with Dvl-GFP (C) is concentrated in discrete membrane domains and colocalized with Dvl-EGFP (D, arrowheads) when adjacent to a Wnt5b expressing cell (C and D, nuclear EGFP). (E-G) The pattern of Fz-mCherry (E) co-localized with Dvl-GFP (F and G) is not affected by co-injection of Ryk (G). (H-J) Ryk-mCherry (H) when coinjected with Dvl-GFP (I) does not colocalize with Dvl-EGFP (J). Note that Ryk-expressing cells develop lamellipodia-like protrusions (H) and Dvl-EGFP is largely located in cytoplasmic areas that are Ryk-mCherry negative (J, arrowheads). Quantification of the ratio of co-localized Dvl-EGFP versus total Dvl-EGFP area (K). Column height represents average ratio in percentage. Error bars represent standard error of seven samples in each experiment. One-way ANOVA and Tukey HSD Test (asterisks, $p<0.01$). Scale bar: 10μm.

Source: Lin, S., Baye, L.M., Westfall, T.A., and Slusarski, D.C. (2010). Wnt5b-Ryk pathway provides directional signals to regulate gastrulation movement. J Cell Biol *190*, 263-278.

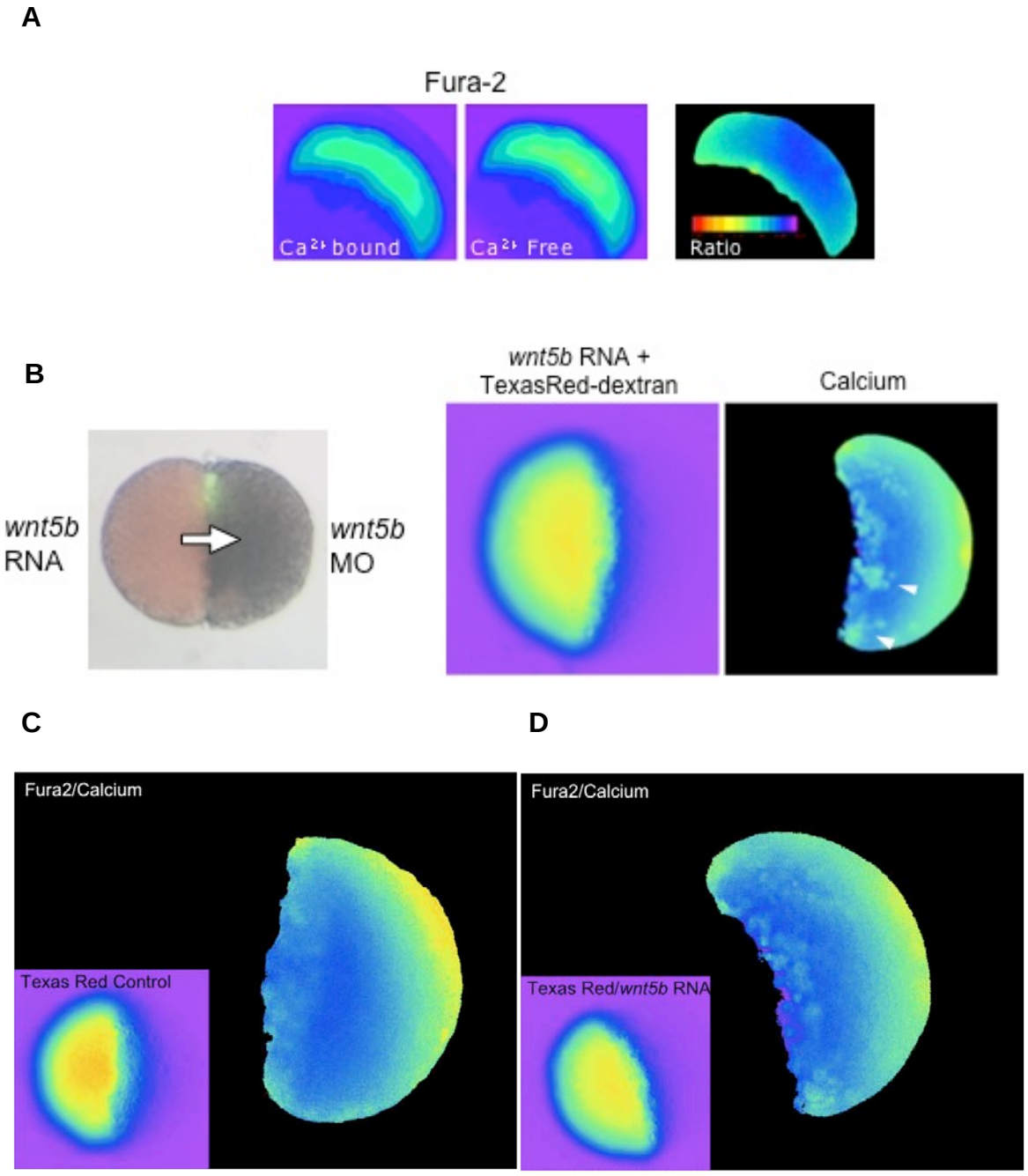

Figure 38: Directional Wnt5b signals propagate Ca^{2+} release events in co-cultured explants. (A) Fura-2 was used for Ca^{2+} imaging purpose. (B) Two explants/animal caps were dissected from embryos injected with *wnt5b* RNA+TexasRed-dextran for lineage tracing and Wnt5b MO+Fura-2 for Ca^{2+}, respectively. (C-D) Ca^{2+} dynamics in explant aggregates. Control aggregates from explants expressing endogenous Wnt5b demonstates baseline calcium activity in the forms of periodic transients on the perimeter and sustained level on the interface (C). In contrast, Wnt5b-depleted explant, when juxtaposed to a Wnt5b-expressing explant, exhibits significantly elevated Ca^{2+} release events in the entire explants (D).

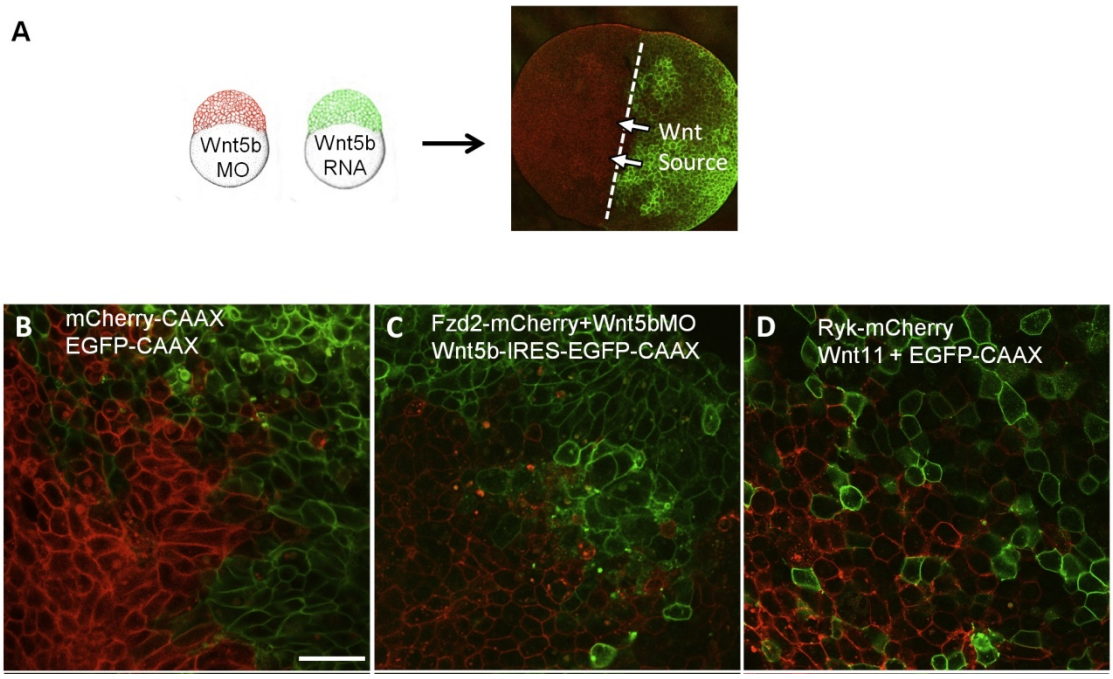

Figure 39: Zebrafish animal cap aggregate assays. (A) Zebrafish animal caps were dissected from embryos injected with Wnt5b-IRES-EGFP-CAAX (100pg, green) and mCherry constructs (100pg) + Wnt5b MO (1.0pmol, red), respectively; a directional Wnt5b signal was created by juxtaposing the two caps. (B-G) Live images at the interface of co-cultured cap aggregates. mCherry-CAAX cap(red) co-cultured with EGFP-CAAX cap (green) showed cell intermingling at the interface (B). Fz2-mCherry+Wnt5b MO cap (red) co-cultured with Wnt5b-expressing cap (green) show similar cell intermingling (C). Wnt11-expressing cap (green) co-cultured with Ryk-mCherry expressing cap (red) show intermingled cells (D). Ryk-mCherry+Wnt5b MO cap (red) co-cultured with Wnt5b-expressing cap (green) do not show intermingled cells (E). The region at the interface of the caps show a distinct border with reduced Ryk-mCherry (E, asterisk). High magnification image of Ryk-mCherry expressing cell projecting a protrusion away from the Wnt5b source (F). Ryk ICD-mCherry cap (red) co-cultured with Wnt5b-expressing cap (green) show cell mixing (G). (H-I) To evaluate cell distribution at the boundary, Ryk-mCherry and Wnt5b-IRES-EGFP-CAAX were injected into H2A-EGFP transgenic embryos resulting in nuclear EGFP in cells of the aggregate. H2A-EGFP cells were present across the boundary of Ryk-mCherry and Wnt5b-IRES-EGFP-CAAX expressing aggregates, indicating absence of cell loss at the interface (H). In an Ryk-mCherry/H2A-EGFP cap co-cultured with a Wnt5b-IRES-EGFP-CAAX cap, juxtaposition of the nuclear H2A-EGFP with membrane EGFP-CAAX (lack of H2A-EGFP and EGFP-CAAX double negative area) suggests the “gap” area originates from mCherry turnover rather than EGFP-CAAX turnover (I). Scale bars: 20μm.

Source: Lin, S., Baye, L.M., Westfall, T.A., and Slusarski, D.C. (2010). Wnt5b-Ryk pathway provides directional signals to regulate gastrulation movement. J Cell Biol *190,* 263-278.

Figure 39 continued

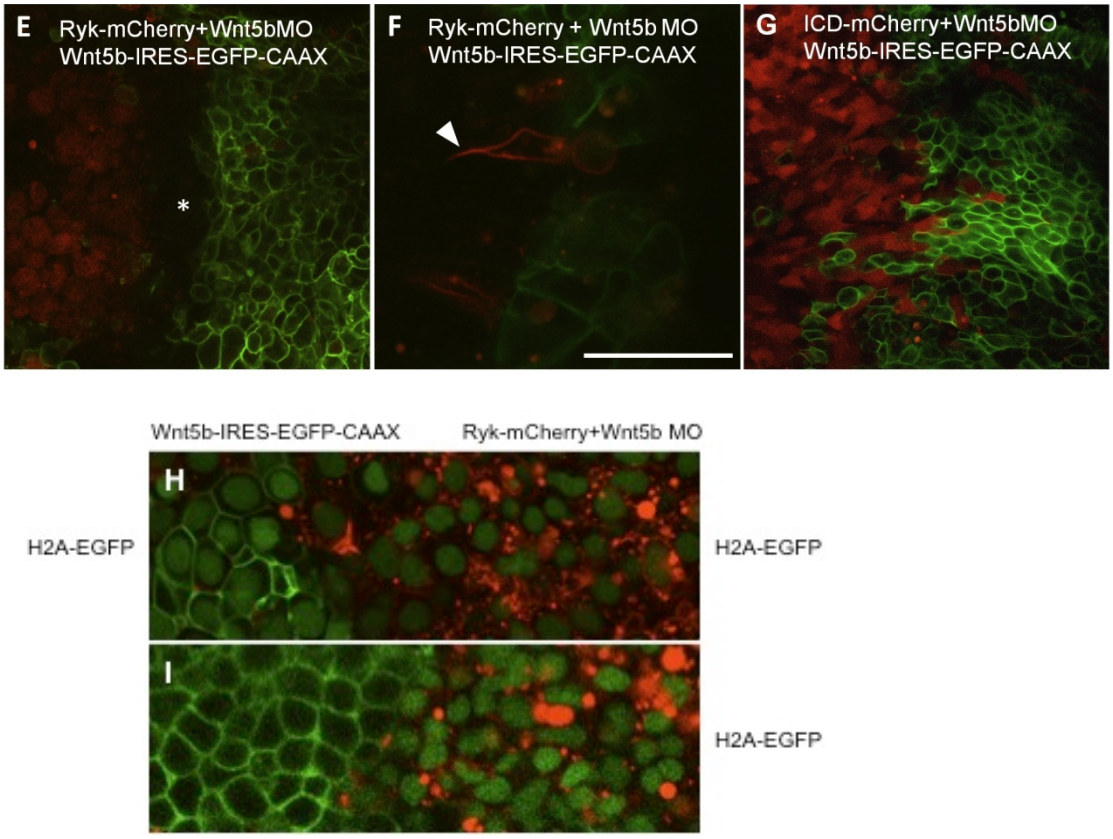

Red Moiety	Green Moiety	Non-intermingled	Intermingled
mCherry-CAAX+Wnt5bMO	Wnt5b-IRES-EGFP-CAAX	0	12
Fzd2-mCherry+Wnt5bMO	Wnt5b-IRES-EGFP-CAAX	1	16
Ryk-mCherry+Wnt5bMO	Wnt5b-IRES-EGFP-CAAX	17	2
Ryk-mCherry	Wnt11 + EGFP-CAAX	1	20
ICD-mCherry+Wnt5bMO	Wnt5b-IRES-EGFP-CAAX	0	15

Table 4. Quantification of the number of cap aggregates that had cell intermingling at the interface.

Source: Lin, S., Baye, L.M., Westfall, T.A., and Slusarski, D.C. (2010). Wnt5b-Ryk pathway provides directional signals to regulate gastrulation movement. J Cell Biol *190*, 263-278.

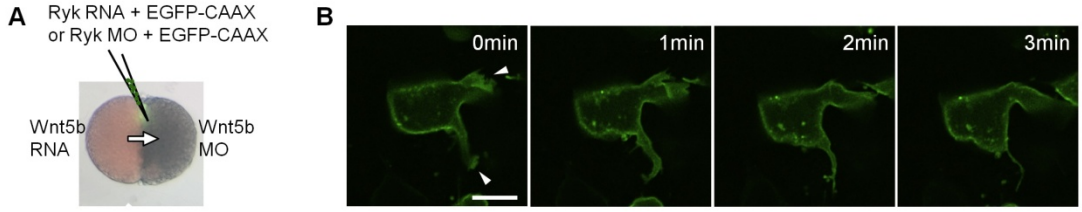

Figure 40: Direction of Wnt5b/Ryk signaling is correlated with cell mobility and polarized cell protrusions. (A) A *wnt5b* RNA injected cap (red) and a Wnt5b MO injected cap were juxtaposed and co-cultured to generate a directional Wnt source. Cells with *ryk* RNA + EGFP-CAAX or Ryk MO + EGFP-CAAX (green) were transplanted to the center of the aggregate interface. (B) An example of cell tracking of one *ryk* RNA injected cell showing active extension and retraction of lamellipodia-like protrusions over time (arrowheads). (C) Overlay traces of a *ryk* RNA injected cell and a Ryk MO injected cell; arrow marks the direction of Wnt5b gradient (high to low) was used to calculate cell roundness and was significantly different between *ryk* RNA and Ryk MO injected cells. Error bars represent standard error (n=24). Student's t-test (asterisks, $p<0.01$). (D) Representative migration path of individual cells recorded by time-lapse imaging over 20 min at 1 min intervals; start and end points are indicated by yellow and red triangles, respectively; Wnt5b source to the left. Total speed in all directions (black curved arrow) and net speed away from the Wnt5b source (red dashed arrow) are charted comparing Ryk MO injected cells to *ryk* RNA injected cells (n=10). Error bars represent standard error. A column chart showing that total speed in all directions (black curved arrow) and net speed away from the Wnt5b source (red dashed arrow) are reduced in Ryk MO injected cells, compared to *ryk* RNA injected cells (E, n=5). (E-F) Cells were transplanted into animal cap aggregates from *wnt5b* RNA injected caps (indicated by mCherry co-injection) and Wnt5b MO injected caps; boxes indicate areas for time-lapse imaging. *ryk* RNA+EGFP-CAAX injected cells preferentially spread into the Wnt5b MO injected moiety (E). Ryk MO+EGFP-CAAX injected cells spread in both moieties (F). Error bars represent standard error. Scale bars: 10μm in B, 5μm in D.

Source: Lin, S., Baye, L.M., Westfall, T.A., and Slusarski, D.C. (2010). Wnt5b-Ryk pathway provides directional signals to regulate gastrulation movement. J Cell Biol *190*, 263-278.

Figure 40 continued

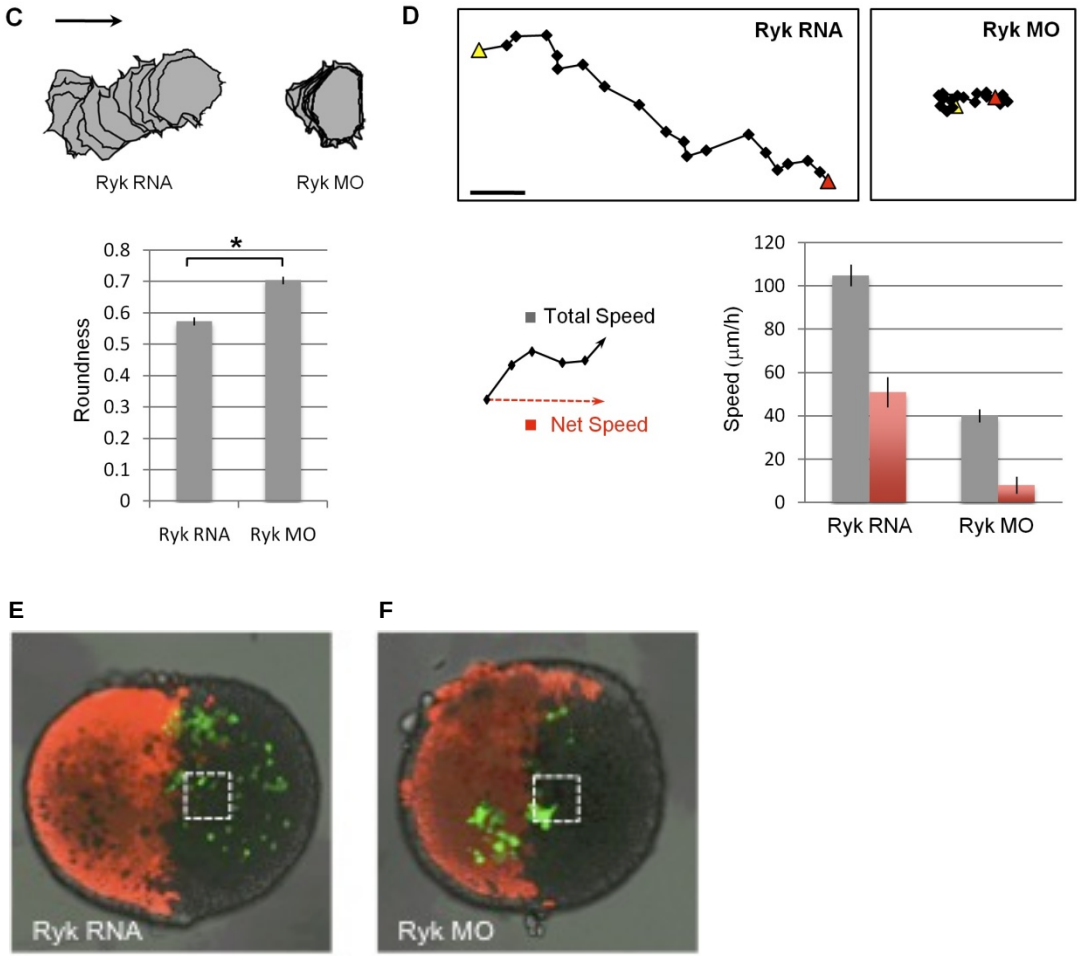

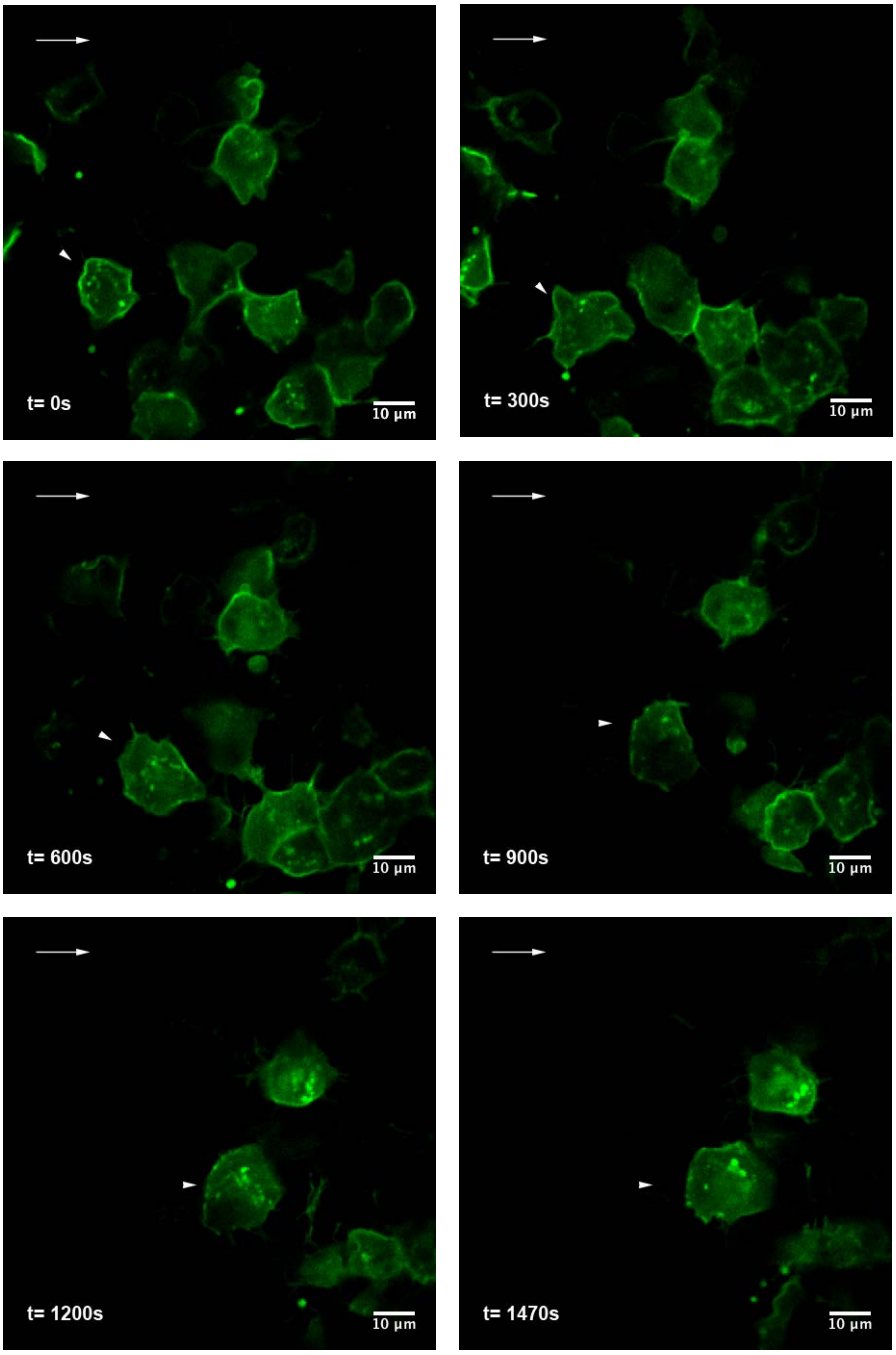

Figure 41: EGFP-CAAX was co-injected with *ryk* RNA in donor embryos. Cells from these embryos were transplanted into the center of the animal cap aggregate generated from a *wnt5b*-RNA injected cap juxtaposed with a Wnt5b MO injected cap. Arrow notes the direction of Wnt5b signal. Arrowhead traces a representative cell. 50 frames were taken at 30 second intervals.

Source: Lin, S., Baye, L.M., Westfall, T.A., and Slusarski, D.C. (2010). Wnt5b-Ryk pathway provides directional signals to regulate gastrulation movement. J Cell Biol *190*, 263-278.

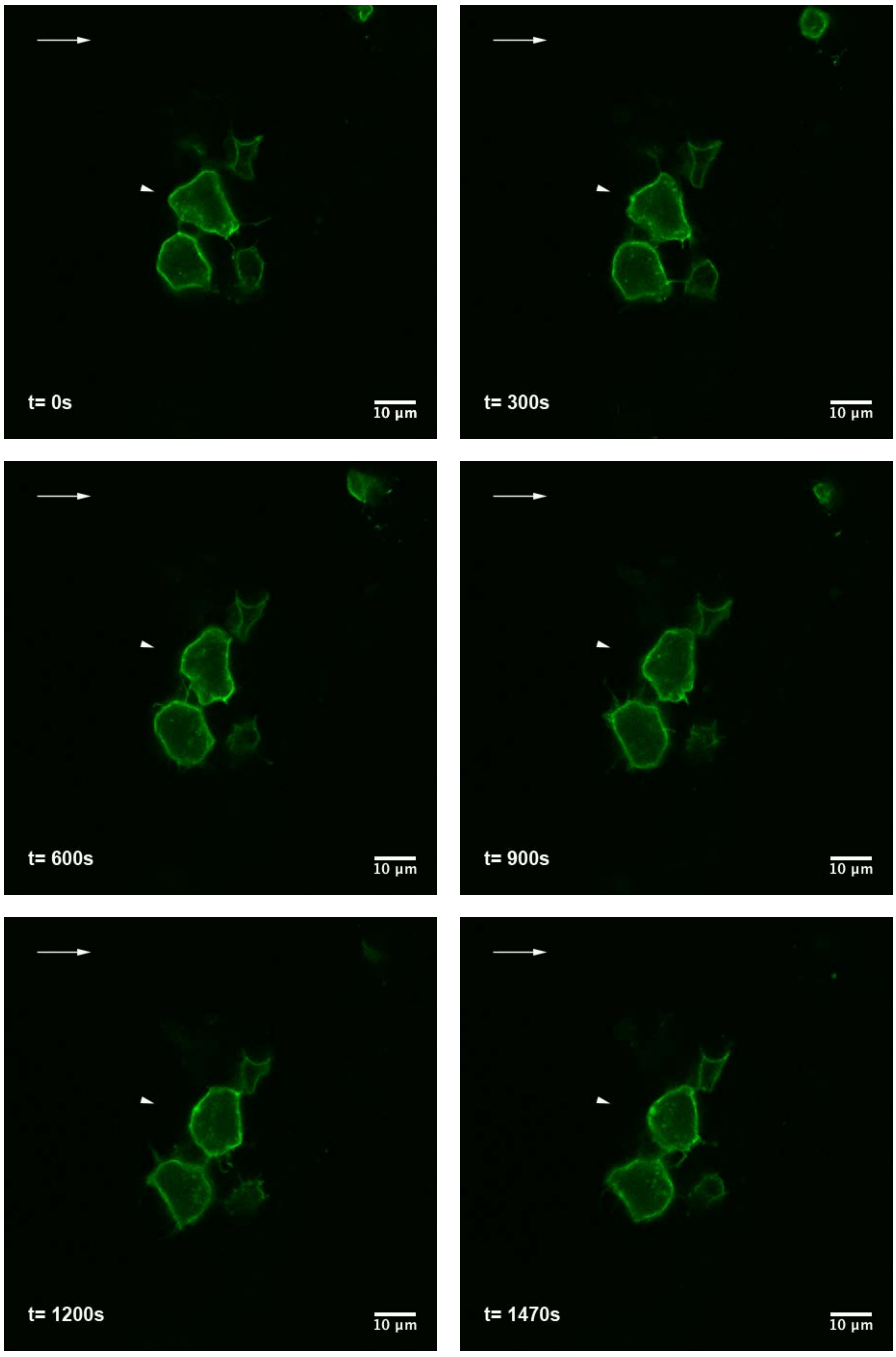

Figure 42: EGFP-CAAX was co-injected with Ryk MO in donor embryos. Cells from these embryos were transplanted into the center of the animal cap aggregate generated from a *wnt5b*-RNA injected cap juxtaposed with a Wnt5b MO injected cap. Arrow notes the direction of Wnt5b signal. Arrowhead traces a representative cell. 50 frames were taken at 30 second intervals.

Source: Lin, S., Baye, L.M., Westfall, T.A., and Slusarski, D.C. (2010). Wnt5b-Ryk pathway provides directional signals to regulate gastrulation movement. J Cell Biol *190*, 263-278.

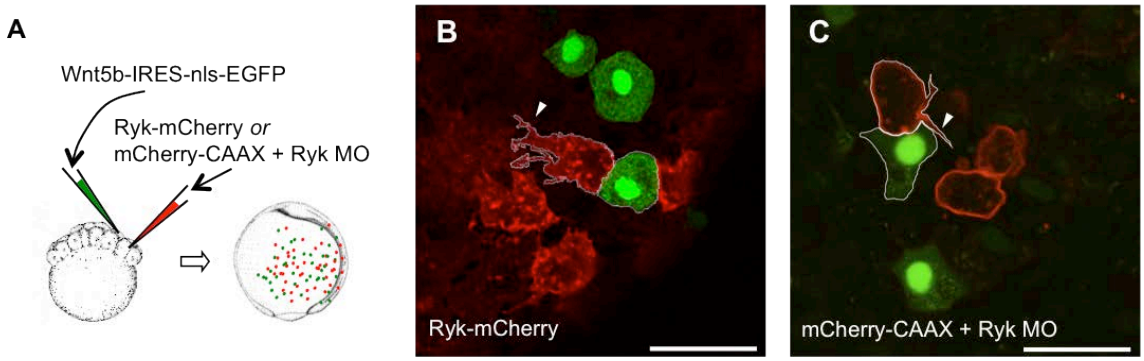

Figure 43: Polarized lamellipodia-like protrusions in 80-90% epiboly stage embryos. Schematic of the mosaic injection experimental approach shown (A). Ryk-mCherry cells (red) adjacent to Wnt5b-IRES-nls-EGFP cells (green) show directional protrusions (B, arrowhead). mCherry-CAAX and Ryk MO cell (red) adjacent to Wnt5b-IRES-nls-EGFP cells (green) display random projections (C, arrowhead). Scale bars: 30μm.

Source: Lin, S., Baye, L.M., Westfall, T.A., and Slusarski, D.C. (2010). Wnt5b-Ryk pathway provides directional signals to regulate gastrulation movement. J Cell Biol *190,* 263-278.

CHAPTER VII
CONCLUSION AND DISCUSSION

Conclusion

This study focuses on two fundamental aspects of Wnt signaling: the differential expression of Wnt ligands and the action of Wnt receptors. We have identified and characterized several novel mechanisms that regulate Wnt5b signaling in zebrafish. We have also applied principles of embryonic development to studies on signaling regulation during adult stages. Our findings shed light on development and disease processes regulated by Wnt5b signaling.

Permissive and instructive roles of Wnt5b

Our work suggests that in the context of gastrulation movement, Wnt5b acts as both permissive and instructive cues. A permissive cue triggers the response of recipient cells when its overall concentration reaches a threshold level. In contrast, an instructive cue provides positional information to the recipient cells by forming a directional concentration gradient. Non-canonical Wnts in the Fz/PCP pathway are known to function as permissive cues that do not provide spatial signals to downstream PCP components (Rohde and Heisenberg, 2007; Simons and Mlodzik, 2008). However, unlike the *wnt11/silberblick* mutant (Heisenberg et al., 2000), *wnt5b/pipetail* phenotype cannot be rescued by *wnt5b* RNA expression (Kilian et al., 2003; Westfall et al., 2003a), suggesting that localized Wnt5b can provide essential spatial information. Consist with the hypothesis that Wnt5 provides spatial cues, zygotic *wnt5b* expression is localized in the ventral-posterior region (Kilian et al., 2003), with a graded expression pattern resembling that of mammalian Wnt5a (Yamaguchi et al., 1999). These initial observations imply that Wnt5b acts as both permissive and instructive cues during development. Dual roles (permissive and instructive) of Wnt5b action suggest intricate control of *wnt5b* expression and the involvement of divergent downstream pathways.

Our studies have led to three tentative propositions that explain the dichotomy of zebrafish *wnt5b*: 1) permissive and instructive roles of *wnt5b* are genetically coded, 2) permissive and instructive roles of *wnt5b* are involved in different developmental processes, and 3) permissive and instructive roles of *wnt5b* are mediated by different receptors. The identification of *wnt5b.1* and *wnt5b.2*, as well as differential phenotypes resulted from individual knockdowns, provides evidence that different roles of *wnt5b* can be genetically separated. The fact that *wnt5b.1* and *wnt5b.2* are expressed at different stages in different levels suggests that their involvement in various developmental processes vary. Lastly, our data showcase that Fz2 and Ryk are associated with permissive and instructive roles of the Wnt5b ligand, respectively.

Signaling Versatility of Wnt5b

We reasoned that a particular signaling event is determined by both the affinity between specific ligand and receptor, and the availability of certain ligand and receptor under a given circumstance. These two factors may explain the remarkable signaling versatility of Wnt5, whose homologs have been associated with all known Wnt pathways under different contexts. To explore the availability of Wnt5 in developing embryos, we characterized *cis*-elements that drive tissue-specific expression of Wnt5 homologs. The identification of multiple *cis*-elements revealed an unexpected level of intricacy of temporal and spatial control of *wnt5b* expression. Future studies using these *cis*-elements to drive dominant-negative forms of either Wnt5b, Fz2 or Ryk would yield insights into the relative importance of a particular Wnt5b-triggered pathway in given tissue or developmental stage.

We further examined whether Wnt5b signals are conveyed by various receptors in gastrulation. Wnt5b is known to signal through Fz2 during CE movement (Kilian et al., 2003). In this study, we provided genetic, embryonic, and biochemical evidence to demonstrate that Wnt5b also bind the Ryk receptor. We showed that a Wnt5b gradient

could be conveyed to Ryk-expressing cells by co-culturing explants expressing Wnt5b and Ryk, respectively. We found that Wnt5b/Ryk interaction restricted cells intermingling, while Wnt11/Ryk cells freely intermingled. We also found that Wnt5b/Ryk and Wnt5b/Fz2 demonstrate differential impacts on cell intermingling. Our study highlights the differences between two non-canonical Wnt ligands, Wnt5 and Wnt11, and explains the high degree of Wnt signaling diversity due to combination of different ligand and receptor.

Our findings show that multiple Wnt receptors, which collectively regulate gastrulation, induce distinct downstream signaling events. This is reminiscent of *C. elegans* vulval development, during which distinct pathways downstream to Fz, Ryk and the Ror receptor tyrosine kinase CAM-1 are all required for proper orientation of vulval cells (Green et al., 2008). We demonstrated that Wnt5b/Ryk and Wnt5b/Fz2 pathways lead to distinct signaling outputs. In the presence of Wnt5b, Fz2 but not Ryk clusters with Dvl on the membrane. This, along with the intermingling of Fz and Wnt5b, but not Ryk and Wnt5b cells in co-cultured explant, is consistent with our hypothesis that Ryk and Fz2 pathways are separate. We postulate that Wnt5b/Fz2 activates a PCP-like pathway similar to Wnt11/Fz7 signaling that is directly associated with Dvl (Carmona-Fontaine et al., 2008; Witzel et al., 2006). In contrast to a previous study in *Xenopus* (Kim et al., 2008), we demonstrate that Wnt5b is largely responsible for Ryk-mediated gastrulation movement by promoting Ryk internalization and efficient persistent cell protrusions with net migration away from the Wnt5b source.

We will perform future experiments to address alternative mechanisms that might also contribute to the signaling versatility of Wnt5b. One possible mechanism is that Fz, Ryk, and Wnt form a ternary signaling complex and promotes canonical Wnt signaling (Lu et al., 2004). Although the possibility of compound signaling from Fz/Ryk complex remains, it is unlikely that this leads to downstream events similar to Fz receptor alone, as Fz and Ryk demonstrate distinct signaling properties when stimulated by external Wnt5b.

Indeed, we showed that neither Ryk overexpression nor Ryk knock-down in embryos results in changes in canonical Wnt signaling by luciferase assays, suggesting that Ryk is not an essential component of canonical Wnt signaling pathway. Nevertheless, signaling events resulted from the potential ternary complex may be different from signaling events triggered by either Ryk or Fz alone. We will perform FRET and Co-IP analysis to address whether Ryk and Fz can form complex on the plasma membrane.

Molecular nature of Ryk signaling

We investigated three previously proposed theories on the molecular nature of Ryk signaling pathways: 1) Ryk functions as a Fz co-receptor (Kim et al., 2008; Lu et al., 2004), 2) Ryk intracellular domain (ICD) is translocated to the nucleus in a Wnt-dependent manner and functions as a transcription factor (Lyu et al., 2008), and 3) Ryk heterodimerizes with other RTKs (Halford et al., 2000) and activates typical RTK effectors like Src kinase (Wouda et al., 2008). Even though all three theories have been tested, conflicting results have been reported. In *Drosophila*, Wnt5A-Derailed pathway seems to be independent of Fz-mediated pathways (Wouda et al., 2008). During vulval cell patterning in *C. elegans*, a Wnt ligand MOM-2 activates the Ryk homolog LIN-18 to signal a pathway separated from Fz homolog LIN-17 mediated pathways (Inoue et al., 2004). In contrast, experiments using HEK293T cells showed that Wnt1, Ryk and Frizzled form a ternary complex (Lu et al., 2004). Overexpressed DVL and RYK interact with each other using the PDZ domain of Dvl and the C-terminal tail of RYK, and RYK is required for Wnt3a-mediated canonical Wnt signaling (Lu et al., 2004). We showed compelling data that Ryk is not associated with Dvl, an essential component of all Fz-mediated pathway. Therefore Ryk is unlikely to participate in Fz-mediated signaling events.

We also tested if potential transcription activity of Ryk intracellular domain (ICD) underlies Ryk's function during zebrafish gastrulation. Others and we previously showed

that vertebrate Ryk proteins are reported to be constitutively cleaved by γ-secretase at a position close to the transmembrane domain (Lin et al., 2010; Lyu et al., 2008). A recent study reported that Wnt3a simulates the cleaved Ryk product to enter the nucleus and function as a transcriptional factor during neuronal differentiation; importantly, this function of Ryk is independent of Fz (Lyu et al., 2008). We confirmed the result that Ryk is constitutively cleaved in a Wnt independent manner. However, the N-terminal and C-terminal products of Ryk are still spatially overlapped and primarily distributed in cytoplasm, arguing against the idea that Ryk functions through transcriptional activation by its ICD. We reasoned that neuronal differentiation, which depends on the transcription activity of Ryk ICD, is a prolonged biological process and may be different from acute cellular responses like Wnt5b-mediated cell migration. Therefore the two processes may utilize different molecular mechanisms. Furthermore, we demonstrate that Ryk ECD processing is necessary for Ryk and Wnt5b binding. Although the ICD portion of Ryk is sufficient to drive neuronal differentiation in cell culture (Lyu et al., 2008), our work demonstrates that Ryk ICD-expressing cells intermingle with Wnt5b-expressing cells in co-cultured explants and expression of ICD alone does not rescue Ryk MO-induced CE defects in zebrafish. We postulate that lack of rescue suggests Wnt5b and Ryk ECD interaction is necessary for directional cell migration and that non-directional Ryk signaling is insufficient to mediate CE movement. Our results show both ECD and ICD portions of Ryk are internalized upon Wnt5b exposure, indicating that Wnt5b-mediated protrusive activities require full-length Ryk. These observations differ from non-directional responses like neuronal differentiation that require accumulation of ICD in the nucleus (Lyu et al., 2008).

Data from my studies suggest that Ryk acts through an RTK-like pathway but possibly does not directly bind an RTK. The notion that Ryk participates in RTK pathway came from early overexpression experiments showing Ryk could heterodimerize with other RTKs and activate typical RTK signaling (Halford et al., 2000). A recent

study in *Drosophila* cell lines also demonstrated phosphorylation of the Ryk receptor upon Wnt activation and subsequent Src kinase activation (Wouda et al., 2008). We confirmed the finding that Ryk can be phosphorylated at tyrosine residues (data not shown). However, paring with a kinase-active RTK is not a necessity for activating RTK pathway. Phosphorylation of Ryk by cytosolic kinases can serve as alternative mechanism for RTK pathway activation. Our preliminary FRET experiments show that Ryk clusters on the plasma membrane without apparent requirement of other RTKs, affirming that alternative RTK activation via cytosolic kinases is possible. Another important molecular event downstream of RTK activation is intracellular Ca^{2+} release. We showed that Ryk is partially responsible for both endogenous and Wnt5-induced Ca^{2+} release, consistent with the idea that Wnt5b/Ryk may activate an RTK-like pathway.

Implications of Wnt5b function in adult zebrafish

We investigated Wnt5b's role in disease by examining abnormality in *wnt5b*$^{Ti265/+}$ zebrafish. We noted > 11% frequency of zebrafish with distended abdomens or external growths in *wnt5b*$^{Ti265/+}$ zebrafish when compared to 0% in wild-type of a similar age and diet. The pathological features assessed by hematoxylin and eosin staining, as well as couter-staining with anti-β-catenin antibody and the nuclear marker Topro3, includes markedly increased proliferation of the undifferentiated cells and accompanying reduction of the differentiated cells, which comprise the spermatozoa. Although the exact tumorigenic event of is unclear, we speculated that loss of Wnt5b has at least two effects on cancer progression. First, due to its ability to antagonize canonical Wnt signaling, Wnt5b may play a role in restricting cell growth via attenuating β-catenin signaling. Conversely, loss of Wnt5b causes elevation of β-catenin signaling and excessive cell growth. Wnt5b is only present in undifferentiated cells that are also devoid of nuclear β-catenin. Second, since Wnt5b regulates angiogenesis (Cirone et al., 2008),

loss of Wnt5b may result in mis-routing of the blood vessel and unrestricted growth of tumor cells.

We also investigated the transcriptional regulation of *wnt5* during regeneration, since *wnt5b* is known to be upregulated in regenerating fins (Lee et al., 2009; Stoick-Cooper et al., 2007). Surprisingly, we found that a human *WNT5A* enhancer driving gene expression in both embryonic and adult caudal fin does not drive gene expression in regenerating caudal fins post amputation. We speculated that *wnt5*-expressing cells in caudal fin can be divided into sub-populations: one that is expressed in regenerating cells, and the other that is expressed in mature pigment cells. Alternatively, enhancers isolated from human *WNT5A* locus may not respond to regenerating signals as human lost most of the regeneration ability during evolution. To distinguish between these two hypotheses, we will closely examine transgenic lines with enhancer elements derived from species with great regenerating abilities like zebrafish in the future.

REFERENCES

Agalliu, D., Takada, S., Agalliu, I., McMahon, A.P., and Jessell, T.M. (2009). Motor neurons with axial muscle projections specified by Wnt4/5 signaling. Neuron *61*, 708-720.

Aigouy, B., Farhadifar, R., Staple, D.B., Sagner, A., Roper, J.C., Julicher, F., and Eaton, S. (2010). Cell flow reorients the axis of planar polarity in the wing epithelium of Drosophila. Cell *142*, 773-786.

Alonso, L., and Fuchs, E. (2003). Stem cells in the skin: waste not, Wnt not. Genes Dev *17*, 1189-1200.

Amack, J.D., and Yost, H.J. (2004). The T box transcription factor no tail in ciliated cells controls zebrafish left-right asymmetry. Curr Biol *14*, 685-690.

Amsterdam, A., Burgess, S., Golling, G., Chen, W., Sun, Z., Townsend, K., Farrington, S., Haldi, M., and Hopkins, N. (1999). A large-scale insertional mutagenesis screen in zebrafish. Genes Dev *13*, 2713-2724.

Angers, S., and Moon, R.T. (2009). Proximal events in Wnt signal transduction. Nat Rev Mol Cell Biol *10*, 468-477.

Angers, S., Thorpe, C.J., Biechele, T.L., Goldenberg, S.J., Zheng, N., MacCoss, M.J., and Moon, R.T. (2006). The KLHL12-Cullin-3 ubiquitin ligase negatively regulates the Wnt-beta-catenin pathway by targeting Dishevelled for degradation. Nat Cell Biol *8*, 348-357.

Baier, H., Klostermann, S., Trowe, T., Karlstrom, R.O., Nusslein-Volhard, C., and Bonhoeffer, F. (1996). Genetic dissection of the retinotectal projection. Development *123*, 415-425.

Bauer, M.P., and Goetz, F.W. (2001). Isolation of gonadal mutations in adult zebrafish from a chemical mutagenesis screen. Biol Reprod *64*, 548-554.

Baye, L.M., and Link, B.A. (2007). The disarrayed mutation results in cell cycle and neurogenesis defects during retinal development in zebrafish. BMC Dev Biol *7*, 28.

Berridge, M.J. (1993). Inositol trisphosphate and calcium signalling. Nature *361*, 315-325.

Berridge, M.J., Bootman, M.D., and Roderick, H.L. (2003). Calcium signalling: dynamics, homeostasis and remodelling. Nat Rev Mol Cell Biol *4*, 517-529.

Broughton, R.E., Milam, J.E., and Roe, B.A. (2001). The complete sequence of the zebrafish (Danio rerio) mitochondrial genome and evolutionary patterns in vertebrate mitochondrial DNA. Genome Res *11*, 1958-1967.

Buratovich, M.A., Anderson, S., Gieseler, K., Pradel, J., and Wilder, E.L. (2000). DWnt-4 and Wingless have distinct activities in the Drosophila dorsal epidermis. Dev Genes Evol *210*, 111-119.

Cadigan, K.M., and Liu, Y.I. (2006). Wnt signaling: complexity at the surface. J Cell Sci *119*, 395-402.

Callahan, C.A., Bonkovsky, J.L., Scully, A.L., and Thomas, J.B. (1996). derailed is required for muscle attachment site selection in Drosophila. Development *122*, 2761-2767.

Carmona-Fontaine, C., Matthews, H.K., Kuriyama, S., Moreno, M., Dunn, G.A., Parsons, M., Stern, C.D., and Mayor, R. (2008). Contact inhibition of locomotion in vivo controls neural crest directional migration. Nature *456*, 957-961.

Chakrabarty, S., Radjendirane, V., Appelman, H., and Varani, J. (2003). Extracellular Calcium and Calcium Sensing Receptor Function in Human Colon Carcinomas: Promotion of E-Cadherin Expression and Suppression of beta-Catenin/TCF Activation. Cancer Res *63*, 67-71.

Chien, A.J., Conrad, W.H., and Moon, R.T. (2009). A Wnt survival guide: from flies to human disease. J Invest Dermatol *129*, 1614-1627.

Cirone, P., Lin, S., Griesbach, H.L., Zhang, Y., Slusarski, D.C., and Crews, C.M. (2008). A role for planar cell polarity signaling in angiogenesis. Angiogenesis *11*, 347-360.

Dale, T.C. (1998). Signal transduction by the Wnt family of ligands. Biochem J *329 (Pt 2)*, 209-223.

Dejmek, J., Dib, K., Jonsson, M., and Andersson, T. (2003). Wnt-5a and G-protein signaling are required for collagen-induced DDR1 receptor activation and normal mammary cell adhesion. Int J Cancer *103*, 344-351.

Dodge, J.E., Ramsahoye, B.H., Wo, Z.G., Okano, M., and Li, E. (2002). De novo methylation of MMLV provirus in embryonic stem cells: CpG versus non-CpG methylation. Gene *289*, 41-48.

Driever, W., Solnica-Krezel, L., Schier, A.F., Neuhauss, S.C., Malicki, J., Stemple, D.L., Stainier, D.Y., Zwartkruis, F., Abdelilah, S., Rangini, Z., *et al.* (1996). A genetic screen for mutations affecting embryogenesis in zebrafish. Development *123*, 37-46.

Du, S.J., Purcell, S.M., Christian, J.L., McGrew, L.L., and Moon, R.T. (1995). Identification of distinct classes and functional domains of Wnts through expression of wild-type and chimeric proteins in Xenopus embryos. Mol Cell Biol *15*, 2625-2634.

Fatemi, M., Pao, M.M., Jeong, S., Gal-Yam, E.N., Egger, G., Weisenberger, D.J., and Jones, P.A. (2005). Footprinting of mammalian promoters: use of a CpG DNA

methyltransferase revealing nucleosome positions at a single molecule level. Nucleic Acids Res *33*, e176.

Feil, R., and Berger, F. (2007). Convergent evolution of genomic imprinting in plants and mammals. Trends Genet *23*, 192-199.

Fisher, S., Grice, E.A., Vinton, R.M., Bessling, S.L., and McCallion, A.S. (2006). Conservation of RET regulatory function from human to zebrafish without sequence similarity. Science *312*, 276-279.

Forrester, W.C., Kim, C., and Garriga, G. (2004). The Caenorhabditis elegans Ror RTK CAM-1 inhibits EGL-20/Wnt signaling in cell migration. Genetics *168*, 1951-1962.

Freisinger, C.M., Fisher, R.A., and Slusarski, D.C. (2010). Regulator of g protein signaling 3 modulates wnt5b calcium dynamics and somite patterning. PLoS Genet *6*, e1001020.

Freisinger, C.M., Schneider, I., Westfall, T.A., and Slusarski, D.C. (2008a). Calcium dynamics integrated into signalling pathways that influence vertebrate axial patterning. Philos Trans R Soc Lond B Biol Sci *363*, 1377-1385.

Freisinger, C.M., Schneider, I., Westfall, T.A., and Slusarski, D.C. (2008b). Calcium dynamics integrated into signalling pathways that influence vertebrate axial patterning. Philos Trans R Soc Lond, B, Biol Sci *363*, 1377-1385.

Gao, C., and Chen, Y.G. (2010). Dishevelled: The hub of Wnt signaling. Cell Signal *22*, 717-727.

Gieseler, K., Graba, Y., Mariol, M.C., Wilder, E.L., Martinez-Arias, A., Lemaire, P., and Pradel, J. (1999). Antagonist activity of DWnt-4 and wingless in the Drosophila embryonic ventral ectoderm and in heterologous Xenopus assays. Mech Dev *85*, 123-131.

Gilland, E., Miller, A.L., Karplus, E., Baker, R., and Webb, S.E. (1999). Imaging of multicellular large-scale rhythmic calcium waves during zebrafish gastrulation. Proc Natl Acad Sci U S A *96*, 157-161.

Gore, A.V., Maegawa, S., Cheong, A., Gilligan, P.C., Weinberg, E.S., and Sampath, K. (2005). The zebrafish dorsal axis is apparent at the four-cell stage. Nature *438*, 1030-1035.

Green, J.L., Inoue, T., and Sternberg, P.W. (2008). Opposing Wnt pathways orient cell polarity during organogenesis. Cell *134*, 646-656.

Habas, R., Kato, Y., and He, X. (2001). Wnt/Frizzled activation of Rho regulates vertebrate gastrulation and requires a novel Formin homology protein Daam1. Cell *107*, 843-854.

Haffter, P., Granato, M., Brand, M., Mullins, M.C., Hammerschmidt, M., Kane, D.A., Odenthal, J., van Eeden, F.J., Jiang, Y.J., Heisenberg, C.P., *et al.* (1996). The identification of genes with unique and essential functions in the development of the zebrafish, Danio rerio. Development *123*, 1-36.

Haines, T.R., Rodenhiser, D.I., and Ainsworth, P.J. (2001). Allele-specific non-CpG methylation of the Nf1 gene during early mouse development. Dev Biol *240*, 585-598.

Halford, M.M., and Stacker, S.A. (2001). Revelations of the RYK receptor. Bioessays *23*, 34-45.

Hammerschmidt, M., Pelegri, F., Mullins, M.C., Kane, D.A., Brand, M., van Eeden, F.J., Furutani-Seiki, M., Granato, M., Haffter, P., Heisenberg, C.P., *et al.* (1996). Mutations affecting morphogenesis during gastrulation and tail formation in the zebrafish, Danio rerio. Development *123*, 143-151.

Harris, K.E., and Beckendorf, S.K. (2007). Different Wnt signals act through the Frizzled and RYK receptors during Drosophila salivary gland migration. Development *134*, 2017-2025.

He, X., Semenov, M., Tamai, K., and Zeng, X. (2004). LDL receptor-related proteins 5 and 6 in Wnt/beta-catenin signaling: arrows point the way. Development *131*, 1663-1677.

Heasman, J. (2002). Morpholino oligos: making sense of antisense? Dev Biol *243*, 209-214.

Heisenberg, C.P., Tada, M., Rauch, G.J., Saúde, L., Concha, M.L., Geisler, R., Stemple, D.L., Smith, J.C., and Wilson, S.W. (2000). Silberblick/Wnt11 mediates convergent extension movements during zebrafish gastrulation. Nature *405*, 76-81.

Hikasa, H., Shibata, M., Hiratani, I., and Taira, M. (2002). The Xenopus receptor tyrosine kinase Xror2 modulates morphogenetic movements of the axial mesoderm and neuroectoderm via Wnt signaling. Development *129*, 5227-5239.

Hoegg, S., Brinkmann, H., Taylor, J.S., and Meyer, A. (2004). Phylogenetic timing of the fish-specific genome duplication correlates with the diversification of teleost fish. J Mol Evol *59*, 190-203.

Hovens, C.M., Stacker, S.A., Andres, A.C., Harpur, A.G., Ziemiecki, A., and Wilks, A.F. (1992). RYK, a receptor tyrosine kinase-related molecule with unusual kinase domain motifs. Proc Natl Acad Sci U S A *89*, 11818-11822.

Inoue, T., Oz, H.S., Wiland, D., Gharib, S., Deshpande, R., Hill, R.J., Katz, W.S., and Sternberg, P.W. (2004). *C. elegans* LIN-18 is a Ryk ortholog and functions in parallel to LIN-17/Frizzled in Wnt signaling. Cell *118*, 795-806.

Isogai, S., Horiguchi, M., and Weinstein, B.M. (2001). The vascular anatomy of the developing zebrafish: an atlas of embryonic and early larval development. Dev Biol *230*, 278-301.

Jing, L., Lefebvre, J.L., Gordon, L.R., and Granato, M. (2009). Wnt signals organize synaptic prepattern and axon guidance through the zebrafish unplugged/MuSK receptor. Neuron *61*, 721-733.

Jonsson, M., Dejmek, J., Bendahl, P.O., and Andersson, T. (2002). Loss of Wnt-5a protein is associated with early relapse in invasive ductal breast carcinomas. Cancer Res *62*, 409-416.

Ju, R., Cirone, P., Lin, S., Griesbach, H., Slusarski, D.C., and Crews, C.M. (2010). Activation of the planar cell polarity formin DAAM1 leads to inhibition of endothelial cell proliferation, migration, and angiogenesis. Proc Natl Acad Sci U S A *107*, 6906-6911.

Katso, R.M., Russell, R.B., and Ganesan, T.S. (1999). Functional analysis of H-Ryk, an atypical member of the receptor tyrosine kinase family. Mol Cell Biol *19*, 6427-6440.

Kawakami, K., Takeda, H., Kawakami, N., Kobayashi, M., Matsuda, N., and Mishina, M. (2004). A transposon-mediated gene trap approach identifies developmentally regulated genes in zebrafish. Dev Cell *7*, 133-144.

Keeble, T.R., and Cooper, H.M. (2006). Ryk: a novel Wnt receptor regulating axon pathfinding. Int J Biochem Cell Biol *38*, 2011-2017.

Keeble, T.R., Halford, M.M., Seaman, C., Kee, N., Macheda, M., Anderson, R.B., Stacker, S.A., and Cooper, H.M. (2006). The Wnt receptor Ryk is required for Wnt5a-mediated axon guidance on the contralateral side of the corpus callosum. J Neurosci *26*, 5840-5848.

Kikuta, H., Laplante, M., Navratilova, P., Komisarczuk, A.Z., Engstrom, P.G., Fredman, D., Akalin, A., Caccamo, M., Sealy, I., Howe, K., *et al.* (2007). Genomic regulatory blocks encompass multiple neighboring genes and maintain conserved synteny in vertebrates. Genome Res *17*, 545-555.

Kilian, B., Mansukoski, H., Barbosa, F.C., Ulrich, F., Tada, M., and Heisenberg, C.P. (2003). The role of Ppt/Wnt5 in regulating cell shape and movement during zebrafish gastrulation. Mech Dev *120*, 467-476.

Kim, G.H., Her, J.H., and Han, J.K. (2008). Ryk cooperates with Frizzled 7 to promote Wnt11-mediated endocytosis and is essential for Xenopus laevis convergent extension movements. J Cell Biol *182*, 1073-1082.

Kimmel, C.B., Ballard, W.W., Kimmel, S.R., Ullmann, B., and Schilling, T.F. (1995). Stages of embryonic development of the zebrafish. Dev Dyn *203*, 253-310.

Kimmel, C.B., and Law, R.D. (1985a). Cell lineage of zebrafish blastomeres. I. Cleavage pattern and cytoplasmic bridges between cells. Dev Biol *108*, 78-85.

Kimmel, C.B., and Law, R.D. (1985b). Cell lineage of zebrafish blastomeres. III. Clonal analyses of the blastula and gastrula stages. Dev Biol *108*, 94-101.

Kohn, A.D., and Moon, R.T. (2005). Wnt and calcium signaling: beta-catenin-independent pathways. Cell Calcium *38*, 439-446.

Kroiher, M., Miller, M.A., and Steele, R.E. (2001). Deceiving appearances: signaling by "dead" and "fractured" receptor protein-tyrosine kinases. Bioessays *23*, 69-76.

Kume, S., Saneyoshi, T., and Mikoshiba, K. (2000). Desensitization of IP3-induced Ca2+ release by overexpression of a constitutively active Gqalpha protein converts ventral to dorsal fate in Xenopus early embryos. Dev Growth Differ *42*, 327-335.

Kwan, K.M., Fujimoto, E., Grabher, C., Mangum, B.D., Hardy, M.E., Campbell, D.S., Parant, J.M., Yost, H.J., Kanki, J.P., and Chien, C.B. (2007). The Tol2kit: a multisite gateway-based construction kit for Tol2 transposon transgenesis constructs. Dev Dyn *236*, 3088-3099.

Lai, S.L., Chien, A.J., and Moon, R.T. (2009). Wnt/Fz signaling and the cytoskeleton: potential roles in tumorigenesis. Cell Res *19*, 532-545.

Langenau, D.M., Traver, D., Ferrando, A.A., Kutok, J.L., Aster, J.C., Kanki, J.P., Lin, S., Prochownik, E., Trede, N.S., Zon, L.I., *et al.* (2003). Myc-induced T cell leukemia in transgenic zebrafish. Science *299*, 887-890.

Lawrence, P.A., Casal, J., and Struhl, G. (2002). Towards a model of the organisation of planar polarity and pattern in the Drosophila abdomen. Development *129*, 2749-2760.

Lawrence, P.A., Struhl, G., and Casal, J. (2007). Planar cell polarity: one or two pathways? Nat Rev Genet *8*, 555-563.

Lawson, N.D., and Weinstein, B.M. (2002). In vivo imaging of embryonic vascular development using transgenic zebrafish. Dev Biol *248*, 307-318.

Lee, Y., Hami, D., De Val, S., Kagermeier-Schenk, B., Wills, A.A., Black, B.L., Weidinger, G., and Poss, K.D. (2009). Maintenance of blastemal proliferation by functionally diverse epidermis in regenerating zebrafish fins. Dev Biol *331*, 270-280.

Liang, H., Chen, Q., Coles, A.H., Anderson, S.J., Pihan, G., Bradley, A., Gerstein, R., Jurecic, R., and Jones, S.N. (2003). Wnt5a inhibits B cell proliferation and functions as a tumor suppressor in hematopoietic tissue. Cancer Cell *4*, 349-360.

Liepinsh, E., Bányai, L., Patthy, L., and Otting, G. (2006). NMR structure of the WIF domain of the human Wnt-inhibitory factor-1. J Mol Biol *357*, 942-950.

Lin, S., Baye, L.M., Westfall, T.A., and Slusarski, D.C. (2010). Wnt5b-Ryk pathway provides directional signals to regulate gastrulation movement. J Cell Biol *190*, 263-278.

Lipkin, M. (1999). Preclinical and early human studies of calcium and colon cancer prevention. Ann N Y Acad Sci *889*, 120-127.

Lister, R., Pelizzola, M., Dowen, R.H., Hawkins, R.D., Hon, G., Tonti-Filippini, J., Nery, J.R., Lee, L., Ye, Z., Ngo, Q.M., *et al.* (2009). Human DNA methylomes at base resolution show widespread epigenomic differences. Nature *462*, 315-322.

Liu, Y., Shi, J., Lu, C.C., Wang, Z.B., Lyuksyutova, A.I., Song, X.J., Song, X., and Zou, Y. (2005). Ryk-mediated Wnt repulsion regulates posterior-directed growth of corticospinal tract. Nat Neurosci *8*, 1151-1159.

Long, Q., Meng, A., Wang, H., Jessen, J.R., Farrell, M.J., and Lin, S. (1997). GATA-1 expression pattern can be recapitulated in living transgenic zebrafish using GFP reporter gene. Development *124*, 4105-4111.

Lu, W., Yamamoto, V., Ortega, B., and Baltimore, D. (2004). Mammalian Ryk is a Wnt coreceptor required for stimulation of neurite outgrowth. Cell *119*, 97-108.

Lyu, J., Yamamoto, V., and Lu, W. (2008). Cleavage of the Wnt receptor Ryk regulates neuronal differentiation during cortical neurogenesis. Dev Cell *15*, 773-780.

Malicki, J., Schier, A.F., Solnica-Krezel, L., Stemple, D.L., Neuhauss, S.C., Stainier, D.Y., Abdelilah, S., Rangini, Z., Zwartkruis, F., and Driever, W. (1996). Mutations affecting development of the zebrafish ear. Development *123*, 275-283.

Mellitzer, G., Xu, Q., and Wilkinson, D.G. (1999). Eph receptors and ephrins restrict cell intermingling and communication. Nature *400*, 77-81.

Mikels, A.J., and Nusse, R. (2006). Purified Wnt5a protein activates or inhibits beta-catenin-TCF signaling depending on receptor context. PLoS Biol *4*, e115.

Montero, J.A., Kilian, B., Chan, J., Bayliss, P.E., and Heisenberg, C.P. (2003). Phosphoinositide 3-kinase is required for process outgrowth and cell polarization of gastrulating mesendodermal cells. Curr Biol *13*, 1279-1289.

Moon, R.T., Christian, J.L., Campbell, R.M., McGrew, L.L., DeMarais, A.A., Torres, M., Lai, C.J., Olson, D.J., and Kelly, G.M. (1993). Dissecting Wnt signalling pathways and Wnt-sensitive developmental processes through transient misexpression analyses in embryos of Xenopus laevis. Dev Suppl, 85-94.

Moon, R.T., Kohn, A.D., De Ferrari, G.V., and Kaykas, A. (2004). WNT and beta-catenin signalling: diseases and therapies. Nat Rev Genet *5*, 691-701.

Mullins, M.C., Hammerschmidt, M., Kane, D.A., Odenthal, J., Brand, M., van Eeden, F.J., Furutani-Seiki, M., Granato, M., Haffter, P., Heisenberg, C.P., *et al.* (1996). Genes

establishing dorsoventral pattern formation in the zebrafish embryo: the ventral specifying genes. Development *123*, 81-93.

Nelson, W.J., and Nusse, R. (2004). Convergence of Wnt, beta-catenin, and cadherin pathways. Science *303*, 1483-1487.

Nusse, R. (2008). Wnt signaling and stem cell control. Cell Res.

Oishi, I., Suzuki, H., Onishi, N., Takada, R., Kani, S., Ohkawara, B., Koshida, I., Suzuki, K., Yamada, G., Schwabe, G.C., *et al.* (2003). The receptor tyrosine kinase Ror2 is involved in non-canonical Wnt5a/JNK signalling pathway. Genes Cells *8*, 645-654.

Oishi, I., Takeuchi, S., Hashimoto, R., Nagabukuro, A., Ueda, T., Liu, Z.J., Hatta, T., Akira, S., Matsuda, Y., Yamamura, H., *et al.* (1999). Spatio-temporally regulated expression of receptor tyrosine kinases, mRor1, mRor2, during mouse development: implications in development and function of the nervous system. Genes Cells *4*, 41-56.

Park, H.C., Kim, C.H., Bae, Y.K., Yeo, S.Y., Kim, S.H., Hong, S.K., Shin, J., Yoo, K.W., Hibi, M., Hirano, T., *et al.* (2000). Analysis of upstream elements in the HuC promoter leads to the establishment of transgenic zebrafish with fluorescent neurons. Dev Biol *227*, 279-293.

Park, M., and Moon, R.T. (2002). The planar cell-polarity gene stbm regulates cell behaviour and cell fate in vertebrate embryos. Nat Cell Biol *4*, 20-25.

Pawson, T. (1995). Protein modules and signalling networks. Nature *373*, 573-580.

Peifer, M., and Polakis, P. (2000). Cancer - Wnt signaling in oncogenesis and embryogenesis - a look outside the nucleus [Review]. Science *287*, 1606-1609.

Pennacchio, L.A., Ahituv, N., Moses, A.M., Prabhakar, S., Nobrega, M.A., Shoukry, M., Minovitsky, S., Dubchak, I., Holt, A., Lewis, K.D., *et al.* (2006). In vivo enhancer analysis of human conserved non-coding sequences. Nature *444*, 499-502.

Rauch, G.J., Hammerschmidt, M., Blader, P., Schauerte, H.E., Strahle, U., Ingham, P.W., McMahon, A.P., and Haffter, P. (1997a). Wnt5 is required for tail formation in the zebrafish embryo. Cold Spring Harbor Symposia on Quantitative Biology *62*, 227-234.

Rauch, G.J., Hammerschmidt, M., Blader, P., Schauerte, H.E., Strahle, U., Ingham, P.W., McMahon, A.P., and Haffter, P. (1997b). Wnt5 is required for tail formation in the zebrafish embryo. Cold Spring Harb Symp Quant Biol *62*, 227-234.

Robu, M.E., Larson, J.D., Nasevicius, A., Beiraghi, S., Brenner, C., Farber, S.A., and Ekker, S.C. (2007). p53 activation by knockdown technologies. PLoS Genet *3*, e78.

Rohde, C., Zhang, Y., Reinhardt, R., and Jeltsch, A. (2010). BISMA--fast and accurate bisulfite sequencing data analysis of individual clones from unique and repetitive sequences. BMC Bioinformatics *11*, 230.

Rohde, L.A., and Heisenberg, C.P. (2007). Zebrafish gastrulation: cell movements, signals, and mechanisms. Int Rev Cytol *261*, 159-192.

Sato, A., Yamamoto, H., Sakane, H., Koyama, H., and Kikuchi, A. (2010). Wnt5a regulates distinct signalling pathways by binding to Frizzled2. EMBO J *29*, 41-54.

Savant-Bhonsale, S., Friese, M., McCoon, P., and Montell, D.J. (1999). A Drosophila derailed homolog, doughnut, expressed in invaginating cells during embryogenesis. Gene *231*, 155-161.

Schambony, A., Hefele, J.A., Gentzel, M., Wilm, M., and Wedlich, D. (2003). A homologue of cysteine-rich secretory proteins induces premature degradation of vitelline envelopes and hatching of Xenopus laevis embryos. Mech Dev *120*, 937-948.

Schier, A.F., and Talbot, W.S. (2005). Molecular genetics of axis formation in zebrafish. Annu Rev Genet *39*, 561-613.

Schmitt, A.M., Shi, J., Wolf, A.M., Lu, C.C., King, L.A., and Zou, Y. (2006). Wnt-Ryk signalling mediates medial-lateral retinotectal topographic mapping. Nature *439*, 31-37.

Schneider, I., Houston, D.W., Rebagliati, M.R., and Slusarski, D.C. (2008). Calcium fluxes in dorsal forerunner cells antagonize beta-catenin and alter left-right patterning. Development *135*, 75-84.

Sheldahl, L.C., Slusarski, D.C., Pandur, P., Miller, J.R., Kuhl, M., and Moon, R.T. (2003). Dishevelled activates Ca2+ flux, PKC, and CamKII in vertebrate embryos. J Cell Biol *161*, 769-777.

Simons, M., and Mlodzik, M. (2008). Planar cell polarity signaling: from fly development to human disease. Annu Rev Genet *42*, 517-540.

Slusarski, D.C., and Corces, V.G. (2000). Calcium imaging in cell-cell signaling. Methods Mol Biol *135*, 253-261.

Slusarski, D.C., Corces, V.G., and Moon, R.T. (1997a). Interaction of Wnt and a Frizzled homologue triggers G-protein-linked phosphatidylinositol signalling. Nature *390*, 410-413.

Slusarski, D.C., Yang-Snyder, J., Busa, W.B., and Moon, R.T. (1997b). Modulation of embryonic intracellular Ca2+ signaling by Wnt-5A. Dev Biol *182*, 114-120.

Solnica-Krezel, L. (2005). Conserved patterns of cell movements during vertebrate gastrulation. Curr Biol *15*, R213-228.

Solnica-Krezel, L., Stemple, D.L., Mountcastle-Shah, E., Rangini, Z., Neuhauss, S.C., Malicki, J., Schier, A.F., Stainier, D.Y., Zwartkruis, F., Abdelilah, S., *et al.* (1996). Mutations affecting cell fates and cellular rearrangements during gastrulation in zebrafish. Development *123*, 67-80.

Spence, R., Gerlach, G., Lawrence, C., and Smith, C. (2008). The behaviour and ecology of the zebrafish, Danio rerio. Biol Rev Camb Philos Soc *83*, 13-34.

Stoick-Cooper, C.L., Weidinger, G., Riehle, K.J., Hubbert, C., Major, M.B., Fausto, N., and Moon, R.T. (2007). Distinct Wnt signaling pathways have opposing roles in appendage regeneration. Development *134*, 479-489.

Summerhurst, K., Stark, M., Sharpe, J., Davidson, D., and Murphy, P. (2008). 3D representation of Wnt and Frizzled gene expression patterns in the mouse embryo at embryonic day 11.5 (Ts19). Gene Expr Patterns *8*, 331-348.

Thisse, C., Thisse, B., Schilling, T.F., and Postlethwait, J.H. (1993). Structure of the zebrafish snail1 gene and its expression in wild-type, spadetail and no tail mutant embryos. Development *119*, 1203-1215.

Topczewski, J., Sepich, D.S., Myers, D.C., Walker, C., Amores, A., Lele, Z., Hammerschmidt, M., Postlethwait, J., and Solnica-Krezel, L. (2001). The zebrafish glypican knypek controls cell polarity during gastrulation movements of convergent extension. Dev Cell *1*, 251-264.

Topol, L., Jiang, X., Choi, H., Garrett-Beal, L., Carolan, P.J., and Yang, Y. (2003a). Wnt-5a inhibits the canonical Wnt pathway by promoting GSK-3-independent {beta}-catenin degradation. J Cell Biol *162*, 899-908.

Topol, L., Jiang, X., Choi, H., Garrett-Beal, L., Carolan, P.J., and Yang, Y. (2003b). Wnt-5a inhibits the canonical Wnt pathway by promoting GSK-3-independent beta-catenin degradation. J Cell Biol *162*, 899-908.

Torres, M.A., Yang-Snyder, J.A., Purcell, S.M., DeMarais, A.A., McGrew, L.L., and Moon, R.T. (1996). Activities of the Wnt-1 class of secreted signaling factors are antagonized by the Wnt-5A class and by a dominant negative cadherin in early Xenopus development. J Cell Biol *133*, 1123-1137.

Ulrich, F., Concha, M.L., Heid, P.J., Voss, E., Witzel, S., Roehl, H., Tada, M., Wilson, S.W., Adams, R.J., Soll, D.R., *et al.* (2003). Slb/Wnt11 controls hypoblast cell migration and morphogenesis at the onset of zebrafish gastrulation. Development *130*, 5375-5384.

van Amerongen, R., Mikels, A., and Nusse, R. (2008). Alternative wnt signaling is initiated by distinct receptors. Sci Signal *1*, re9.

van Es, J.H., Barker, N., and Clevers, H. (2003). You Wnt some, you lose some: oncogenes in the Wnt signaling pathway. Curr Opin Genet Dev *13*, 28-33.

Veeman, M.T., Axelrod, J.D., and Moon, R.T. (2003a). A second canon. Functions and mechanisms of beta-catenin-independent Wnt signaling. Dev Cell *5*, 367-377.

Veeman, M.T., Slusarski, D.C., Kaykas, A., Louie, S.H., and Moon, R.T. (2003b). Zebrafish prickle, a modulator of noncanonical wnt/fz signaling, regulates gastrulation movements. Curr Biol *13*, 680-685.

von der Hardt, S., Bakkers, J., Inbal, A., Carvalho, L., Solnica-Krezel, L., Heisenberg, C.P., and Hammerschmidt, M. (2007). The Bmp gradient of the zebrafish gastrula guides migrating lateral cells by regulating cell-cell adhesion. Curr Biol *17*, 475-487.

Wallingford, J.B., Ewald, A.J., Harland, R.M., and Fraser, S.E. (2001). Calcium signaling during convergent extension in Xenopus. Curr Biol *11*, 652-661.

Wargovich, M.J., Jimenez, A., McKee, K., Steele, V.E., Velasco, M., Woods, J., Price, R., Gray, K., and Kelloff, G.J. (2000). Efficacy of potential chemopreventive agents on rat colon aberrant crypt formation and progression. Carcinogenesis *21*, 1149-1155.

Webb, S.E., and Miller, A.L. (2006). Ca2+ signaling and early embryonic patterning during the blastula and gastrula periods of zebrafish and Xenopus development. Biochim Biophys Acta *1763*, 1192-1208.

Weeraratna, A.T., Jiang, Y., Hostetter, G., Rosenblatt, K., Duray, P., Bittner, M., and Trent, J.M. (2002). Wnt5a signaling directly affects cell motility and invasion of metastatic melanoma. Cancer Cell *1*, 279-288.

Westfall, T.A., Brimeyer, R., Twedt, J., Gladon, J., Olberding, A., Furutani-Seiki, M., and Slusarski, D.C. (2003a). Wnt-5/pipetail functions in vertebrate axis formation as a negative regulator of Wnt/beta-catenin activity. J Cell Biol *162*, 889-898.

Westfall, T.A., Hjertos, B., and Slusarski, D.C. (2003b). Requirement for intracellular calcium modulation in zebrafish dorsal-ventral patterning. Dev Biol *259*, 380-391.

Wettschureck, N., and Offermanns, S. (2005). Mammalian G proteins and their cell type specific functions. Physiol Rev *85*, 1159-1204.

Wharton, K.A. (2003). Runnin' with the Dvl: Proteins That Associate with Dsh/Dvl and Their Significance to Wnt Signal Transduction. Developmental Biology *253*, 1-17.

Whitfield, T.T., Granato, M., van Eeden, F.J., Schach, U., Brand, M., Furutani-Seiki, M., Haffter, P., Hammerschmidt, M., Heisenberg, C.P., Jiang, Y.J., *et al.* (1996). Mutations affecting development of the zebrafish inner ear and lateral line. Development *123*, 241-254.

Witzel, S., Zimyanin, V., Carreira-Barbosa, F., Tada, M., and Heisenberg, C.P. (2006). Wnt11 controls cell contact persistence by local accumulation of Frizzled 7 at the plasma membrane. J Cell Biol *175*, 791-802.

Wodarz, A., and Nusse, R. (1998). Mechanisms of WNT Signaling in Development. Annu Rev Cell Dev Biol *14*, 59-88.

Wong, G.T., Gavin, B.J., and McMahon, A.P. (1994). Differential transformation of mammary epithelial cells by Wnt genes. Mol Cell Biol *14*, 6278-6286.

Wouda, R.R., Bansraj, M.R., de Jong, A.W., Noordermeer, J.N., and Fradkin, L.G. (2008). Src family kinases are required for WNT5 signaling through the Derailed/RYK receptor in the Drosophila embryonic central nervous system. Development *135*, 2277-2287.

Yamaguchi, T.P., Bradley, A., McMahon, A.P., and Jones, S. (1999). A Wnt5a pathway underlies outgrowth of multiple structures in the vertebrate embryo. Development *126*, 1211-1223.

Yin, C., Kiskowski, M., Pouille, P.A., Farge, E., and Solnica-Krezel, L. (2008). Cooperation of polarized cell intercalations drives convergence and extension of presomitic mesoderm during zebrafish gastrulation. J Cell Biol *180*, 221-232.

Yoshikawa, S., Bonkowsky, J.L., Kokel, M., Shyn, S., and Thomas, J.B. (2001). The derailed guidance receptor does not require kinase activity in vivo. J Neurosci *21*, RC119.

Zallen, J.A. (2007). Planar polarity and tissue morphogenesis. Cell *129*, 1051-1063.

Zhang, J., Lefebvre, J.L., Zhao, S., and Granato, M. (2004). Zebrafish unplugged reveals a role for muscle-specific kinase homologs in axonal pathway choice. Nat Neurosci *7*, 1303-1309.